University of Alberta

Meteorological Analysis of Four Rainstorms that Caused Severe Flooding in Alberta during June 2005

by

Aihong Alice Ou

A thesis submitted to the Faculty of Graduate Studies and Research
in partial fulfillment of the requirements for the degree of

Master of Science

Department of Earth and Atmospheric Sciences

Edmonton, Alberta
Spring 2008

Library and Archives Canada

Published Heritage Branch

395 Wellington Street
Ottawa ON K1A 0N4
Canada

Bibliothèque et Archives Canada

Direction du Patrimoine de l'édition

395, rue Wellington
Ottawa ON K1A 0N4
Canada

Your file Votre référence
ISBN: 978-0-494-45867-9
Our file Notre référence
ISBN: 978-0-494-45867-9

NOTICE:
The author has granted a non-exclusive license allowing Library and Archives Canada to reproduce, publish, archive, preserve, conserve, communicate to the public by telecommunication or on the Internet, loan, distribute and sell theses worldwide, for commercial or non-commercial purposes, in microform, paper, electronic and/or any other formats.

The author retains copyright ownership and moral rights in this thesis. Neither the thesis nor substantial extracts from it may be printed or otherwise reproduced without the author's permission.

AVIS:
L'auteur a accordé une licence non exclusive permettant à la Bibliothèque et Archives Canada de reproduire, publier, archiver, sauvegarder, conserver, transmettre au public par télécommunication ou par l'Internet, prêter, distribuer et vendre des thèses partout dans le monde, à des fins commerciales ou autres, sur support microforme, papier, électronique et/ou autres formats.

L'auteur conserve la propriété du droit d'auteur et des droits moraux qui protège cette thèse. Ni la thèse ni des extraits substantiels de celle-ci ne doivent être imprimés ou autrement reproduits sans son autorisation.

In compliance with the Canadian Privacy Act some supporting forms may have been removed from this thesis.

While these forms may be included in the document page count, their removal does not represent any loss of content from the thesis.

Conformément à la loi canadienne sur la protection de la vie privée, quelques formulaires secondaires ont été enlevés de cette thèse.

Bien que ces formulaires aient inclus dans la pagination, il n'y aura aucun contenu manquant.

Canada

ABSTRACT

We analyze the synoptic and mesoscale evolution of four rainstorms that produced extensive floods in June 2005, in Alberta, Canada. The dates and point-measured peak accumulated rainfalls of the four rainstorms were: 1-5 June (140 mm), 5-9 June (248 mm), 16-19 June (152 mm), and 27-29 June (90 mm). All four rainstorms were associated with short wave troughs and cold lows at 500 hPa. Some common features were: positive vorticity advection at mid level present during the heaviest rainfall episode, low level moisture tongues, and quasi-stationary inverted troughs or trowals (trough of warm air aloft) with lee cyclone genesis or intensification. Stability analysis of the balloon soundings suggests that convection was important for the June 16-19 case, but not important for the other cases. A simple calculation suggests that mechanical lifting by upslope wind contributed to about half of the precipitation accumulation in southern Alberta for the June 5-9 case.

DEDICATION

To My Loving Husband and Parents

Whose Encouragement, Support, Understanding and Strong Belief in Education Have

Made This Work Possible

ACKNOWLEDGEMENTS

I wish to express my sincere gratitude to Professor Gerhard W. Reuter for his warm guidance, advice and encouragement throughout the course of this work, and especially for his help in editing this manuscript. My heartfelt thanks are given to Professor Paul G. Myers for his kind co-supervision, teaching, and constructive suggestions. My appreciation is also due to Professor John D. Wilson for his kind teaching, continuing interest, and consideration.

I would like to convey my special acknowledgments to the following organizations:

* The Canadian Foundation for Climate and Atmospheric Sciences (CFCAS) and the Natural Sciences and Engineering Research Council (NSERC) of Canada who provided research grants for supporting this thesis project.
* Environment Canada (EC) who provided meteorological analysis charts, synoptic observations, radar and satellite images.
* Alberta Environment (AE) who provided hourly precipitation data and stream flow information.
* The Plymouth State Weather Center (PSWC) and NOAA/ESRL - Physical Science Division who provided reanalysis data through their Webs.
* NOAA/NCDC - Forecast System Laboratory who provided radiosonde data through their Web.

Table of Contents

		Page
Chapter 1:	Introduction	1
1.1	Brief introduction to the June 2005 Alberta flood	1
1.2	Research objectives	2
1.3	Background on heavy precipitation events	3
1.3.1	Synoptic features	3
1.3.2	Organization of precipitation	4
1.3.3	Orographic effects	4
1.3.4	Convective overturning	5
1.3.5	Atmospheric moisture	5
1.4	Climatology of extreme rainfall events in Alberta	5
1.5	Outline of content of thesis	8
Chapter 2:	Theory and overview of the flood events	9
2.1	Theory relevant for precipitation production	9
2.1.1	Water flux balance at cloud base	9
2.1.2	Mechanical lifting due to sloping terrain	11
2.1.3	Synoptic forcing of ascending air motion	11
2.1.4	Orographic effects	16
2.1.5	Vertical wind shear	17
2.1.6	Convective instability	18
2.1.7	Precipitable water	19
2.2	Observational data	20
2.2.1	Radar and satellite imageries	20
2.2.2	Synoptic weather maps	21
2.2.3	Balloon soundings	22
2.3	Overview and background on the June 2005 Alberta flood	22
2.3.1	Features of the four rainstorms in Alberta during June 2005	22

2.3.2 Impacts of the June 2005 Alberta flood..... 24
2.3.3 Alberta's June precipitation climatology..... 25

Chapter 3: Study of the extreme rainstorm case of June 5-9, 2005..... 27
3.1 Brief review of the case..... 27
3.2 Analyses of radar and satellite imageries..... 27
3.2.1 Precipitation organization and evolution of the radar echoes..... 27
3.2.2 Organization and evolution of clouds and airstreams on satellite imagery..... 31
3.3 Synoptic flow features..... 34
3.3.1 Flow pattern at the surface 34
3.3.2 Flow pattern at upper levels..... 36
3.4 Moisture condition..... 42
3.4.1 Water vapor distribution at 850 hPa..... 42
3.4.2 Precipitable water and vapor mixing ratio..... 43
3.5 Mechanisms contributing to heavy precipitation..... 44
3.5.1 Synoptic forcing..... 44
3.5.2 Orographic forcing and orographic rainfall..... 48
3.5.3 State of the atmosphere and buoyant forcing..... 50
3.5 Summary and concluding remarks for extreme rainstorm case 2. 53

Chapter 4: Study of the other 3 rainstorms during June 2005..... 54
4.1 Study of rainstorm case 1 (June 1-5)..... 54
4.1.1 Brief review of the case..... 54
4.1.2 Organization and evolution of precipitation..... 54
4.1.3 Overview of the synoptic flow pattern..... 56
4.1.4 Moisture condition..... 57
4.1.5 Mechanisms contributing to the rainstorm..... 58
4.1.6 Summary and concluding remarks for rainstorm case 1.. 59

4.2 Study of rainstorm case 3 (June 16-19)..... 60

4.2.1 Brief review of the case..... 60

4.2.2 Organization and evolution of precipitation..... 60

4.2.3 Overview of the synoptic flow pattern..... 62

4.2.4 Moisture condition..... 63

4.2.5 Mechanisms contributing to the rainstorm..... 63

4.2.6 Summary and concluding remarks for rainstorm case 3.. 65

4.3 Study of rainstorm case 4 (June 27-29)..... 65

4.3.1 Brief review of the case..... 65

4.3.2 Organization and evolution of precipitation..... 66

4.3.3 Overview of the synoptic flow pattern..... 66

4.3.4 Moisture condition..... 67

4.3.5 Mechanisms contributing to the rainstorm..... 68

4.3.6 Summary and concluding remarks for rainstorm case 4.. 69

Chapter 5: Comparison of the four rainstorms..... 70

5.1 Introduction..... 70

5.2 Comparison of the surface weather systems..... 70

5.3 Comparison of the upper air circulations..... 70

5.4 Water vapor supply for the four rainstorms..... 72

5.5 Contributions of PVA and PTA..... 73

5.6 Contribution of thermodynamics..... 73

Chapter 6: Summary and Conclusions..... 75

6.1 Summary of the cases and the research project..... 75

6.2 Conclusions..... 76

6.2.1 Flow environment..... 76

6.2.2 Dynamics, thermodynamics and physical mechanisms.. 77

6.2.3 Water vapor supply..... 78

6.3 Comments and suggestions for future work..... 79

Tables..... 81
Figures..... 86
References..... 132

List of Tables

		Page
1-1	Rainstorms with rainfall of 200 mm or more during their life time in southern Alberta for the period 1921 to 2006	81
2-1	Summary of the four rainstorms during the June 2005 Alberta flood	82
2-2	Summary of the record high stream flow during the June 2005 Alberta flood	83
3-1	Relation of vorticity advection, temperature advection and vertical wind shear to measured mean rain rate of extreme rainstorm case 2	84
3-2	Updrafts contributing to extreme rainstorm case 2	84
5-1	Summary of the meteorological parameters of the four rainstorms during the June 2005 Alberta flood	85

List of Figures

		Page
1-1	Precipitation accumulation of the four rainstorms during the June 2005 Alberta flood	86
1-2	Major Alberta river basins	87
2-1	Geometric illustration of orographic forcing	87
2-2	Digital Alberta terrain elevation	88
2-3	Central affected area of the June 2005 Alberta flood	88
2-4	Maximum 24-hour rainfall distribution of the four rainstorms during the June 2005 Alberta flood	89
2-5	Precipitation anomaly of June 2005 in Alberta	90
3-1	24-hour precipitation distribution of rainstorm case 2	91
3-2	Evolution of composite CAPPI radar echoes of rainstorm case 2	92
3-3	Snapshot composite CAPPI image of rainstorm case 2 at 1950 UTC 6 June 2005	95
3-4	(a) Correlation of the estimated radar rain rate (at synoptic hour) to the observed rain rate during 5-9 June 2005; (b) Ratio of the estimated radar rainfall accumulation to the observed rainfall accumulation	95
3-5	Sequence of visible and infrared GOES satellite images of rainstorm case 2	96
3-6	Sequence of surface analysis during 6-8 June 2005	98
3-7	Sequence of 250-hPa analysis during 6-8 June 2005	99
3-8	Sequence of 500-hPa analysis during 6-8 June 2005	100
3-9	Sequence of 700-hPa analysis during 6-8 June 2005	101
3-10	Sequence of 850-hPa analysis during 6-8 June 2005	102
3-11	Superimposition of the synoptic circulations at typical levels at 1200 UTC 6-7 June 2005	103
3-12	Distribution of specific humidity at 850 hPa during 5-8 June 2005	104
3-13	Reanalysis 850-hPa geopotential height, wind field, specific humidity and observed 6h rainfall during 6-7 June 2005	105

3-14 Evolution of precipitable water and vapor mixing ratio at Stony Plain (Alberta) and Great Falls (Montana), along with space-averaged 6h rainfall in southern Alberta during 5-9 June 2005..... 106
3-15 Sequence of absolute vorticity advection at 500 hPa during 6-8 June 2005..... 107
3-16 Sequence of temperature advection at 850 hPa during 6-7 June 2005..... 107
3-17 Sequence of hodographs of Stony Plain, Alberta during 5-8 June 2005.. 108
3-18 Time series of horizontal vapor flux, estimated orographic rainfall rate and rain gauge measured rainfall rate for Sundre, Calgary, and Lethbridge during 5-9 June 2005..... 109
3-19 (a) Accumulated observed rainfall and, (b) Accumulated estimated orographic rainfall of 3 locations during 5-9 June 2005..... 110
3-20 Time series of sounding parameters and precipitation during 5-9 June 2005. (a) Tropopause height and space-averaged 6h rainfall; (b) Ambient lapse rate; (c) CAPE and space-averaged 6h rainfall..... 111
4-1 24-hour precipitation distribution of rainstorm case 1..... 112
4-2I Evolution of composite CAPPI radar echoes of rainstorm case 1..... 113
4-2II Evolution of the zoom-in CAPPI radar echoes over southwestern Alberta during the early hours on 5 June 2005..... 115
4-3 Superimposition of the synoptic circulations at typical levels at 0000 UTC 2-3 June 2005..... 116
4-4 Distribution of specific humidity at 850 hPa during 1-4 June 2005..... 117
4-5 Time series of dynamic and thermodynamic parameters and precipitation during 1-5 June 2005. (a) Vorticity advection, temperature advection and time-space-averaged rainfall rate; (b) Precipitable water, tropopause height and space-averaged 6h rainfall; (c) Ambient lapse rate; (d) CAPE and space-averaged 6h rainfall..... 118
4-6 24-hour precipitation distribution of rainstorm case 3..... 118
4-7I Evolution of composite CAPPI radar echoes of rainstorm case 3..... 119
4-7II Evolution of the zoom-in CAPPI radar echoes over southeastern

	Alberta from 2100 UTC 17 June to 0230 UTC 18 June 2005.....	121
4-8	Superimposition of the synoptic circulations at typical levels at 0000 UTC 17-18 June 2005.....	122
4-9	Distribution of specific humidity at 850 hPa during 17-19 June 2005....	123
4-10	Time series of dynamic and thermodynamic parameters and precipitation during 16-19 June 2005. (a) Vorticity advection, temperature advection and time-space-averaged rainfall rate; (b) Precipitable water, tropopause height and space-averaged 6h rainfall; (c) Ambient lapse rate; (d) CAPE and space-averaged 6h rainfall.....	124
4-11	24-hour precipitation distribution of rainstorm case 4.....	124
4-12	Composite CAPPI radar echoes on 28 June 2005, with topographic background.....	125
4-13	Superimposition of the synoptic circulations at typical levels at 1200 UTC 27-28 June 2005.....	126
4-14	Distribution of specific humidity at 850 hPa during 27-29 June 2005....	127
4-15	Time series of dynamic and thermodynamic parameters and precipitation during 26-29 June 2005. (a) Vorticity advection, temperature advection and time-space-averaged rainfall rate; (b) Precipitable water, tropopause height and space-averaged 6h rainfall; (c) Ambient lapse rate; (d) CAPE and space-averaged 6h rainfall.....	128
5-1	Characterized sea-level synoptic flow patterns of the four rainstorms....	128
5-2	Evolution of the 500-hPa lows of the four rainstorms.....	129
5-3	Evolution of vorticity advection, temperature advection and time-space-averaged rainfall rate of the four rainstorms.....	130
5-4	Time series of sounding parameters and precipitation of June 2005. (a) Precipitable water and space-averaged 6h rainfall; (b) Ambient lapse rate; (c) CAPE and space-averaged 6h rainfall.....	131

Chapter 1: Introduction

1.1 Brief introduction to the June 2005 Alberta flood

In June 2005, extensive rainfall caused severe flooding in Alberta. A total of 16 Albertan municipalities declared states of emergency due to widespread river flooding. Thousands of people were forced to leave their homes. Hundreds of houses were damaged and many farms were flooded. The damage was estimated to be about $400 million in total. Four people died during the flood. This devastating flood was described as a "one-in-200-year event" (2005 Global Register of Major Flood Events - 2005 Flood Archive, http://www.dartmouth.edu/~floods/Archives/2005sum.htm). The flood in June 2005 is regarded as the worst flood for Alberta in history. Environment Canada declared the June 2005 Alberta flood as the "Number One Weather Event" of the year, because of its impact on the public.

A flash flood is defined as a short-term, localized, and often unexpected rise in river or stream level, causing flooding. It usually occurs in response to torrential rain falling over a small geographical area (Moran 2002, p261). A family of four consecutive major rainstorms passed over Alberta in June 2005 and produced extraordinary rainfall amounts for the southern half of the province. The first storm contributed 50 to 140 mm of rain to an area centered over Cardston (49.16°N 113.26°W) in the Oldman River basin (Fig. 1-1a, 1-2), saturating the basins in the southern regions and providing pre-existing conditions for the later floods. The second storm had rainfall amounts of 50 to 248 mm (Fig. 1-1b, 1-2). Heavy rainfall was centered near Pekisko (50.37°N 114.42°W) in the Highwood River basin of the lower Bow River basin, bringing in the first widespread flood. The third storm added 50 to 152 mm of rain to the foothills centered near Sundre (51.97°N 114.45°W) in the Red Deer River basin (Fig. 1-1c, 1-2), producing the second extensive flood. The fourth rainstorm contributed another 50 to 90 mm of rain into southern and central Alberta with its maximum located near Highwood (50.55°N 114.37°W) in the lower Bow River basin (Fig. 1-1d, 1-2). A secondary centre was evident between the North Saskatchewan River basin and the southern Athabasca River

basin. Although the fourth storm did not cause a major flood, it re-struck the areas that had suffered the first and second severe floods, and impeded the disaster clean-up and assistance.

The precipitation that fell during the episodes of the four major rainstorms in Alberta in June 2005 was much higher than normal as evidenced by the rainfall climatology. For example, the recorded monthly rainfall in the lower Bow River basin was approximately 6 times the precipitation for the month of June in a normal year, which was more than half the normal annual precipitation.

Consideration of these four consecutive rainfall events suggests that something interesting and unusual had occurred. Some obvious questions need to be addressed: Where did this huge amount of rain originate from? How can the precipitation dropped (locally) in a month be more than half the normal annual precipitation? Why did successive rainstorms occur in such a short time span? Does the forecaster have any information about the likely recurrence interval of consecutive major rainstorms? Is it possible to predict the likely recurrence of consecutive rainstorms well in advance? And in a practical sense, is it possible to improve the forecasting of flooding events in Alberta, with a lead-time sufficiently long to allow for necessary action to prevent the loss of life and catastrophic damage to property?

1.2 Research objectives

The occurrence of a flash flood is affected by antecedent conditions such as soil moisture content, pre-occurring precipitation, the size and topography of the drainage basin, snow melt runoff and peak river discharge. Therefore, a flash flood is the concatenation of a meteorological event with a particular hydrological circumstance (Doswell III et al. 1996).

The major objective of my thesis research is to document the June 2005 Alberta flood with a focus on meteorological developments rather than hydrological processes. Specifically, I will investigate the presence of the typical "ingredients" that are usually

associated with the flood-producing storms. I analyze the synoptic scale airflow and the mesoscale features of the four previously mentioned rainstorms. Particular emphasis will be given to the organization of the precipitation pattern, and orographic effects. Specifically, I will address the following two questions:

1. What are the main mechanisms that contributed to the extreme rainfall which caused severe flooding in southern Alberta on 5-9 June 2005?
2. What are the similarities and differences of the meteorological conditions for the development of the four Alberta rainstorms during June 2005?

To discuss the significance of the above questions, some background is reviewed in the following sections.

1.3 Background on heavy precipitation events

1.3.1 Synoptic features

Heavy precipitation requires the presence of a favorable environment of synoptic and mesoscale forcing that can maintain a sustained high rainfall rate (Doswell III et al. 1996). Heavy rainfall events in Alberta are usually associated with a well-developed surface cyclone (or lee cyclogenesis) coupled with the passage of a cutoff cold low (or a deep short wave trough) aloft (Hage 1957, Burrows 1966, Verschuren and Wojtiw 1980, Nguyen 1987, Reuter and Nguyen 1993, Lin et al. 2001). An upstream cyclonic vorticity maximum (or vortex) and overhead positive vorticity advection (PVA) at 500 hPa accentuates a favorable synoptic pattern for significant widespread precipitation (Lin et al. 2001). Diffluent flow in the upper troposphere often links to surface lee cyclone development or intensification that is in conjunction with heavy precipitation (Petterssen 1956, Chung and Reinelt 1973, Kocin and Uccellini 1990). The transport of humidity is often found in the moist warm conveyor belt or the low level jet (LLJ) from distant sources. The combination of the above conditions provides strong lower-level convergence and the consequent strong updraft for incoming moist airstreams to develop heavy precipitation. This project will document the synoptic settings at mandatory pressure levels and their superposition during the four heavy rainfall events.

1.3.2 Organization of precipitation

The spatial organization of rain is often categorized into three types based on the synoptic system background: air-mass precipitation, frontal precipitation and cyclonic (storm) precipitation. It is also divided into two types based on the intensity and duration: steady precipitation (or stratiform precipitation), which lasts longer with lesser intensity variation; and showery precipitation (or convective precipitation), which lasts shorter with larger intensity variation. This project will document the precipitation pattern of the four rainstorms based on analyses of the synoptic features, radar images, geo-stationary satellite images, and the available surface precipitation observations.

1.3.3 Orographic effects

Orography plays an important role in the atmospheric circulation as mountainous terrain intensifies cyclonic weather systems on all scales of atmospheric motion (Chung et al. 1976, Lin et al. 2001). The orography of Alberta has a significant influence on the weather of the province. It provides some preferred regions of convective development caused by differential slope heating, orographically forced convergence and thermally driven upslope winds (Smith and Yau 1987, Reuter and Nguyen 1993).

There are two major precipitation enhancement processes due to orographic influences: lee cyclogenesis and orographic lifting. Lee cyclogenesis is defined as synoptic-scale development of an atmospheric cyclonic circulation on the downwind side of a mountain range. Orographic lifting is defined as ascending airflow caused by rising mountainous terrain (Moran 2002). Both these dynamic processes contribute to the convergence of the moisture-bearing airflow, resulting in upward motion for precipitation development. This project will examine the reinforcement of precipitation due to lee cyclogenesis and mechanical orographic lifting during the June 5-9 extreme rainfall event.

1.3.4 Convective overturning

For heavy convective rainfall, convective instability is required. Convective instability provides energy released by latent heat due to cloud condensation. The thermal energy is then converted into kinetic energy for vertical motion for precipitation formation. I will analyze the vertical profiles of temperature, humidity and wind using a tephigram and a hodograph. The tephigram analysis will reveal the amount of convective available potential energy (CAPE), the precipitable water (PW), the vapor mixing ratio (VMR), the capping lid characteristics, and the level of free convection (LFC). The hodograph will show the magnitude of vertical wind shear. These quantities will be interrelated to the observed rainfall rates of the four heavy rainfall events.

1.3.5 Atmospheric moisture

Moisture supply is a crucial basic ingredient for a flashflood-producing rainstorm (Lin et al. 2001). Without a large amount of moisture, synoptic systems, orographic effects and conditional instability alone can not produce long-lasting, widespread and heavy precipitation for Alberta. Previous water vapor transportation studies suggest that some of the water vapor supplied for Alberta's summer rainstorms might have originated from the Gulf of Mexico, and been carried northwards in a LLJ stream (Brimelow and Reuter 2005). However, there are other possible sources of atmospheric moisture such as the Eastern Pacific Ocean and the Hudson Bay (Liu and Stewart 2003). Furthermore, local supply of moisture exists in the form of evapotranspiration from soil, agricultural fields and small water bodies (Szeto 2002). The synoptic scale moisture distribution at the cloud base level and water vapor advection (i.e. transportation) fields of the four heavy rainfall events will be examined in this study.

1.4 Climatology of extreme rainfall events in Alberta

Verschuren and Wojtiw (1980) compiled a climatology of Alberta rainfall events that had local rainfall accumulations exceeding 50 mm. Their data covered the period

from 1921 to 1978. From this inventory of cases Reuter (2000) selected all storms that produced accumulated rainfall amounts exceeding 150 mm during their lifetime. These extreme events had the following characteristics:

1) Storms with 150+ mm rainfall are rather rare in Alberta. During the 58 years, 27 cases occurred.
2) Storms with 150+ mm rainfall occurred primarily during spring and summer. The monthly occurrences were: June (12), August (7), July (5), April (2) and May (1). During the 58 years, no cases occurred during the seven month period from September to March.
3) Storms with 150+ mm rainfall typically lasted from 3 to 5 days. Only one storm lasted for 2 days.

It is interesting to note that between April 1921 and May 2005, Alberta never had two storms with rainfall amounts exceeding 150 mm within the same month. June 2005 was the first month on record when two 150+ mm storms occurred.

Historical rainstorms in southern Alberta with rainfall of 200 mm or more during their life time were recorded only 6 times since 1921. These rainstorms are summarized in Table 1-1. Four out of the six extreme events occurred in the foothills. The Oldman River and the Bow River basins were likely the regions that have higher frequency of extreme rainfall events. Waterton Lakes Red Rock and Pekisko likely had the highest frequency of being hit by rainstorms with rainfall in excess of 200 mm. The rainstorm during 5-9 June 2005 ranks the fourth in terms of its peak event rainfall.

Warner (1973) analyzed in detail the weather system that caused the flood of 7-8 June 1964 in the Oldman River and Milk River basins. The severe rainstorm was a cross-border flood event that covered the eastern slope of the Rocky Mountains in southwestern Alberta, Canada and northwest Montana, United States (U.S.). The central affected area in Alberta was near Waterton Lakes Red Rock in the Oldman River basin. The flood was primarily attributed to an extreme rainfall of 252 mm. The flood was also affected by pre-existing saturated moisture condition due to above normal precipitation

in May and below normal temperature during late spring that delayed the usual peak snowmelt-runoff into early June. The meteorological contributions to this event included that lee cyclogenesis caused upslope flow, vorticity advection aloft sustained the ascending motion, and strong southerly low-level wind channeled moisture from far south (Warner 1973).

Similar synoptic conditions were identified during the 17-20 June 1975 rainstorm (356 mm) that caused flooding in the Oldman River basin (Phinney 1982). Reuter and Nguyen (1993) investigated the 17 July 1986 rainstorm (104.5 mm in 24 hours) that caused wide-spread flooding along the North Saskatchewan, the Red Deer and the Athabasca Rivers. Again, lee cyclogenesis deepened the upper cold low when the systems crossed the Rocky Mountain range.

Another intense rainstorm on 6-7 June 1995 caused extensive flooding affecting mainly the Oldman River basin. Peak event rainfall of 310 mm was recorded at Spionkop Creek, located just north of Waterton Lakes Park. In addition to the heavy rainfall, the June 1995 flood was affected by the peak mountain snowmelt runoff (Alberta Environment 1995, Browne 1996).

Brimelow and Reuter (2005) analyzed the atmospheric moisture transport for three Alberta extreme rainfall events in central Alberta: 22-23 June 1993, 18-19 June 1996, and 28-29 July 2001. For all three cases, the parcel trajectories were identified as originating near the Gulf of Mexico (GOM). The time required to complete the journey varied between 6 and 10 days. The transport of GOM moisture to Alberta was realized when northward extension of the Great Plains low level jet to the Dakotas occurred in synchrony with rapid cyclogenesis over Alberta. In this way, low-level moisture from the GOM arrived over the northern Great Plains at the same time as strong southerly flow developed over the Dakotas and Saskatchewan, in advance of the deepening cutoff low over Alberta. The moist air was then transported over Saskatchewan and finally westwards over the Athabasca River basin, where heavy rainfall occurred.

1.5 Outline of content of thesis

This thesis consists of 6 chapters. Chapter 1 provides some background of the thesis problem and motivation for investigation. In Chapter 2 I present the theory of precipitation production based on water flux balance at the cloud base level. I also summarize the theory of orographic lifting and synoptic-scale dynamics. After introducing the observational data sets being used, I provide an overview of the four June 2005 Alberta heavy rainfall cases.

In Chapter 3, a detailed analysis is given for the June 5-9 extreme rainfall event. I first discuss the evolution of the precipitation making use of radar and satellite observations, and then describe the synoptic flow environment, dynamics, thermodynamics, physical mechanisms, and mechanical orographic forcing that contributed to the heavy rainfall.

In Chapter 4, studies on the other 3 heavy rainfall cases are carried out to discuss their synoptic flow patterns, dynamics, thermodynamics, as well as the physical mechanisms which caused the heavy rainfall. In Chapter 5, a comparison of the synoptic settings and the associated dynamics and thermodynamics of the four rainstorms is carried out. Finally, in Chapter 6, a summary and a conclusion on the discussions and findings are presented.

Chapter 2: Theory and overview of the flood events

2.1 Theory relevant for precipitation production

2.1.1 Water flux balance at cloud base

The theory of precipitation production is based on the conservation of water mass. This conservation law states that the total mass of water is constant even when vapor is condensed in clouds. For long-lasting precipitating systems, the upward flux of water in the form of vapor is balanced by the downward flux of water in the form of rain or snow. Let us examine this balance of fluxes at the cloud base of a nimbus cloud by considering a unit horizontal cross-section of a vertical air column. The fact that the air may be rising along a gentle slope rather than vertically up in the column is irrelevant as on average, there is no net horizontal divergence of the water flux as a result.

Suppose that a moisture-bearing air parcel rises at the cloud base level with upward velocity or updraft w (m s^{-1}) and vapor content Q (g m^{-3}). Then the upward flux of water vapor is given by the product wQ (g m^{-2} s^{-1}). The downward flux of rain is given by the product of rainfall rate r (m s^{-1}) and the density of the rain water q_r (g m^{-3}). Equating these two fluxes result in

$$rq_r = wQ \qquad (2.1)$$

Noting that $q_r = 10^6$ g m^{-3}, re-arranging *(2.1)* and expressing rainfall rate in its usual units of mm h^{-1} (instead of m s^{-1}) we have

$$r = 3.6wQ \qquad (2.2)$$

where r is in mm h^{-1}, w is in m s^{-1} and Q is in g m^{-3}.

How accurate is the water flux balance equation *(2.2)* assuming that one has accurate values for w and Q? Reuter and Xin (1998) found that equation *(2.2)* provides a good estimate of rainfall rate of nimbostratus clouds for typical Alberta summer conditions. However, for short-lived convective type rain showers, *(2.2)* tends to be an

overestimate. The presence of evaporative loss of liquid water from the sides of the cumulonimbus and the flux of ice crystals into the cloud anvil suggests that the upward flux of vapor at the cloud base should exceed the downward flux of precipitation. Therefore *(2.2)* can be improved by writing

$$r = 3.6wQE \qquad (2.3)$$

where E is the precipitation efficiency, which is defined as the ratio of the mass of water falling as precipitation to the mass of water vapor ascending at the cloud base (Doswell III et al. 1996). The precipitation efficiency depends mainly on the size of the storm, the magnitude of the vertical wind shear, and the dryness of the upper air (Cotton and Anthes 1989, Doswell III et al. 1996, Lin et al. 2001). A precipitation efficiency of 80% - 90% is typical for Alberta summer convective storms (Reuter 1990).

From *(2.3)* we identify the two basic "ingredients" needed for heavy rainfall: strong ascending motion (w) at the cloud base level, and high vapor content (Q). Q values range from about 5 g m^{-3} to 15 g m^{-3} at the cloud base. In precipitating clouds, w ranges from about 0.01 m s^{-1} to 5 m s^{-1} at the cloud base (Djurić 1994). The greater range of updraft at the cloud base shows that the instantaneous rainfall rate is primarily determined by the magnitude of updraft. *(2.3)* shows that r is proportional to w with a proportionality constant depending on the vapor content.

The accumulated rainfall (R) from time 0 to time t at a point (x,y) is given by time integration of the instantaneous rainfall rate r at (x,y) such that

$$R(s) = \int_0^t r(s)ds \qquad (2.4a)$$

where s denotes the integration variable. For simplicity, R at a location (x,y) is

$$R(t) = \bar{r}\, t \qquad (2.4b)$$

where $\bar{r}$ denotes the average rainfall rate at (x,y) for a duration t. Thus, heavy rainfall arises from the product of high rainfall rate and long duration.

2.1.2 *Mechanical lifting due to sloping terrain*

Consider a slab mountain range in an *(x,y,z)* coordinate system such that, *x* points perpendicular to the mountain range, *y* points parallel to the mountain range, and *z* points vertically upward. The velocity vector has components denoted by *(u,v,w)*. Component *v* vanishes by selecting *y* coordinate to be parallel to the mountain range (see Fig. 2-1). Assuming the airflow to be freely terrain following, the vertical velocity (w_o) near the earth's surface forced by orographic lifting is given by

$$w_o = u(\Delta z / \Delta x) \qquad (2.5)$$

where u is the wind component perpendicular to the mountain slope, Δz is the increment of the terrain, Δx is the horizontal extent perpendicular to the slope, and the slope of the terrain is given by $\Delta z/\Delta x$. Equation *(2.5)* gives a good estimate of the component of the vertical velocity (at the cloud base) that is caused by the mechanical orographic forcing. Of course, there are other forcing mechanisms contributing to the vertical velocity at the cloud base, but it is convenient to consider each individual contributing factor separately. For an incident horizontal wind V with direction α, w_o is given by

$$w_o = V\cos(\alpha - \beta)\,(\Delta z / \Delta x) \qquad (2.6)$$

where β is the orientation of the terrain slope. Equation *(2.6)* shows that the vertical component (w_o) of the terrain-following flow depends on the horizontal wind speed and its direction relative to the sloping terrain.

2.1.3 *Synoptic forcing of ascending air motion*

A favourable synoptic flow environment is required to provide strong dynamic support for incoming moist airstreams that can be continuously uplifted to the condensation level and develop heavy precipitation. The analysis of synoptic circulations at mandatory pressure levels of the troposphere allows us to look into the airflow background of the dynamics contributing to a heavy precipitation event.

a) 300-hPa or 250-hPa features

In addition to waves, troughs and ridges, diffluence, confluence and jet streams are the characteristics of the flow pattern in the upper troposphere. Diffluence (confluence) is defined as a lateral divergence (convergence) of the 300-hPa (or 250-hPa) geopotential contours. The jet stream is defined as the elongated zone of high wind velocities exceeding about 30 m s^{-1} (or 60 knots). Previous studies suggest that diffluence is a signature of increasing upper-level divergence downstream of a trough axis (Bjerknes 1954, Palmén and Newton 1969, Kocin and Uccellini 1990). Further, diffluence in the left flank of the exit region of a jet stream in the upper troposphere enhances the upper-level divergence (Bjerknes 1951, Petterssen 1956, Kocin and Uccellini 1990). Divergence in the upper troposphere implies a contribution towards a net reduction of column air mass per unit area which must be replaced by ascending air from lower levels where convergence occurs in response to the vertical motion (Petterssen 1956). The magnitude of convergence is also a measurement of the change of vorticity that is an indication of the development or intensification of cyclonic circulation, namely cyclogenesis. Based on conservation of mass, the continuity equation for an incompressible fluid is given by

$$\frac{\partial w}{\partial z} = -\left(\frac{\partial u}{\partial x} + \frac{\partial v}{\partial y}\right) \qquad (2.7)$$

where u, v are the horizontal wind components, and w is the vertical velocity in the (x,y,z) coordinate system. Equation *(2.7)* states that the change of vertical velocity with height is the result of horizontal convergence. The simplified vertical vorticity equation in the absence of twisting and solenoidal effects is given by

$$\frac{1}{\zeta}\frac{d\zeta}{dt} = -\left(\frac{\partial u}{\partial x} + \frac{\partial v}{\partial y}\right) \qquad (2.8)$$

where ζ is the vertical component of absolute vorticity, and $d\zeta/dt$ is the rate of change of absolute vorticity of an air parcel (see Equ. 4.22b in Holton 2004). Thus, equation *(2.8)* shows that divergence aloft (or low-level convergence) contributes to the change of vertical absolute vorticity (ζ) at the lower levels, which is in connection with the vertical velocity indicated by equation *(2.7)*.

b) 500-hPa features

Waves, lows and troughs near the 500-hPa level provide significant forcing for the mid-level upward motion and the associated formation of cloud and precipitation (Petterssen 1956, Djurić 1994). An upstream cutoff vortex (or a cold core low) and PVA downstream of the vortex at 500 hPa has long been recognized to be a characteristic flow pattern that contributes to cyclonic development or intensification in the lower troposphere during a long-lasting heavy precipitation event in Alberta (e.g. Hage 1957, Chung and Reinelt 1973, Nguyen 1987). A trough line is another feature of upper airflow pattern providing dynamical support for heavy precipitation. The trough line is defined as a line of maximum curvature of isopleths (of geopotential height or pressure) such that the isopleths bend cyclonically around the lower values of the scalar associated with the isopleths. The geostrophic wind approximation indicates that wind blows parallel to the geopotential contours. Thus, a trough line is also a zone of maximum horizontal cyclonic wind shear. As the vertical vorticity is the curl of the horizontal wind vector (see Equ. (4-3) in Djurić 1994), a zone of horizontal cyclonic wind shear is an indication of existence of positive vertical vorticity, which is in conjunction with horizontal convergence and its ultimate product – the upward motion (see Equ. *(2.7)* and *(2.8)*).

Thickness, related to the mean temperature between two selected isobaric surfaces, is a convenient tool for describing the thermal structure of the atmosphere (see Equ. (6-1) and C-6 in Djurić 1994). The intersection of the contours of 500-hPa geopotential height and the 500-1000 hPa thickness is an indication of the existence of atmospheric baroclinicity. A lagged behind thickness ridge (where the thicknesses intersect the geopotential heights) suggests that there exists a zone of baroclinic instability which is favorable for cyclogenesis at the lower level and occlusion at the surface (Petterssen 1956, Bluestein 1986, Djurić 1994, Holton 2004).

c) 700-hPa features

The geopotential height at 700 hPa is about 3 km above sea level (ASL), and the elevation of the Alberta Rocky Mountains is in the 2-3 km ASL range. Analysis of the

patterns of the 700-hPa height contours and isotherms allows for an assessment of temperature (or thickness) advection with less influence of the underling surface. In absence of other vertical forcing, ascending motion is associated with warm air advection (WAA), while cold air advection (CAA) is associated with descending motion. Furthermore, at a given tropospheric layer, WAA at its base destabilizes the layer by decreasing the temperature lapse rate, whereas CAA at its base stabilizes the layer by increasing the temperature lapse rate. The effect of CAA is indicative for the occurrence of adiabatic drying subsidence in the layer. The sinking motion of the air tends to amplify the mid-level downstream wave or trough and converts geopotential energy to kinetic energy which eventually contributes to the updraft that is required for the development of cyclonic circulation and precipitation (Holton 2004). The main influence of temperature advection is to increase vorticity in the region of WAA, while decreasing vorticity in the region of CAA (Petterssen 1956).

d) 850-hPa features

In mid-latitudes the observed cloud base of nimbus is usually located close to the 850-hPa level. The wind field and temperature distribution at 850 hPa provide valuable information on temperature advection and the associated thermal forcing on upward motion for precipitation development in Alberta. The 850-hPa updraft caused by WAA quantifies the contribution of thermal advection to precipitation. We can estimate the 850-hPa updraft with the adiabatic method which is based on the thermodynamic energy equation such that

$$c_p \frac{DT}{Dt} - \frac{1}{\rho}\frac{Dp}{Dt} = J \qquad (2.9)$$

where c_p is the specific heat of dry air at constant pressure, T is the temperature, ρ is the moist air density, p is the pressure, J is the diabatic heating rate, DT/Dt and Dp/Dt are the rates of change of temperature and pressure following a fluid element, respectively. By letting $Dp/Dt = \omega$ (vertical velocity in isobaric coordinates), and expanding DT/Dt in isobaric coordinates, *(2.9)* can be rewritten as

$$\frac{\partial T}{\partial t} + V \cdot \nabla_p T - S_p \omega = \frac{J}{c_p} \qquad (2.10)$$

where V is the horizontal wind velocity, ∇_p is the horizontal del operator in isobaric coordinates, $\nabla_p T$ is the horizontal temperature gradient such that $V \cdot \nabla_p T$ gives the thermal advection, and S_p is the stability parameter in isobaric coordinates. With the aid of the equation of state ($p = \rho R_d T$) and the hydrostatic equation ($\partial p / \partial z = -\rho g$), S_p has the form

$$S_p = \frac{R_d T}{c_p p} - \frac{\partial T}{\partial p} = (\Gamma_d - \Gamma) / \rho g$$

where R_d is the specific gas constant for dry air (≈287 J $kg^{-1}K^{-1}$), Γ_d is the dry adiabatic lapse rate ($\Gamma_d = -\partial T / \partial z = g / c_p$), Γ is the ambient lapse rate ($\Gamma = -\partial T / \partial z$), and g is the acceleration due to gravity. By neglecting the diabatic heating and local rate of change of temperature, re-organizing *(2.10)* yields

$$\omega = S_p^{-1} V \cdot \nabla_p T \qquad (2.11)$$

With the aid of the hydrostatic approximation ($\omega = -\rho g w$), the updraft w in z coordinates can be estimated as follows

$$w = -(\Gamma_d - \Gamma)^{-1} V \cdot \nabla_p T \qquad (2.12)$$

Thus, substituting *(2.12)* into *(2.3)* yields a rainfall rate contributed by thermal advection.

The location of the low pressure centres, trough lines, and ridge lines at 850 hPa provides valuable information for analyzing the low-level synoptic flow regime affecting precipitation production. Special attention is usually given to the cyclonic sheared wind field as it is an indication of occurrence and region of convergence and vertical vorticity. Much attention is often paid to the narrow band of concentrated largest temperature gradients as it is an indication of existence of baroclinic zone or thermal front (Holton 2004). Intersections between contours (streamlines of geostrophic wind) and isotherms suggest that there exists thermal advection (Djurić 1994). Analysis of the 850-hPa synoptic pattern provides a better understanding of the lower tropospheric flow characteristics and the contribution of WAA toward precipitation.

2.1.4 Orographic effects

The influence of mountain topography on precipitation is well documented. The range of the Rocky Mountains, extending some 2400 km from Yukon to Texas is an impressive north-south mountain barrier that has a major impact on the local weather of North America. The impact is particularly evident in Alberta, whose boundaries extend from 49°N to 60°N and 120°W to 110°W, with the southwestern border following the Continental Divide (Fig. 2-2). The impact of Alberta orography on the spatial distribution of precipitation was documented by McKay (1965), Reinelt (1970), and Thompson (1976).

The orographic influence on Alberta's weather ranges from microscale to synoptic scale. During the summer, the impact on the mesoscale convective development over some preferred regions owes to differential slope heating, thermally driven upslope winds and topographically forced convergence (Smith and Yau 1987). The orographic influence on synoptic-scale precipitation patterns mainly occurs in two ways: lee cyclogenesis and orographic lifting. Lee cyclogenesis dynamically enhances the self-development of the precipitating system, and in turn reinforces the precipitation. Orographic lifting mechanically superimposes the updraft that is supported by the atmospheric dynamics and thermodynamics, and reinforces the precipitation over the rising terrain. Lee cyclogenesis and orographic lifting in summer often result in quasi-steady rainfall causing extensive river flooding (Reinelt 1970, Chung et al. 1976, Reuter and Nguyen 1993, Lin et al. 2001, and Pan et al. 2004).

The topography in central and southern Alberta consists of three regions: the mountain region, the foothills region, and the plains region. The mountain region has an elevation of 2-3 km ASL, the foothills region has an elevation of 1-2 km ASL, and the plains region has an elevation of 0.6-1 km ASL (Fig. 2-2). The lowering terrain from west to east allows vertical stretching of the cross-barrier flow in the lee of the Rocky Mountains, and that often leads to lee cyclogenesis (Chung et al. 1976, Lin et al. 2001). Lee cyclogenesis occurs in association with a pre-existing synoptic-scale trough or

cyclone (namely the "parent low") that interacts with the orography (Tibaldi et al. 1990). Lee cyclogenesis largely owes to orographic impacts on the increase of vertical cyclonic vorticity (Petterssen 1956, Pierrehumbert 1986, Holton 2004), as the local rate of change of vorticity is affected by the stretching (or shrinking) of the fluid columns due to divergence (or convergence). The downslope orography leads to vertical vortex stretching of the air columns that cross the cordillera onto the lee slope (Chung et al. 1976, Pierrehumbert 1986). As indicated in equations *(2.8)* and *(2.7)*, cyclogenesis (i.e. increase of vertical vorticity) is in connection with horizontal convergence and its associated updraft. Therefore, downslope vortex stretching ultimately enhances the lee slope updraft and the consequent precipitation.

2.1.5 Vertical wind shear

Vertical wind shear (*SHEAR*) quantifies the change of wind velocity with height. For a layer from height z_1 to height z_2, the shear vector is given by

$$SHEAR = \frac{\vec{V}_2 - \vec{V}_1}{z_2 - z_1} \qquad (2.13)$$

where $\vec{V}_1$ and $\vec{V}_2$ are the horizontal wind vectors at heights z_1 and z_2, respectively. As *SHEAR* is a vector quantity, it consists of both speed shear and directional shear. A local storm developing in a sheared environment tends to have a tilting storm updraft leaning in the direction of *SHEAR*. The slanted updraft and downdraft (strengthened by water loading, i.e. precipitation) are formed on the upshear and downshear flank of the storm, respectively. In a sheared environment, the water loading occurs mainly on the downshear side of the storm, thus the downdraft will not cut-off the updraft and the updraft remains almost undisturbed. Directional shear in the lower troposphere helps to initiate a rotating updraft for development of a mesocyclone (Bleckman 1981). Based on the thermal wind theory, thermal wind is the vertical shear of the geostrophic wind (Djurić 1994), and it is directed along isotherms with warm air to the right and cold air to the left (in the Northern Hemisphere). Thus directional shear dynamically reflects thermal advection: WAA is associated with anticyclonic wind shear (i.e. veering), while CAA is associated with cyclonic wind shear (i.e. backing). The analysis of vertical wind

shear helps to understand the sheared wind environment and vertical profile of the thermal advection that are favorable for heavy precipitation over a specific location.

2.1.6 Convective instability

Considering a (thin) layer of moist air extending from height z_1 to z_2, temperature lapse rate Γ quantifies the decrease in temperature for a unit height difference such that

$$\Gamma = -\frac{T_2 - T_1}{z_2 - z_1} \qquad (2.14)$$

where T_1 and T_2 are the temperature values at heights z_1 and z_2, respectively. The temperature lapse rate describes the stability properties of the air layer depending on whether the air is saturated or unsaturated such that

$\Gamma < \Gamma_s$	Absolutely stable
$\Gamma = \Gamma_s$	Saturated neutral
$\Gamma_s < \Gamma < \Gamma_d$	Conditionally unstable
$\Gamma = \Gamma_d$	Dry neutral
$\Gamma > \Gamma_d$	Absolutely unstable

where Γ_s is the saturated adiabatic lapse rate, and Γ_d is the dry adiabatic lapse rate (Rogers and Yau 1989). Super adiabatic or absolutely unstable air layers do not occur for sustained periods in the free atmosphere as convective overturning will immediately release the instability. However, conditionally unstable layer occurs frequently as the air may not be saturated. Once condensation occurs, the instability is released and overturning occurs. If the amount of kinetic energy being released is significant, moist convection occurs resulting in thunderstorms.

For assessment of the likelihood of moist convection and its intensity, it is useful to quantify the energy which will be released by the convective instability. This quantity is known as CAPE which estimates the maximum possible kinetic (buoyant) energy that a hydrostatically unstable parcel can acquire by neglecting the influences of water vapor and condensed water droplets on the buoyancy (Holton 2004, p295). CAPE is evaluated on the basis of a parcel of air that is being adiabatically lifted through the atmosphere

from the LFC (level of free convection), p_{LFC}, to the equilibrium level above, p_e, such that

$$CAPE = R_d \int_{p_{LFC}}^{p_e} [T(p) - T_a(p)] \, d \ln p \qquad (2.15)$$

where R_d is the specific gas constant for dry air, $T(p)$ is the lifted parcel temperature and $T_a(p)$ is the ambient temperature, both being functions of pressure p (Djurić 1994).

2.1.7 *Precipitable water*

As discussed in section 2.1.1, the instantaneous rainfall rate depends on the water vapor content at the cloud base. Thus, the local storage, the temporal and spatial distributions, as well as the transportation of water vapor are important parameters for analyzing precipitation. Precipitable water that quantifies the local vapor storage is of particular interest in this study.

Precipitable water (PW) is defined as the total water vapor contained in a vertical column of unit cross-sectional area extending from the earth's surface to the "top" of the atmosphere such that

$$PW = \frac{1}{g} \int_{p_0}^{p_{top}} q_v(p) \, dp \qquad (2.16)$$

where q_v is the vapor mixing ratio at level p, and g is the acceleration due to gravity. The integration limits are from p_0 to p_{top}, denoting the pressures at the ground and top of the air column, respectively (Djurić 1994). Typically, $p_{top} = 150$ hPa. The resulting units of PW in *(2.16)* are $kg\ m^{-2}$. To compare PW with the accumulated rainfall amount, it is convenient to convert PW into an equivalent depth of liquid water expressed in *mm*.

Atmospheric conditions characterized by high PW values ($\geq$ 15 mm, see Taylor 1999) tend to have ample water vapor supply for conversion to precipitation. Studies carried out by Hoskins (1990) and Uccellini (1990) suggest that latent heat released during water vapor transformation to liquid water acts to amplify the anomaly of the vertical potential vorticity and acts in the sense of increasing the low-level cyclonic

circulation, which ultimately enhances the vertical motion and the consequent precipitation.

2.2 Observational data

2.2.1 Radar and satellite imageries

C-band (5 cm wavelength) weather radar is the main observational tool available for monitoring the intensity and organization of the mesoscale precipitation field. Radar-derived products are used routinely in operational weather analysis and forecasting. The principle of radar is to send packets of electromagnetic waves (with frequency of 6.0 GHz for C-band) about 1°-2° wide, horizontally and above horizon, in repetitive frequencies of about 1000 Hertz. Part of the back-scattered energy, mainly from the rain droplets, is received by the radar between the pulses, during which the delay time of the echo gives the indication of the distance to the target (Djurić 1994). Radar echo, namely the reflectivity of the precipitation particle, can be interpreted in terms of size, shape, motion, location and thermodynamic phase of the particle. On the constant altitude plan position indicator (CAPPI) imagery, the relationship of the radar reflectivity, Z, to the falling speed of the water particles, r, can be approximately expressed as

$$Z = 200\, r^{1.6} \qquad (2.17)$$

(Rogers and Yau 1989). This provides a means to estimate the evolution of the spatial distribution of the instantaneous rainfall rate (r). Integrating r over time provides an estimate of the spatial distribution of rainfall accumulation. We will employ the composite CAPPI radar images to analyze the precipitation system in our studies for the four June 2005 Alberta rainstorms.

The weather satellite records cloud patterns, where one may infer airstreams and cyclone systems (Weldon 1979, Beckman 1987, Young et al. 1987). Visible (VIS) and infrared (IR) satellite images are the two major imageries used in the operational setting. VIS imagery is taken in the visible spectrum (wavelength of 0.4-1.1 μm). The brightness of the VIS is related to the reflectivity of the detected objects (e.g. cloud droplets). The

reflectivity depends on the color, brightness, and roughness of the objects. The brightness of VIS during day time is proportional to the altitude and thickness of the cloud. The brightness of VIS is reduced during the sunrise and sunset hours due to lower solar altitude (angle). Shadows of the clouds during the sunrise and sunset hours help to distinguish the cloud layers and the boundaries. IR imagery is taken in the infrared spectrum (wavelength of 10.5-12.5 μm). IR images of wavelength 10.7 μm are used in this study. In the IR spectrum, clouds at different heights have different radiances which differ also from that of the ground level. As the radiances varying with cloud height can be expressed in temperatures, the cloud-top temperature on IR reflects the height of the cloud which is associated with the cloud type. For example, deep moist convective (cumuliform) cloud has higher cloud top with lower cloud-top temperatures whereas weak convective (stratiform) cloud has lower cloud top with higher cloud-top temperatures. The cloud-top temperatures on IR help to identify convection. With the aid of VIS and IR, the shapes, sizes, brightness, radiances (temperature), boundaries and layers of the clouds can be used to analyze the cloud formation (moist air ascent) and dissipation (dry air subsidence), cloud pattern, system structure and movement, and the associated air flow (Browning 1990, Djurić 1994). We will employ geo-stationary VIS and IR images to analyze the cloud system in the study for rainstorm case 2.

2.2.2 Synoptic weather maps

A synoptic weather map is a chart that presents a quasi-horizontal depiction of the synoptic airflow at a given time. A standard set of synoptic maps includes a sea-level surface chart and the upper-level charts at mandatory-pressure levels (e.g. 850, 700, 500, and 300 (or 250) hPa). The surface map provides information about sea-level pressure, pressure tendency, temperature, dewpoint temperature, wind observation, cloud cover, visibility and precipitation. The upper-level maps provide data commonly including wind velocity, temperature, temperature-dewpoint depression and geopotential height. Vorticity and thickness are usually included on the 500-hpa maps. We will employ weather maps to analyze the flow environment for the four June 2005 Alberta rainstorms.

2.2.3 Balloon soundings

In-situ measurements at different heights can be sampled using a radiosonde mounted on a balloon released from the ground. With the application of balloon sounding, the vertical structure and the state of the atmosphere, such as inversion, stable and unstable layers, tropopause, fronts, air masses, and humid layers, can be described by the basic quantities and the derived thermodynamic variables. The basic quantities from the sounding include temperature, relative humidity, and wind as functions of pressure. The derived thermodynamic parameters include temperature lapse rate, CAPE, PW, vertical wind shear, and helicity. Sounding data are particularly useful in assessing cloud layers and the potential for convective instability. We will employ the soundings of Great Falls (47.45°N 111.38°W), Montana and Stony Plain (53.55°N 114.11°W), Alberta in our studies for the four June 2005 Alberta rainstorms.

2.3 Overview and background on the June 2005 Alberta flood

2.3.1 Features of the four rainstorms in Alberta during June 2005

This thesis analyzes the four Alberta rainstorms that occurred on 1-5, 5-9, 16-19 and 27-29 June 2005, respectively. The last three events, roughly a week apart from each other, caused extensive flooding. Based on the impacting weather system and in order to clarify the accumulation of each event, we separated the first and the second rainstorm at 0600 UTC 5 June. The second and the third storms were the most severe ones in terms of their flooding damage. These four rainstorms in June together produced extraordinary rainfall over the central and southern Alberta foothills and created record-breaking water levels in four of the major river basins of the province. The event rainfall accumulation of each rainstorm is shown on Figure 1-1. The affected area of the June flood is illustrated on Figure 2-3. The hydrological features of the four rainstorms are summarized in Tables 2-1 and 2-2. The distribution of the maximum 24-hour rainfall accumulation of each rainstorm is displayed on Figure 2-4.

Rainstorm case 1 lasted for 96 hours from 0600 UTC 1 June to 0600 UTC 5 June. It produced a maximum precipitation accumulation of 140 mm to the area near Cardston and a maximum 24-hour rainfall of 49.5 mm on 2 June (accumulation ending at 0600 UTC) at Milk River (49.13°N 112.05°W) (Fig. 2-4a). This rainstorm produced a secondary high 24-hour rainfall accumulation of 48.1 mm on the same day at Del Bonita (49.05°N 112.82°W). The Oldman River basin was the centrally affected region, where an area of about 32,000 km^2 recorded $\geq$ 50 mm of rain (Fig. 1-1a, 1-2). In response to the heavy rainfall, the below seasonal normal water level of the streams in the Bow River and Oldman River basins rose to normal or slightly above normal. This rainstorm drenched the soil and swelled the streams in the areas surrounding the Oldman River basin, providing a saturated antecedent condition for the upcoming floods.

Rainstorm case 2 lasted for 96 hours from 0600 UTC 5 June to 0600 UTC 9 June. The maximum precipitation accumulation was 248 mm. The maximum 24-hour rainfall was 131.8 mm recorded on 7 June at Pekisko (Fig. 2-4b). This rainstorm produced a secondary high 24-hour rainfall accumulation of 110.5 mm at Beauvais Park (49.42°N 114.10°W) on 5 June. The extreme rainfall over the southern Alberta foothills from the rainstorm caused overflows of the Sheep River, upper Oldman River, Willow Creek and the Highwood River. The bank of the Highwood River burst due to the heavy load of water flow. The overflow and bank burst of the above rivers set out the first widespread flash flood of the month. The lower Bow River basin and the upper Oldman River basin were the centrally affected regions, where an area of about 62,500 km^2 received $\geq$ 50 mm of rain (Fig. 1-1b, 1-2). The mainly affected communities included Black Diamond, Turner Valley, Okotoks, High River, Bragg Creek, Pincher Creek, Lethbridge (Fig. 2-3). Medicine Hat (50.02°N 110.72°W) in the South Saskatchewan River basin also suffered a minor flood threat due to the peak flow from upstream (Oldman and Bow Rivers).

Rainstorm case 3 lasted for 78 hours from 1200 UTC 16 June to 1800 UTC 19 June. It produced a maximum precipitation accumulation of 152 mm and a maximum 24-hour rainfall of 128.4 mm on 17 June at Springbank (51.1°N 114.37°W) (Fig. 2-4c). This rainstorm gave a secondary high 24-hour rainfall of 114.9 mm to the Bow Valley

(51.08°N 115.07°W) on 18 June. Lightning and thunderstorms were reported at Calgary, Lethbridge and Medicine Hat during the event. Heavy rainfall fell over the Red Deer River and upper Bow River basins. The consequent overflow of the Elbow and Bow Rivers, and bank burst of the Red Deer River and Bearberry Creek induced the second catastrophic flood within the month. The centrally affected regions covered an area of nearly 50,500 km^2 in the Red Deer River and Bow River basins that received $\geq$ 50 mm of rain (Fig. 1-1c, 1-2). The mainly affected communities included Sundre, Red Deer, Drumheller, Drayton Valley, Rocky Mountain House, Edmonton, Priddis, Calgary, High River, Black Diamond, Turner Valley, Okotoks, and Bragg Creek (Fig. 2-3).

Rainstorm case 4 lasted for 54 hours from 0600 UTC 27 June to 1200 UTC 29 June. A peak precipitation accumulation of 90 mm was recorded in the area near Highwood, and a maximum 24-hour rainfall of 59.8 mm was reported at Cop Upper (51.08°N 114.22°W) on 28 June (Fig. 2-4d). This rainstorm also gave a secondary high 24-hour rainfall accumulation of 57.7 mm at Beaver Mines (49.47°N 114.18°W) on 27 June. The rainstorm re-hit the areas that had suffered the previous two floods and caused the third flood within the month. The centrally affected regions covered the same basins hit by the second rainstorm, where an area of about 10,500 km^2 receiving $\geq$ 50 mm of rain (Fig. 1-1d). The mainly affected communities included High River and Okotoks, where both were hit 3 times in a month.

2.3.2 Impacts of the June 2005 Alberta flood

With the extraordinary rainfall during June 2005, rapid response of rivers and streams in the central and southern Alberta foothills produced extreme high water levels. The Bow, Oldman and Red Deer Rivers were engorged carrying 10-30 times their usual volume. About 22 of the swollen rivers broke the highest or next highest flow records, and 17 of them had a chance of occurrence of similar magnitude less than 1% in any given year (see Table 2-2).

Consecutive severe floods caused by torrential rain from the four rainstorms affected 16 major communities, with 14 of them declaring unprecedented official states of emergency. Floodwater washed out many roads and parks, destroyed bridges, flooded hundreds of homes and businesses, damaged sewers and other infrastructure, wrecked buildings and drowned livestock. In Calgary alone, one in ten dwellings reported damage. In total about 40 municipalities identified infrastructure damage. Thousands of people were forced to evacuate their homes. Four people died due to turbulent waters of the floods. The insured losses were about $275 million. The total uninsured and insured losses were approximately $400 million. Besides the extensive damage of properties and businesses, there were countless occurrences of soil erosion and hydraulic structure damage. The cleanup and rebuilding across central and southern Alberta lasted months, even years for some towns that had experienced two to three major floods in a space of one week.

In addition to economic losses, there were losses impossible to be calculated in dollars and cents during the June 2005 Alberta flood. Entire communities and lives of individuals were seriously disrupted, and the disruption lasted for long periods afterwards. The consecutive floods with only one week space did not give a break to the affected people and communities. Most importantly, the lives of people in the flood hazard areas were in danger. The impacts of the June 2005 Alberta flood on the public were far greater than one might quantify in terms of money.

2.3.3 Alberta's June precipitation climatology

Rainfall climatology indicates that June tends to have the highest monthly precipitation amount. For southern Alberta, June of 2005 was the wettest one ever recorded. The precipitation accumulation of June 2005 in the central and southern Alberta foothills was mainly contributed by the four successive rainstorms. For example, the total rainfall accumulation of the four storms was about 70% of the precipitation of June 2005 between Red Deer and Calgary, and more than 90% of that south of Calgary. At Calgary, the accumulation of the four consecutive rainstorms was 237.4 mm and the

total rainfall of June was 247.6 mm, giving a ratio of 96%. Accumulation of the four rainstorms along the central and southern Alberta foothills was about two to six times the normal precipitation for the June rainfall climatology (Fig. 2-5), making it the biggest June rainfall in more than a century. For instance, total rainfall of June 2005 at Calgary was more than three times the normal June precipitation of 79.8 mm. Total rainfall of June 2005 reported in the lower Bow River basin was about six times the normal June Alberta precipitation climatology that usually ranged from 75 to 100 mm (Phillips 1990).

An in-depth study of Alberta's precipitation climatology was carried out by Verschuren and Wojtiw (1980). Their analysis of point measurements of maximum accumulated storm rainfall indicates that in a 100 year period, the climatological probability of a storm producing $\geq$ 50 mm of rain ranges from 100% (i.e. once per year) in the central-west region to 200% (i.e. twice per year) in the extreme southwest foothills (Waterton Lakes Park area); the probability of a storm producing $\geq$ 100 mm of rain ranges from 10% in the central-west region to 25% in the southwest foothills; the probability of a storm producing $\geq$ 150 mm of rain ranges from 2% in the central-west region to 5% in the southwest foothills. The overall probability of a storm producing $\geq$ 150 mm of rain in Alberta is about 5.6% during the summer months, and about 2.6% in June alone; the probability of a storm producing $\geq$ 200 mm of rain in Alberta is about 1% during the summer months and less than 1% in June (see Fig. 11, 12, 13 and Table 1 in Verschuren and Wojtiw 1980). Based on the above results, the June 2005 Alberta rainstorms case 1 and case 3 had a probability of 25% and 10%, respectively, and case 2 had a probability of less than 1%. According to the Verschuren-Wojtiw frequency analysis of the average storm total precipitation over the southern Alberta foothills, the greatest frequency is about 0.09 for rainfall exceeding 150 mm, and about 0.38 for rainfall exceeding 100 mm. This suggests a mean return period of about 10 years and 3 years for the rainfall of $\geq$ 150 mm and $\geq$ 100 mm, respectively. The occurrence of three consecutive rainstorms (cases 1, 2, 3) in June 2005 with rainfall in excess of 100 mm and a space of one week or less was rare in the Alberta history.

Chapter 3: Study of the extreme rainstorm of June 5-9, 2005

3.1 Brief review of the case

Between 5 and 9 June 2005, the second rainstorm of the month hit southern Alberta and produced extensive rainfall covering an area larger than 60,000 km^2. Figure 3-1 shows the distribution of 24-hour rainfall accumulation during the event. 6 June and 7 June were the heaviest rainfall days in which an area of about 25,000 km^2 recorded $\geq$ 50 mm of rain during a 24-hour period. A highest 24-hour rainfall accumulation of 131.8 mm and a secondary high one of 110.5 mm were recorded on 7 June at Pekisko and on 5 June at Beauvais Park, respectively. An accumulated event rainfall of 248 mm was recorded at Pekisko in the middle Highwood River basin of the Bow River basin.

Streams originating in and along the southern mountains and foothills responded very quickly to the heavy rainfall as these areas were already saturated due to high rainfall recorded in the previous week (case 1). Rivers and streams in the Bow River and Oldman River basins were swollen and many of their peak flows broke the highest record in previous history. Overflows from the Sheep River, Willow Creek, outflow from the Oldman River dam and bank burst of the Highwood River caused extensive flooding in the above river basins.

3.2 Analyses of radar and satellite imageries

A detailed discussion on the organization and evolution of the rainstorm during 5-9 June 2005 displayed on radar images and the associated structures of clouds and airflows shown on VIS and IR satellite images will be presented as follows.

3.2.1 Precipitation organization and evolution of radar echoes

A sequence of radar images at 3-hour intervals during the extreme rainstorm case 2 will be dissected and discussed. The radar images employed here are the composite

CAPPI images at the level of 1.5 km above ground level (AGL). (Notice there are echoes of ground clutters of the Rocky Mountains and Cypress Hills ranges (49.40°N 109.30°W) presented on all radar images, located about 80 km west and southwest of Calgary and 55 km southeast of Medicine Hat, respectively.)

Figure 3-2(I, II, III) shows the time series of the composite CAPPI images of case 2. Two precipitation spans were identified from the radar sequence. The first one was from 0600 UTC 5 June to 0000 UTC 6 June with scattered localized heavy rain showers along the central and southern Alberta foothills. The second and the major precipitation span began at 0000 UTC 6 June and ended by about 1200 UTC 8 June with mostly uniform rainfall covering an area more than 5000 km^2 in southwestern Alberta.

Panels (a) to (f) of Figure 3-2I show that prior to 0000 UTC 6 June, there were some localized mesoscale convective clusters scattered along the Alberta foothills. A signature of a cyclonic development was located near Lethbridge between 0800 UTC and 1500 UTC 5 June. Peak radar reflectivity briefly reached 42 decibel (dBz) at 0840 UTC 5 June, suggesting an instantaneous rainfall rate of about 18-20 mm/h. The surface rain gauge reported about 21 mm of rain within 4 hours (0500-0900 UTC) in the Lethbridge area under this localized feature. In the meantime, two other clusters developed to the south and southeast of Drumheller (51.50°N 112.76°W) and south-southeast of Calgary. The maximum radar reflectivity of the cluster south-southeast of Drumheller fluctuated between 40 and 45 dBz (suggesting an instantaneous rainfall rate of 12-25 mm/h) from 0600 UTC to 1600 5 June. This cluster actually produced about 20.5 mm of rain at Hussar (51.18°N 112.5°W) during this period. The cluster south-southeast of Calgary presented a peak reflectivity of 46 dBz at 1550 UTC 5 June, and it produced 34 mm of rain in the Calgary area from 0600 to 1800 UTC 5 June.

In the evening hours local time (LCT) on 5 June, some local convection developed in the area between Waterton Park Gate (49.08°N 113.48°W) and Cardston. Intense radar echoes higher than 45 dBz occurred from 2130 UTC 5 June to 0110 UTC 6 June with a peak of 55-60 dBz presented near Cardston from 2250 UTC 5 June to 0000

UTC 6 June. This suggests the presence of deep convection and hail potential, and it suggests an instantaneous rainfall rate of 30 mm/h or higher. The recorded rainfall rates at Cardston and Waterton Park Gate were both about 3 mm/h at 2300 UTC 5 June and at 0000 UTC 6 June, respectively. However, the higher rain rate in between these locations might not be recorded. Another small area of high echoes of 40-50 dBz (suggesting a rainfall rate of 12-64 mm/h) was presented near Pincher Creek between 0000 and 0600 UTC 6 June. The hourly rainfall reported at Pincher Creek was 12.6 mm at 0200 UTC 6 June, and remained at 6.2-8.2 mm/h within the next couple hours. Lightning at the above regions was detected by the Canadian Lightning Detection Network (CLDN) between 2100 UTC 5 June and 0500 UTC 6 June. The high rainfall rate during these hours was associated with high CAPE that was derived from the sounding data at 0000 UTC 6 June (see further discussion in section 3.5.3, Fig. 3-20 c).

The major precipitation span of case 2 from 0000 UTC 6 June to 1200 UTC 8 June was shown on panels (g) to (x) on Figure 3-2I, II, III (images omitted after 0300 UTC 8 June). At 0000 UTC 6 June, a broad elongated rain cluster began to approach the west Alberta-Montana border from the southwest. A few small intense convective clusters (echoes briefly peaked at 55-60 dBz) that previously developed south of Lethbridge merged into the broad rain cluster as it pushed north of the border (Fig. 3-2I g). Heavy rainfall began to spread over southern Alberta at this time. Within the next 6 hours, the broad rain cluster continued moving north-northeast with its core passing Lethbridge and the east area. Peak echoes of 46 dBz covered an area of about 100 km^2 at 0700 UTC 6 June (image omitted, refer to Fig. 3-2II i). The corresponding rainfall rate of 14 mm/h was reported at the Lethbridge Alberta Environment hydrological station at 0800 UTC. By 0900 UTC 6 June, the weakening broad rain cluster swung slightly north and separated into a few smaller clusters. The major one with echoes of 30-40 dBz was lingering over the foothills near High River (Fig. 3-2II j-k).

By 1500 UTC 6 June, a second broad rain cluster approached southeastern Alberta from central Montana (Fig. 3-2II l). This cluster reached its peak intensity at 1800-2100 UTC 6 June, with a peak of 45-50 dBz at 1950 UTC (Fig. 3-2II m, n and Fig.

3-3) located approximately 55 km north of Medicine Hat. The corresponding peak instantaneous rainfall rate would be 30 mm/h or higher. The reported rainfall at the Medicine Hat Airport was 9.5 mm/h at 1900 UTC. During this period (1800-2100 UTC) three curved strips of 35-50 dBz circled around a centre about 30 km east of Medicine Hat when the entire cluster moved north of Cypress Hills. The curve of the echoes became insignificant after 2100 UTC 6 June. The broad rain cluster weakened significantly after 0000 UTC 7 June, and separated into smaller clusters propagating west over the southern Alberta foothills (Fig. 3-2II o-p).

By 0600 UTC 7 June, those smaller clusters redeveloped and merged to form another huge cluster by 0900 UTC 7 June, orientating NW to SE over southern Alberta. Peak echoes of 45 dBz were presented at 1200 UTC 7 June, suggesting an instantaneous rainfall rate of 30 mm/h or higher. At this time, the strongest echoes band (40-45 dBz) roughly appeared to be a "J " shape and located about 40 km northeast of Medicine Hat (Fig. 3-2III s). The averaged rainfall rate recorded at Medicine Hat and Schuler (45 km northeast of Medicine Hat) was about 3.5 mm/h during the intense rain period (1000-1300 UTC). The strongest echoes of the broad cluster remained at 40 dBz within the next one and a half hour when the cluster swung west-northwestward about a centre near the eastern Alberta-Montana border (refer to the red solid circle on Fig. 3-2III t). The cyclonic rotational motion of the cluster continued until 0600 UTC 8 June (Fig. 3-2III t-x). This cluster rapidly weakened after 1800 UTC 7 June indicating that the heavy rainfall episode headed for its end.

During the major span of the extreme rainstorm case, radar echoes along the Alberta foothills (e.g. the Highwood River basin on Fig. 2-3) remained mostly uniform and steady, and were relatively weak ($\leq$ 30 dBz, suggesting a rainfall rate of 2 mm/h or less). But the accumulation over these areas was the highest of the event (refer to Fig. 1-1b, Fig. 3-1). This implies that precipitation along the foothills was mainly produced by stratiform clouds with a lower cloud top that might not be able to be detected by the radar, especially of a longer range from the radar (Doswell III et al. 1996).

In this study, an analysis of the estimated CAPPI radar rain rate against the surface rain gauge measurement of selected locations is carried out. Figure 3-4a shows the relation of the estimated synoptic hour radar rain rate at 1.5 km AGL to the rain gauge measured rain rate (6h mean) of Sundre, Calgary and Lethbridge during the event. The result suggests a nearly linear correlation with a correlation coefficient of about 0.7 between the estimated radar rain rate and the measured rain rate. Figure 3-4b gives the ratios of integration of the estimated radar rain rate to the accumulated rainfall of the three locations. The highest ratio of 80% is that of Calgary which is close to the radar station, and the lowest one of 66% is that of Lethbridge which is far away from the radar station. The averaged ratio for the three locations is about 72.7%. The surface observation was a collection of all rain water that fell from the entire column of air, including possible rain water advected from surrounding areas. Thus one of the reasons for the lesser rainfall rate detected on the CAPPI radar images may be due to the fact that the radar measures rain droplets at a constant level 1.5 km above ground, and rainfall contributed below this level could not be detected. The higher ratio at Calgary and lower ratio at Lethbridge may be due to the attenuation increase with distance from the radar.

In summary, the time series of radar images suggests that the extreme rainstorm case during 5-9 June 2005 was produced by three large elongated rain clusters that migrated from south of Alberta, as well as some local mesoscale convective developments prior to the major rainfall span. Three peaks of intense echoes, which appeared at 0700 UTC 6 June near Lethbridge, 1950 UTC 6 June north of Medicine Hat, and 1200 UTC 7 June northeast of Medicine Hat, were associated with high recorded rainfall rates. Radar measurement of precipitation was well correlated to the surface rain gauge measurement, and the accuracy largely depended on the attenuation associated with the distance away from the radar location.

3.2.2 Organization and evolution of clouds and airstreams on satellite imagery

We use high resolution visible (pixel size 1 km) and infrared (pixel size 4 km) satellite images originating from the Geostationary Operational Environmental Satellite

(GOES) series in this study. Figure 3-5(I, II) depicts the sequence of the VIS (left panels) and IR (right panels) images with a centralized view of western Canada and the Northwest U.S. The selected times of the IR images were 0000 and 1200 UTC, and that of the VIS ones were 0000 and 1300 UTC on 6-8 June 2005 for better visual result except that the 0000 UTC 6 June image was replaced by the 2300 UTC 5 June one due to missing data.

Panels (a) and (d) on Figure 3-5I indicate that there was an elongated leaf-shaped cloud shield lying from southern British Columbia (hereafter BC) to western Montana and Idaho (U.S.) at 2300 UTC 5 June. Embedded convection (bubble-like white spots - Cumulus) with low cloud top temperature (minus 60°C and lower) can be identified near the Alberta-Montana border and the south. The anvil cirrus plumes of the convection extended northeast from the arch of the leaf-shaped cloud shield (denoted by "A" on Fig. 3-5I a). The convection was also detected by the CAPPI radar images (Fig. 3-2I g, h) where the echoes reached 50 dBz with corresponding rainfall rate records that were associated with high CAPE (see section 3.2.1, 3.5.3).

By 1300 UTC 6 June, the initial leaf-shaped cloud shield developed to be a comma-shaped cloud system extending from a primary cyclone centre off the Washington-Oregon coast ("C" on Fig. 3-5I b). An anticyclonic curving scalloped cloud ("B" on Fig. 3-5I b) developed on the right edge of the comma tail over the cross border of Alberta-Montana-Saskatchewan. Studies by Weldon (1979), Carlson (1980), and Browning (1990) suggest that the tail of the extratropical comma-shaped cloud systems is identified as a warm conveyor belt, and the signature of anticyclonic curving is identified as a baroclinic cloud leaf. The presence of a warm conveyor belt with the signature of baroclinic cloud leaf suggests an initial stage of surface cyclogenesis (Weldon 1979, Carlson 1980, Browning 1990). Both the 1300 UTC VIS image and the 1200 UTC IR image (Fig. 3-5I b, e) show a gap of the cloud top between the comma tail and the baroclinic cloud leaf, indicating a divergent southerly steering flow at the cloud top layer. A narrow clear belt on the west edge of the comma tail was identified lying from southeastern BC to the Idaho-Montana border. The clear belt of no or least cloud

suggests that there were dry airstreams associated with a sinking cold airmass encroaching on the area. The clear belt implies that there exited an upper frontal zone between the moist cloud shield and the dry airstreams (Carlson 1980, Browning 1990, Kocin and Uccellini 1990).

By 0000 UTC 7 June, the comma tail swung northeast away from the primary offshore comma head. Another cloud crest formed over southern Alberta with a cyclone centre dimly discerned near the Alberta-Montana border ("D" on Fig. 3-5I c). A lambda-shaped cloud pattern was established by the comma tail ("A" on Fig. 3-5I c) extending southeast to the Midwest U.S., and the baroclinic cloud leaf ("B" on Fig. 3-5I c) extending northeast to central Saskatchewan. This signature suggests an occlusion and the onset of surface cyclogenesis (Carlson 1980, Young et al. 1987, Browning 1990) which was responsible for the heavy rainfall episode between 1800 UTC 6 June and 0000 UTC 7 June, as indicated by the radar images (Fig. 3-2II m-o).

By 1300 UTC 7 June, the cloud crest organized to be a well defined comma head lying over the cross border of BC-Alberta-Montana ("D" on Fig. 3-5I g). This comma head with a cloud top temperature of minus 50°C was associated with the heaviest rainfall episode over southern Alberta that was indicated by radar images (Fig. 3-2III s-t) and the ground observations. A cloud free region ("E" on Fig. 3-5II g, h) immediately southeast of the comma head indicates the encroachment of a dry cold air flow that was responsible for rapid surface cyclogenesis (Hoskins et al. 1985, Young et al. 1987, Browning 1990).

By 0000 UTC 8 June, a well defined cyclone centre with a hook-shaped dry encroachment was located just north of Lethbridge on both the VIS and IR images (Fig. 3-5II h, k). As the dry encroachment undercut (i.e. cut off) the moisture supply, widespread precipitation began to dissipate. A narrow convective band (featured by a non-uniform bright boundary on the VIS image) can be identified at the leading edge of the dry encroachment near the southern Alberta-Saskatchewan border. This convective band was also displayed as a narrow comma-shaped cluster on the next 3-hour radar

images (e.g. Fig. 3-2III x). Carr and Millard (1985) documented that the wedge of dry cold air flow encroachment is a favored region for convection.

By 1300 UTC 8 June, the cyclone centre over southern Alberta disappeared beneath the thick cloud cover, instead, another comma-head-like cloud shield developed to the southeast of the province ("F" on Fig. 3-5II i). Precipitation over southern Alberta moderated under the thinning low-cloud layer (this can be identified on Fig. 3-5II l).

In summary, the sequence of satellite images indicates that the extreme rainfall event during 5-9 June 2005 occurred under the development of a large scale comma-shaped cloud system that was associated with surface occlusion (see further discussion on occlusion in section 3.3.1). Heavy rainfall occurred beneath the comma-head clouds. The encroachment of dry cold air flow was responsible for rapid development of surface cyclone and leading edge convection, and led to the end of the widespread precipitation.

3.3 Synoptic flow features

The synoptic flow patterns at typical levels will be discussed in the following sections to reveal the dynamic support for the extreme rainfall event during 5-9 June 2005. The synoptic analysis charts used in our study were derived from the surface (sea-level), 850-, 700-, 500-, 300-, and 250-hPa operational analysis maps provided by Environment Canada (EC) and reanalysis maps provided by Plymouth State Weather Center (PSWC).

3.3.1 Flow pattern at the surface

A centralized view of the flow pattern during 6-8 June at the surface over the southern section of Western Canada and northwest United States is illustrated on Figure 3-6. It indicates that there were two cold fronts at 0000 UTC 6 June (separated from a major cold front previously laid west of the Rocky Mountains on 5 June). The north one lay windward of the Canadian Rockies, and the south one extended southward over

central Montana where a weak low pressure center (1001 hPa) developed on the lee side of the Rocky Mountains. By 1200 UTC 6 June, the north cold front crossed the Continental Divide and merged into an inverted trough of the deepening and southeast-moving Montana low, extending northwest over southern Alberta. The Montana low continued to slip southeast into the Midwest U.S. and deepened to be of 995 hPa at 0000 UTC 7 June (Fig. 3-6c). Under the influence of the orography (the lee slope serves as a cold front, see Petterssen 1956), a moving-in warm front from east-southeast was forced to uplift and formed a trowal (**tr**ough of **w**arm air **al**oft, namely an occlusion front as shown by the dashed arrows) lying roughly parallel to the Continental Divide. By 0600 UTC 7 June (map omitted), a secondary low developed in the trowal over Montana and slipped northwest to be over the Alberta-Montana border with a minimum pressure of 999 hPa at 1200 UTC 7 June (Fig. 3-6d). North of the low centre there were three isobars orientated east-northeast over central to southern Alberta (roughly perpendicular to the slope of the Rocky Mountains) from 0000 to 1200 UTC 7 June. This suggests a tighter pressure gradient and consequently a stronger upslope flow over the foothills (see geostrophic wind Equ. (4.2.3) in Petterssen 1956) existed during the heaviest rainfall episode. As a cold air mass wedged in from the northeast while a warm air mass pushed up from the south (evidence of a temperature gradient), the trowal retreated east and evolved to be a quasi-stationary front stalling over the area by 0000 UTC 8 June. It then weakened to be an inverted trough in 12 hours. The Alberta-Montana low remained nearly stationary and slightly weakened before it tracked southeast, merging into the primary low that already moved into the Midwest U.S. by 1200 UTC 8 June (out of the map's margin). As the merged low continued moving east, the inverted trough was pulled away from Alberta and weakened with the large scale precipitation dissipating.

In summary, the surface flow pattern during 6-8 June 2005 suggests that active fronts, lee inverted trough/trowal systems and their interchanges, plus lee cyclogenesis provided favorable synoptic conditions for the heavy rainfall event. The time of lee cyclogenesis and presence of the trowal was associated with the heaviest rainfall episode on 7 June. Prominent northeasterly upslope flow mechanically reinforced the rainfall over the southern Alberta foothills.

3.3.2 Flow pattern at upper levels

1) Synoptic setting at 250 hPa

A centralized view of the flow pattern over Western Canada and Northwest United States at the 250-hPa level during 6-8 June is depicted on Figure 3-7. By 0000 UTC 6 June, a closed blocking high with a central geopotential height of 1048 decameters (dam) was located south of the Great Slave Lake (61.23°N 115.38°W), and a cutoff low was located off the Washington coast. By 1200 UTC 6 June, the cutoff low landed and dropped its minimum height to 1016 dam with two contours closed. During the heavy precipitation episode on 7 June, the blocking high retrogressed slightly southwest and gradually weakened, and the cutoff low migrated east towards the north U.S. Rocky Mountains. On 8 June, the cutoff low flattened and continued drifting east, and the blocking high over northern Alberta also weakened. The weakening blocking high and flattening cutoff low were in conjunction with the weakening rainfall.

A diffluence was well established by 1200 UTC 6 June over southern Alberta and Montana which were located downstream of a trough lying over the Northwest U.S. and immediately upstream of a ridge extending from Midwest U.S. to southeastern Alberta. A nearly closed polar jet stream that was initially surrounding the cutoff low (at 0000 UTC 6 June) gradually opened, with its exit of the axis swinging east to be lying over eastern Montana on 7 June (Fig. 3-7b, c, d). At this time, the surface lee cyclogenesis occurred near the Alberta-Montana border which was located left of the exit of the jet's axis. When the cutoff low moved further inland on 8 June, the diffluence migrated east to the Midwest U.S., coinciding with the weakening of the surface lee cyclone and the dissipating of precipitation.

In summary, the synoptic setting at 250 hPa during 6-8 June 2005 displayed a slowly-moving blocking high coupling with a cutoff low over western North America, and a divergent flow over southern Alberta and western Montana during the extreme rainfall event. This pattern maintained the upper-level divergence that provided strong

dynamic support for the surface lee cyclogenesis and the lower-level vertical motion for the heavy precipitation of southern Alberta.

2) Synoptic setting at 500 hPa

A centralized view of the flow pattern at the 500-hPa level during 6-8 June is depicted on Figure 3-8. A cutoff low with a close by cold core (shaded area) was located offshore of the Northwest U.S. on 6 June. The central geopotential height of the low was 545 dam and the minimum thickness of the cold core was 536 dam. A closed blocking high with a central geopotential height fluctuating from 570 to 567 dam stalled near the Alberta-Northwest Territories border during 6-7 June. A high pressure ridge extended over the Great Plains on 6 June. It strengthened and nearly joined the blocking high on 7 June. The cold low drifted inland to stall over the west Washington-Oregon border with its central geopotential height raised to 551 dam on 7 June. At 0000 UTC 8 June, the blocking high and the ridge began to migrate southeast and weakened while a new high centre formed over the middle BC coast. At the same time, the cold low migrated east-southeast and split into two centers with the new one lying over the lee slope near the west Alberta-Montana border (Fig. 3-8e). The split-off low then tracked east-southeast to the Midwest U.S. by 1200 UTC 8 June.

A saddle region (between the blocking high and the Great Plains ridge) initially lying over the southern Canadian Prairies on 6 June was cut away when the Great Plains ridge strengthened to nearly connect with the blocking high on 7 June. Replacing the saddle, a zonal trough (the roughly latitudinal trough that was subjectively analyzed and denoted by the double brown dashed line on Fig. 3-8) that extended east from the cold low swung north to be lying over the southern region of BC and Alberta by 0000 UTC 7 June. The trough then pushed back to the south of the border (*by the strengthened easterly wind*) by 12 hours later, with its eastern end tilting northeast over southeastern Alberta and southern Saskatchewan. The trough remained nearly stationary over the area by 0000 UTC 8 June, and finally moved southeast with the split-off low to the south of the border by 1200 UTC 8 June. Between 0000 UTC 7 June and 0000 UTC 8 June, strong horizontal cyclonic wind shear (southerlies shifted to easterlies) and convergence

(west wind component south of the trough and east wind component north of the trough) in the trough area were evident. This coincided with the heaviest rainfall episode over southern Alberta. As horizontal cyclonic wind shear results in positive vertical vorticity and horizontal convergence which eventually contribute to upward motion (see section 2.1.3), horizontal cyclonic wind shear and convergence that were discerned at 500 hPa over southern Alberta during 6-7 June provided dynamic support for the updraft for the heavy rainfall.

During 6-7 June, a thickness ridge (marked by the 558 dam black short dashed line) built from the north Great Plains to the southern Canadian Prairies. The thickness ridge was initially in phase with the contour ridge at 0000 UTC 6 June but lagged slightly behind after 12 hours. This pattern suggests that there existed a zone of baroclinic instability that is favourable for the cyclogenesis at the lower level and occlusion at the surface (see section 2.1.3). The thickness ridge slowly retreated east as the cold core edged inland on 7 June. CAA south of the trough in the southwest wind over western Montana and WAA north the trough in the easterly wind over southern Alberta became evident (where winds blew across the thickness contours (e.g. crossing the 552 dam)) at 1200 UTC 7 June (Fig. 3-8d). The presence of WAA to the north and CAA to the south of the border was in conjunction with the lee cyclogenesis at the lower level and the surface (see further discussion in subsection 3)).

In summary, the presence of a coupled cold low and blocking high, pronounced horizontal wind shear and convergence all together at the 500-hPa level provided ideal dynamic support for sustained uplift for the heavy rainfall during 6-7 June.

3) Synoptic setting at 700 hPa

A centralized view of the flow pattern at the 700-hPa level during 6-8 June is depicted on Figure 3-9. It indicates that there was a narrow area of low pressure lying over the southern Canadian Prairies on 6 June and connecting two low centers that were located over western Ontario and offshore of Washington. By 0000 UTC 7 June, the offshore low weakened when it landed on the Washington-Oregon coast. In the

meantime, a new cyclone developed at the apex of a thermal ridge (marked by the zero degree isotherm) to the lee of the Rocky Mountains near the Alberta-Montana border, which was underneath the 500-hPa zonal trough and the diffluent zone in the upper troposphere (see panel (c) on Fig. 3-7, 8, 9). The new cyclone continued to deepen with a central pressure of 290 dam at 1200 UTC 7 June, and it remained nearly stationary during the next 12 hours. It began to weaken and tracked southeast into the Midwest U.S., merging with another low moved up from the south by 1200 UTC 8 June.

In response to the cyclone development on 7 June, an S-shaped isotherm configuration (marked by the zero degree isotherm) formed lying from the southern Canadian Prairies to the north Great Plains. East-southeasterly wind across the isotherms from warm to cold over southern Alberta and northeast Montana suggests that there was WAA over this region (Fig. 3-9c, d). Meanwhile, northwest and southwest wind across the isotherms from cold to warm over the north Great Plains suggests that there was CAA over this region (missing wind bars over the interested area at 1200 UTC 7 June were estimated from the orientation of the geopotential contours, and were confirmed by the PSWC reanalysis wind data). The prominent WAA to the northeast and CAA to the southwest of the convergent zone at the 700-hPa level indicates a presence of strong baroclinic instability that contributed to the cyclonic development over the Alberta-Montana border. The time of appearance of strong baroclinic instability coincided with the extreme rainfall episode.

In summary, the 700-hPa synoptic circulation during 6-8 June 2005 suggests that the enhanced baroclinic instability due to the co-existence of WAA and CAA contributed to the lee cyclogenesis over the Alberta-Montana border. The occurrence of pronounced WAA and lee cyclogenesis coincided with the extreme rainfall episode.

4) Synoptic setting at 850 hPa

A centralized view of the flow pattern at 850-hPa level during 6-8 June is depicted on Figure 3-10. It shows that on 6 June there was a broad area of low pressure (enclosed by the 144 dam contour) located in western Canada and the Northwest U.S.

with multiple centers within it. A meridional trough (that was subjectively analyzed and denoted by the double brown dashed line on Fig. 3-10) connecting three low centres lay near the Rocky Mountain ridge at 0000 UTC 6 June. By 1200 UTC 6 June, the low centered over western Montana (with a minimum geopotential height of 137 dam) drifted east-southeast with the southern section of the meridional trough swung east and a short zonal trough developed east of the low. The Montana low moved further east and deepened slightly (-2 dam/12h) by 0000 UTC 7 June. In the meantime, the zonal trough and the meridional trough re-organized to a ⊤-shaped configuration lying over southern Alberta and the north Great Plains (Fig. 3-10c). The Montana low moved into the Midwest U.S. and weakened by 1200 UTC 7 June with a secondary low developed near the Alberta-Saskatchewan-Montana border within the area enclosed by the 138 dam contour of the weakening Midwest low (Fig. 3-10d). The new cyclone weakened slightly (+4 dam/12h) when it migrated northwest to be lying over southern Alberta at 0000 UTC 8 June, and quickly tracked southeast along the northwest-tilting zonal trough to be over the central Montana-North Dakota border (Fig. 3-10e, f). The northwest tilting of the trough over southern Alberta between 1200 UTC 6 June and 1200 UTC 8 June indicates the existence of a persistence convergent zone supporting sustained uplift for the continuous rainfall during the event.

A thermal tongue (marked by the 10 degree isotherm) previously extending from the Great Plains, west of the Rocky Mountains to northern Alberta was undercut by a wedged-in cold air mass from central Saskatchewan, and retreated south of the Canadian Prairies by 1200 UTC 7 June. The wedged-in cold air mass at this level increased the temperature lapse rate of the layer immediately above this level, and forced the warm air mass to uplift (where the position of the zero degree isotherm did not change much at 700 hPa) enhancing the vertical motion in the lower troposphere over southern Alberta.

In summary, the 850-hPa flow pattern during 6-8 June 2005 suggests that the combination of lee cyclogenesis near the Alberta-Saskatchewan-Montana border, a stationary ⊤-shaped trough over southern Alberta and the Great Plains, and a wedged-

in cold air mass from central Saskatchewan provided ideal lower tropospheric dynamic support for the heavy rainfall.

5) Superposition of the synoptic circulations of typical levels

The reanalysis charts of typical levels (300-, 500-, 850-hPa and surface) on Figure 3-11 give an overview of the atmospheric circulations over North America at 1200 UTC on 6-7 June. It shows that a cutoff low coupling a blocking high was presented at both the 300- and 500-hPa levels over western North America on both days. On 6 June, a diffluence was presented from southern Alberta to the Great Plains at 300 hPa, and from Montana to the Great Plains at 500 hPa. A primary surface low with a minimum pressure of 1001 hPa (marked as 999 hPa on the EC map Fig 3-6b) was located over the Montana-Wyoming border (Fig. 3-11d), stretching vertically to the 850 hPa. An inverted surface trough of the low trailed northwest to southern Alberta. As the low pressure centers slanted to the west-northwest from the surface to the upper levels, the surface low and its inverted trough consequently lay underneath the diffluent cross-barrier flow of the upper troposphere.

On 7 June, both the cutoff low and the blocking high weakened when they drifted east further inland. The Montana-Wyoming low at the surface and the 850 hPa also migrated eastward with a secondary lee cyclone developed near the Alberta-Montana-Saskatchewan border, where the surface centre had a central pressure of 1002 hPa (marked as 999 hPa on the EC map Fig 3-6d) and the 850-hPa centre had a central height of 1370 gpm (marked as 132 dam on the EC map Fig 3-10d). East to northeast wind was evident from the surface to the upper troposphere over southern Alberta.

In summary, the analysis of weather maps at individual levels and their overlays suggests that the extreme rainfall event during 5-9 2005 was produced under a favorable superposition of the upper and lower atmospheric circulations. A cutoff low coupling a blocking high in the upper troposphere, a ⊤-shaped trough in the lower troposphere, a lee surface inverted trough/trowal and their interchanges, as well as lee cyclogenesis from surface to the middle troposphere comprised an ideal dynamic support of the heavy

rainfall. Analysis of the 500- and 700-hPa flow pattern suggests that lee cyclogenesis was the consequence of a combination of PVA at 500 hPa, baroclinic instability below 700 hPa and vertical vortex stretching of the crossing mountain airflow. Sustained upslope wind due to the tight pressure gradient over southern Alberta also provided reinforcement of the updraft for the heavy rainfall on 6-7 June.

3.4 Moisture condition

As discussed in Chapter 1, water vapor for precipitation formation comes from two major feedings: local supply (i.e. storage) and advection from sources in the distance. Analyzing the backward trajectories of the moist air during the June 5-9 extreme rainfall event suggests that the major source region was the Midwest U.S. (Dupilka et al. 2007). For a given area, specific humidity, PW and VMR are important parameters to quantify the local vapor supply. The specific humidity and VMR quantify the extent of the moisture at a specific level, especially practical at the cloud base that is usually the LCL (lifting condensation level, which is usually close to the 850 hPa). PW quantifies the amount of vapor stored in a column of air. These parameters will be discussed as follow.

3.4.1 Water vapor distribution at 850 hPa

Figure 3-12 shows the distributions of the 850-hPa specific humidity over the central area of North America during the event. On 5 June there existed a moisture tongue (specific humidity $\geq$ 6.0 g/kg) extending northwest along the Rocky Mountains and the region to the east. Two maxima of 7.58 and 8.60 g/kg were located the north Alberta-BC border and the Montana-Wyoming border, respectively. The moisture tongue was undercut by a relatively dry belt on 6 June, but the two maxima increased to be of 9.37 and 11.20 g/kg, respectively. The moisture tongue re-strengthened to be a narrow band along the Alberta foothills on 7 June before it shrunk and retreated southeast away from the area on 8 June. The moisture field at 850 hPa during 5-8 June suggests that there was high vapor content over the Rocky Mountains, the south Canadian Prairies, the Midwest and eastern Northwest U.S. where vapor could be

immediately transported into southern Alberta by convergent flow (see Fig 3-10). Obviously, the water vapor maxima over the Midwest and eastern Northwest U.S. served as source regions.

Figure 3-13 depicts the distributions of geopotential height, wind field, specific humidity field at 850 hPa and the 6h rainfall amount (inch/6h) at 1200 UTC on 6-7 June. The figure shows that the high rainfall amount in southern Alberta on both days was beneath the moisture tongue where the specific humidity was larger than 6.0 g/kg. The peak rainfall on 7 June (0.58 inch/6h, equivalent to 14.5 mm/6h) over southern Alberta was underneath a newly developed cyclone at 850 hPa. Another rainfall peak near the Montana-Wyoming border on 6 June was corresponding to a moisture maximum which also was in conjunction with a cyclone centre at 850 hPa. The Montana-Wyoming rainfall centre moved east along with the moisture maximum into the Midwest U.S. on 7 June. The superimposition of the cyclone at 850 hPa, the moist maxima and the high rainfall region suggests that the cyclonic flow contributed to moisture circulation and convergence for supporting the heavy rainfall over southern Alberta.

3.4.2 Precipitable water and vapor mixing ratio

The evolution of PW (dark green dashed line) and VMR (brown dashed line) at the LCL are depicted on Figure 3-14 along with the space-averaged 6h rainfall of southern Alberta (bright green solid line). The PW and the VMR were derived from the balloon soundings of Stony Plain, Alberta and Great Falls, Montana. The space-averaged 6h rainfall was taken by the average of 6 stations of the 6 hour rainfall ending at 0000 and 0600 (1200 and 1800) UTC as the mean rainfall at 0000 (1200) UTC. The 6 stations are Sundre, Calgary, Lethbridge, Pincher Creek, Milk River, and Medicine Hat.

Figure 3-14a indicates that the PW at Stony Plain had a corresponding peak (nearly 20 mm) to the rainfall peak at 1200 UTC 7 June. The VMR at Stony Plain also had a corresponding peak to the rainfall peak. Figure 3-14b shows that the PW at Great Falls did not have its peak (nearly 19 mm) corresponding to the rainfall peak, rather it

was about 24 hours prior. The VMR at Great Falls also had a similar trend as that of the PW. The above evidences suggest that the high antecedent vapor content south of Alberta may have been transported through southern Alberta into central Alberta when heavy precipitation occurred in the southern area (indicated by the in-phase peaks of PW and VMR at Stony Plain, and the mean rainfall in southern Alberta). It also implies that the extreme rainfall in southern Alberta during this event may not only be contributed by local available water vapor, but also by advection of rain water from surrounding regions.

In summary, the presence of a prominent moisture tongue over the lee slope of the Rocky Mountains and the vicinity during 5-8 June provided ample vapor supply for the heavy rainfall in southern Alberta. The cyclonic flow at 850 hPa contributed to moisture circulation and convergence for supporting the heavy rainfall. High antecedent vapor content (high PW and VMR) to the south and in-phase high vapor content to the north of the heavy rainfall area suggests that both the local vapor supply and advection of vapor and rain water contributed to the heavy rainfall event.

3.5 Mechanisms contributing to heavy precipitation

Under a favorable synoptic environment, dynamic, thermodynamic and physical mechanisms act synergistically to produce sustained upward motion for moisture-bearing air to the condensation level and result in heavy precipitation. The following section will give a detailed discussion about the mechanisms by the synoptic forcing, orographic forcing and buoyant forcing that contributed to the extreme rainfall event during 5-9 June 2005.

3.5.1 Synoptic forcing

1) Positive vorticity advection

As geostrophic advection of absolute vorticity is one of the important factors which contributes to the local rate of change of absolute vorticity that is in conjunction with cyclogenesis and upward motion (Holton 2004, p146-168), analysis of vorticity

advection at mandatory level may give an estimation of the PVA contribution to the heavy rainfall. The distributions of the absolute vorticity advection at 500 hPa during 6-8 June are displayed on Figure 3-15. The relation of the vorticity advection to the observed rainfall rate is depicted on Table 3-1. Figure 3-15 shows that the 500-hPa PVA existed over southern Alberta on 7 June, and it retreated northwest by 0000 UTC 8 June. Table 3-1 also tells that there existed a peak of 500-hPa PVA ($0.997 \times 10^{-9} s^{-2}$) at 1200 UTC 7 June which is shown near the south Alberta-BC border on Figure 3-15. The occurrence of the peak 500-hPa PVA coincided with the episode of the lower-level lee cyclogenesis and the heaviest precipitation. Negative vorticity advection dominated southern Alberta on 5-6 June and at 1200 UTC 8 June before and after the heavy rainfall episode. It is evident that the PVA at 500 hPa contributed to the heavy rainfall.

2) Positive temperature advection

As geostrophic advection of temperature is a factor responsible for cyclogenesis and vertical motion (see sections c) and d) in 2.1.3), analysis of temperature advection at mandatory level may provide an estimation of the positive temperature advection (PTA, namely WAA) contribution to the heavy rainfall. The contribution of the temperature advection at 700 hPa to cyclogenesis had been discussed in section 3.3.2. Here particular attention will be paid to the contribution of the 850-hPa PTA to updraft and the consequent rainfall.

The distributions of the temperature advection at 850 hPa during 6-7 June are depicted on Figure 3-16. The relation of the 850-hPa temperature advection to the observed rainfall rate is shown on Table 3-1. The largest 850-hPa PTA over southwestern Alberta is seen at 0000 UTC 6 June (Fig. 3-16a) and it was associated with localized convection (showery precipitation and lightning) that was detected as high echoes on radar images (Fig. 3-2I g) and by the CLDN (map omitted). Weak negative temperature advection (NTA) was evident at 1200 UTC 6 June and coincided with the relatively weak rainfall. A secondary high 850-hPa PTA that occurred at 0000 UTC 7 June was about 12 hours prior to the heaviest rainfall episode in southern Alberta.

Table 3-2 quantifies the contribution of the 850-hPa PTA to precipitation. It shows that from zero up to about 60% of the observed rainfall came from lifting resulting from the 850-hPa PTA. The highest contribution was associated with the occurrence of embedded convection (0000 UTC 6 June). A small contribution was found during the heaviest rainfall day (7 June). This indicates that the 850-hPa PTA at the synoptic scale contributed to heavy rainfall to some extent but not significantly throughout the event.

3) Vertical wind shear

As vertical wind shear provides a sheared environment interacting dynamically with a storm system to either enhance or lessen the vertical draft strengths within the storm, it is valuable to quantify the extent of the contribution of the vertical wind shear to heavy precipitation. In this study, particular attention is paid to the relationship of the speed shear and the rainfall rate.

For a best representation of the upper wind over southern Alberta, we employed the soundings of Stony Plain, Alberta. Figure 3-17 gives the sequence of the hodographs from 1200 UTC 5 June to 0000 UTC 8 June 2005 at intervals of 12 hours. The hodographs were generated by the RAOB program (Rawinsonde Observation Program) provided by the Environmental Research Services, Washington, U.S. The winds were plotted from the surface to the level 6 km AGL on the radius scale with the vector traces from the graph's origin. The wind vector's heads were connected by a red curve. Winds at standard upper levels were labeled in hPa, and at the surface labeled with its mean sea-level pressure value in hPa. The storm motion vector (brown arrow) was derived using the traditional method by taking 30 degrees deviation to the right and 75% of the magnitude of steering flow, which is the mean wind from surface to the level 6 km AGL with thickness weighted (see RAOB User's Guide).

Figure 3-17 shows that mean wind from the surface to the level 6 km AGL was from the east (either southeast or northeast). At 1200 UTC 5 June (prior to the heavy rainfall episode), winds were basically backing with height (negative shear) up to 750

hPa. Wind veering with height (positive shear) up to 850 hPa began at 0000 UTC 6 June, and extended further up to 600 hPa at 1200 UTC 6 June. On 7 June, wind backed between 800 hPa and 650 hPa at 0000 UTC (Fig. 3-17d) and the backing layer shrunk and lifted to lie between 700 hPa and 600 hPa at 1200 UTC. The strongest wind shear between the surface and 850 hPa occurred at 0000 and 1200 UTC 7 June (also see Table 3-1). By 0000 UTC 8 June, wind backed again with height below the level of 875 hPa, and the veering above 875 hPa became insignificant.

Table 3-1 gives the relation of the vertical wind shear of the layer, between the surface and the 850 hPa, to the observed rainfall rate. It suggests that the strongest positive wind shear was associated with the largest rainfall rate on 7 June. Small positive shear and negative shear were associated with lower rainfall rate on the other days. Overall, the larger the speed shear, the higher the rainfall rate, and vice versa. This suggests that the vertical wind shear in the lower troposphere reinforced the precipitation to some extent. It also implies that the amount of lower-level vertical wind shear was interrelated to rainfall rate but may not be directly quantified due to the complex combination of the speed shear and directional shear.

The storm motion vector on the hodograph indicates that the rainstorm moved mainly west to northwest over southern Alberta during the event, and it was consistent with the motion of the rain clusters shown on radar images. The radar series suggests that the rain clusters initially moved north from Montana into southern Alberta, and migrated slowly west-northwestward thereafter. The initial northward motion of the rain clusters were steered by the mean southerly flow south of the border (refer to Fig 3-8). An exception was identified at 1200 UTC 6 June that the storm motion vector pointed to west-southwest, in which the evolution of radar echoes suggests that rain clusters remained nearly stationary or drifted slowly west over the southern Alberta foothills. One possible explanation is that the rainstorm's movement was blocked by the NW-SE orientated mountain range and the initially west-southwest motion of the rainstorm was detoured to west-northwest by the mountain range.

In summary, PVA and PTA reveal the major dynamics of synoptic forcing. The 500-hPa PVA significantly contributed to the uplift required for the heaviest rainfall on 7 June. Rainfall produced by the 850-hPa PTA ranged from zero up to about 60% of the observation throughout the event. The amount of vertical wind shear was interrelated with the rainfall rate. Heavy rainfall of the event was contributed synergistically by the 500-hPa PVA, the 850-hPa PTA and the vertical wind shear from the surface to the middle troposphere. The storm motion vector derived from the steering flow of the layer below 6 km AGL coincided with the direction of movement of the rainstorm.

3.5.2 Orographic forcing and orographic rainfall

As the underlying orography of Alberta has a significant influence on weather, it is valuable to quantify the orographic influence on large scale precipitation. The rising terrain from east to west in central and southern Alberta results in mechanically forced lifting when wind has a component perpendicular to the terrain's slope. The following section will examine the contribution of orographic lifting to the extreme rainfall event.

Based on the water budget at the cloud base and the vertical velocity forced by orographic lifting illustrated by equations *(2.3)* and *(2.6)*, an estimate of the orographic rainfall rate can be made when V, Q, E and the terrain slope are known. Substituting *(2.6)* into *(2.3)* yields

$$r_o = 3.6\ V\cos(\alpha-\beta)\ (\Delta z/\Delta x)\ Q\ E \qquad (3.1)$$

where r_o denotes the orographic rainfall rate. *(3.1)* implies that for a given precipitation efficiency, the orographic rainfall rate is proportional to the horizontal wind velocity V (when it has a component perpendicular to the terrain's slope), the slope of the terrain $\Delta z/\Delta x$, and the vapor content Q.

Employing the NCEP/NCAR reanalysis of wind and vapor content (derived from specific humidity) with an assumption that E is 90% in a uniform synoptic-scale precipitating system, we computed the horizontal vapor flux ($u\ Q$), the orographic rainfall rate at every 6 hours (0000, 0600, 1200, 1800 UTC) during the event, and

compared them with the observed mean synoptic rainfall rate at three ground locations. We also integrated the estimated orographic rainfall rates and compared them with the observed rainfall accumulation for each locations. Based on the average LCL (the level at which a parcel of moist air lifted dry-adiabatically from the surface would become saturated (Rogers and Yau 1989)) derived from the soundings (at Stony Plain, Alberta and Great Falls, Montana), we selected the 925-hPa level as the cloud base and used the 925-hpa horizontal wind and vapor content for orographic rainfall estimation. The three locations we selected are Sundre (1115 m ASL), Calgary (1084 m ASL) and Lethbridge (929 m ASL). The results are plotted on Figure 3-18 and 3-19.

Figure 3-18 shows that the time series of horizontal vapor flux at the 3 locations were similar. At Sundre, the vapor flux and the orographic rainfall rate were roughly in phase with the observed rainfall rate. At Calgary, the vapor flux was also roughly in phase with the observed rainfall rate except around 1200 UTC 7 June. At Lethbridge, the vapor flux and the orographic rainfall rate were mainly out of phase with the observation. Analysis of the radar imagery indicates that the peak rainfall at Lethbridge at 0600 UTC on 5 and 6 June was associated with the west-to-east moving systems, and this suggests that the precipitation occurring during that period was unlikely to have been affected by orographic lifting (with weak or absent upslope wind).

Generally, the time series of the vapor flux, orographic rainfall rate and observed rainfall rate on Figure 3-18 all show 3 major peaks during the event. The orographic rainfall rate was not well correlated with the observations. We know that each synoptic observation is an average over a 6 hour period, and the actual rainfall rate is often not evenly distributed within the period. Also, the observed rainfall includes water substance that is locally lifted to condense as well as that is transported from surrounding areas. Moreover, the orographically lifted water substance may not be reported as precipitation over the area that it originally forms (e.g. rain water may be transported out of the observed station). Thus, it is not surprising to see that the 6h orographic rainfall rate was not correlated well with the observation through time. Two of the local minima of the time series of the vapor flux (at 1200 UTC 6 June and after 1800 UTC 8 June) at 3

locations were well interrelated with the observation of least or no precipitation. The roughly in-phase horizontal vapor flux and observation at Sundre and Calgary suggest that the observed rainfall rate was proportional to the vapor influx during the event.

Figure 3-19 gives an illustration of the overall contribution of orographic lifting to the precipitation. It shows that the estimated orographic rainfall accumulation at each of the 3 locations over the entire period was near 50 mm, and the observed rainfall accumulation varied from 64 mm to 148 mm from the north to the south. The ratios of the estimated orographic rainfall to the observed rainfall are 78% for Sundre, 45% for Calgary, and 32% for Lethbridge. The average ratio of the above stations is about 52% suggesting that about half of the precipitation in southern Alberta came from orographic lifting when the precipitation efficiency was high (as assumed 90%).

Table 3-2 quantifies the contribution of orographic lifting to the measured mean precipitation of southern Alberta during the event. Apparently, at a minimum, 10% of the observed rainfall came from orographic lifting. The computed orographic rainfall rate exceeded the measured rainfall rate at 0000 UTC 6 June, which can be interpreted in relation to the fact that local deep convection was occurring (as shown by Fig. 3-2I g). On average, the ratio of the estimated orographic rainfall rate to the measured rainfall rate during the entire event is about 49%.

In summary, the influence of Alberta orography on precipitation was significant. The rainfall contributed by orographic lifting during the event was sustained. About half of the observed rainfall came from orographic lifting, and even more for the higher terrains.

3.5.3 State of the atmosphere and buoyant forcing

In order to further understand the state of the atmosphere during the extreme rainfall event and the contribution of thermodynamics to the rainstorm development, we analyzed the daily evolution of the tropopause height, ambient lapse rate and CAPE. The

tropopause height and CAPE were derived from the sounding of Great Falls, Montana which is the nearest sounding station that has a similar elevation to that of the southern Alberta foothills. The ambient lapse rate was the mean value derived from the soundings of Great Falls, Montana and Stony Plain, Alberta. The evolution of the tropopause height, ambient lapse rate, and CAPE along with the space-averaged 6h rainfall of southern Alberta during the extreme rainfall event is illustrated on Figure 3-20 (The space-averaged 6h rainfall was taken the same way as stated in section 3.4.2).

1) Tropopause height

The thickness of the troposphere is proportional to its mean temperature. A higher tropopause level indicates a thicker troposphere, and accordingly a higher mean tropospheric temperature. The evolution of the tropopause height (orange dashed line) on Figure 3-20a indicates that the tropopause level peaked prior to the rainfall peak (bright green curve), and dropped when the heavy rainfall began. The high tropopause prior to the heavy rainfall suggests a warm antecedent condition, and the lowering tropopause during the heavy rainfall suggests the existence of a cooling process that may be due to precipitation in the lower troposphere and the possible cold advection aloft.

2) Ambient lapse rate

The time series of the ambient lapse rate, representative of the atmospheric hydrostatic stability, is illustrated on Figure 3-20b. The blue dashed curve is the lapse rate of the lower layer 850-700 hPa ($\Gamma_{850\text{-}700}$), and the purple solid curve is that of the middle troposphere 700-500 hPa ($\Gamma_{700\text{-}500}$). With an average temperature of 5 to 15 C at 850 hPa, and -15 to -20 C at 500 hPa, the moist adiabatic lapse rate Γ_s is roughly $\Gamma_{s\_850\text{-}700} \approx 5.0$ C/km, and $\Gamma_{s\_700\text{-}500} \approx 6.6$ C/km (Holton 2004 provided an approximate observed value of ~ 4 C/km for the lower warm humid air mass and ~ 6-7 C/km in the middle troposphere). The two lapse rate series show that $\Gamma_{850\text{-}700}$ satisfied $\Gamma_{s\_850\text{-}700} \leq \Gamma_{850\text{-}700} < \Gamma_d$, where the dry adiabatic lapse rate, Γ_d, is approximately 10 C/km, and $\Gamma_{700\text{-}500}$ mostly satisfied $\Gamma_{700\text{-}500} \leq \Gamma_{s\_700\text{-}500}$. It suggests that the 700-500 hPa layer was saturated neutral in the early span of the extreme rainfall event (prior to 0000 UTC 6 June) and was nearly stable through out the rest of the event. The fluctuating curve of

$\Gamma_{850\text{-}700}$ with large departure from $\Gamma_{s\_850\text{-}700}$ suggests that the layer 850-700 hPa was conditionally unstable during the event. The evolution of the ambient lapse rate suggests that hydrostatic instability was limited to the lower troposphere during the event and provided a buoyant force for the ascent of the moist air within this layer.

3) CAPE

As CAPE is an index of the convective instability that can be used for evaluating the maximum buoyant (kinetic) energy for potential convection (refer to section 2.1.6), it is valuable to quantify the contribution of CAPE to the heavy precipitation that may be caused by deep convection. The CAPE values employed in this study were computed by the RAOB program and are plotted on Figure 3-20c. (Estimation of some small CAPE values that were not computed by the RAOB program was performed to make the data set completed.)

The evolution of CAPE (red dashed curve) indicates that a peak CAPE (1057 J/kg) occurred one day prior to the peak rainfall, and it was associated with the peak radar echoes of 55-60 dBz between 2250 UTC 5 June and 0000 UTC 6 June over Cardston. The measured rainfall rate at Cardston was just about 3 mm/h at 2300 UTC 5 June, but lightning was detected by the CLDN. The CAPE series shows very small values (nearly zero) during the heaviest rainfall episode. This was consistent with the neutral to stable ambient lapse rate at the middle troposphere during the event. The fact that convection (over the southwest Alberta as shown by high echoes on Fig. 3-2I g and extreme low cloud-top temperatures on Fig. 3-5I a, d) occurred one day before the heaviest rainfall and no convection during the heaviest rainfall episode suggests that CAPE was an instantaneous energy released in the beginning of the heavy rainfall, and convection was unlikely a major factor contributing to the extreme rainstorm case 2.

In summary, the thermodynamic parameters derived from the soundings suggest that a high tropopause level along with high PW (see section 3.4.2) prior to the heavy rainfall episode provided a warm moist antecedent condition for the event. The troposphere was saturated neutral to nearly stable at the middle level (700-500 hPa) and

conditionally unstable at the lower level (850-700 hPa). Conditional instability in the lower troposphere provided buoyant forcing for the extreme rainfall. High CAPE at the early stage and small CAPE during the heavy rainfall episode indicates that convection was instantaneous, and unlikely a primary factor contributing to the extreme rainfall.

3.6 Summary and concluding remarks for extreme rainstorm case 2

Extreme rainstorm case 2 during 5-9 June 2005 in southern Alberta was a large scale precipitation event which occurred under the combination of an ideal synoptic flow environment and orographic effects. Saturated neutrality to conditional instability of the middle and lower troposphere, and an abundant water vapor supply, provided essential conditions for the heavy rainfall. The synergizing of a slowly moving and interchanging synoptic scale quasi-stationary front/trough/trowal at the surface, a zonal trough or a convergence line in the middle and lower troposphere, a coupled quasi-steady cold low and blocking high above the middle troposphere, and diffluence in the upper troposphere, provided a long-lasting synoptic scale forcing for the uplift of moist incoming airflow to produce heavy precipitation. The 500-hPa PVA, coupling with the WAA and CAA at 700 hPa, plus leeward stretching of the cross-barrier flow, all contributed to the lee cyclogenesis and vertical motion, which ultimately reinforced the rainfall in the lee foothills. Weak PTA at 850 hPa plus wedged-in NTA from the northeast of the region further destabilized the moist atmosphere and dynamically reinforced the updraft for heavy precipitation. Vertical wind shear in the lower troposphere enhanced the precipitation during the heavy rainfall episode. Moisture-bearing easterly wind from the surface to the middle troposphere over southern Alberta was mechanically uplifted over increasing terrain, reinforcing the ascending motion and adding to the orographic rainfall in the foothills. About 50% of the accumulated rainfall over southern Alberta was attributed to orographic lifting. Convection was only contributing initially to the early rainfall on 5 June 2005.

Chapter 4: Study of the other 3 rainstorms during June 2005

4.1 Study of rainstorm case 1 (June 1-5)

4.1.1 Brief review of the case

Between 1 and 5 June 2005, the first rainstorm of the month passed over southern Alberta and produced a maximum rainfall accumulation of 140 mm to extreme southwest Alberta near Cardston. 2 June and 3 June were the heaviest rainfall days of this event (Fig. 4-1). A highest 24-hour rainfall of 49.5 mm and a secondary high one of 48.1 mm were recorded on 2 June at Milk River and Del Bonita, respectively. During the event, lightning and thunderstorms were recorded on 2 June from 1250 to 1400 UTC at Calgary and from 1820 to 2040 UTC at Lethbridge, on 4 June from 1710 UTC to 1830 UTC at Red Deer, and on 5 June from 0300 to 0400 UTC at Lethbridge. Due to the heavy rainfall, antecedent low water level of the streams in the Bow River and Oldman River basins increased to normal or slightly above normal level. This rainstorm relieved the dry spring condition and moistened the soil in the early summer season.

4.1.2 Organization and evolution of precipitation

The organization and evolution of the precipitation of rainstorm case 1 are shown on the sequences of composite CAPPI radar images on Figure 4-2 (I, II). On 1 June, a couple of narrow and elongated rain clusters developed and moved west-southwest towards the Alberta Rocky Mountains from central Saskatchewan and set up the event. Two parallel banded clusters indicated thundershowers over southern Alberta. One of the clusters (left of label "A" on Fig 4-2I a) developed into a squall line oriented NNE-SSW over Lethbridge-Drumheller-Vegreville (53.52°N 112.1°W) by 2100 UTC 1 June. The strongest echo reached 48 dBz at the leading edge of the squall line near Stettler (52.35°N 112.6°W) by 2300 UTC 1 June. Lighting was detected between 2150 UTC 1 June and 0110 UTC 2 June over where the squall line passed. A corresponding high rainfall rate of 9.8 mm/h was reported at 2200 UTC 1 June at Drumheller. Another

southwest-moving squall line ("D" on Fig 4-2I f, orienting NE-SW) passed over Calgary indicating thundershowers *(6h rain rate averaged about 1.8 mm/h)* from 1250 to 1410 UTC 2 June. By 1500 UTC 2 June, a larger cluster (above label "E" on Fig 4-2I f, g) swung southwest from central Saskatchewan and began to bring heavy precipitation to southern Alberta. Cluster E developed and split into two major clusters, which were labeled as "E1" remained over central Saskatchewan, and "E2" lying N-S over southeastern Alberta by 1800 UTC 2 June (Fig. 4-2I h). Rotational motion of the rain clusters around a loose centre between the E1 cluster and a new moving-in E3 cluster was evident from 1800 UTC 2 June to 0600 UTC 3 June. The centre is clearly seen on the midline between clusters E1 and E3 at 0000 and 0300 UTC 3 June. The rotation centre tracked south into central Montana after 0600 UTC 3 June (Fig. 4-2I l). A N-S oriented squall line developed at the leading edge of cluster E2 (Fig. 4-2I h, i). The 6h rain rate averaged about 2.3 mm/h, peaking at 10.7 mm/h in the area near Lethbridge from 1830 to 2040 UTC 2 June. While cluster E1 moved south of the province by 0300 UTC, cluster E3 together with some arriving smaller clusters developed into another large cluster over southern Alberta by 0600 UTC 3 June. Heaviest rainfall occurred between 1800 UTC 2 June and 0600 UTC 3 June when the rotational clusters reached the southern Alberta foothills. 6h rainfall rate of southern Alberta during this period ranged from 1.0 to 4.5 mm/h. During the entire event, all rain clusters slipped southeast parallel to the mountain ridge after they reached the southern Alberta foothills. The southeast-moving clusters gradually weakened along the foothills after 0600 UTC 3 June with large scale precipitation dissipating.

Scattered convection continued to spread over southern Alberta and slipped southeast along the foothills and plains regions throughout 4 June and early on 5 June. Figure 4-2II illustrates the evolution of the development of the convective clusters along the foothills at the early hours on 5 June. In the late afternoon and early evening hours LCT on 4 June, scattered small convective clusters began to develop over the plains and along the foothills of southern Alberta. By 0030 UTC 5 June, the scattered clusters merged and formed a larger cluster located south of Calgary (station ID of YYC on Fig 4-2II) with a linear convective band extending southeast, about 20 km northeast of

Claresholm (station ID of WDK). At this time, spots of high echoes of 45 dBz formed along the cluster's southeast-extruded section. By 0100 UTC, a new convection developed about 28 km northwest of Lethbridge (station ID of YQL) and merged into the large southeast-moving cluster (from north of Claresholm) by 0230 UTC. The merged cluster continued to track southeast with convection developing and propagating to the right at the leading edge of the cluster near Lethbridge. By 0400 UTC, another cluster developed over Pincher Creek (station ID of ZPC) also had significant convection on its leading edge. By 0430 UTC, the two convective clusters merged to form a small zonal squall line lying between Lethbridge and Pincher Creek. The maximum radar echoes reached 50 dBz at 0410, 0440 and 0530 UTC to the southwest, south and southeast of Lethbridge, respectively. This squall line then propagated southeast and gradually weakened over the next hour and a half. Lightning was detected over the southern foothills between 1800 UTC 4 June and 0630 UTC 5 June, and thunderstorms were reported between 0300 and 0400 UTC 5 June at Lethbridge. A peak precipitation rate of 23.5 mm/h was reported at 0600 UTC 5 June at the Lethbridge airport. The scattered heavy convective precipitation on 4 June and in the early hours on 5 June continued to add to the rainfall accumulation of the entire event.

In summary, several convective rain clusters moved from central Saskatchewan into central Alberta and then turned southwards into southern Alberta, bringing in periods of heavy rainfall. The precipitation varied from intermittent to continuous.

4.1.3 Overview of the synoptic flow pattern

Figure 4-3 depicts an overview of the synoptic circulations of typical levels over North America at 0000 UTC on 2 and 3 June 2005. On 2 June, a deep cutoff low was presented at both the 300- and 500-hPa levels, where the 300-hPa centre (of 9144 gpm) located over Idaho and the 500-hPa centre (of 5553 gpm) slanted to the northeast to be over the west Saskatchewan-Montana border. A trough of low pressure at 300 hPa trailing NE from the low centre extended to southern Saskatchewan. An Omega-shaped blocking high was presented over the north Canadian Prairies at both the 300- and 500-

hPa levels. There were also low centres presented at 850 hPa and the surface (sea-level), where the 850-hPa centre (of 1358 gpm) located over eastern Montana and the surface centre (of 999 hPa) lay over the west border of North and South Dakota. An inverted trough of the surface low extended to Yukon. Northerly surface wind was observed south of the inverted trough. Northeasterly upper wind blew over southern Alberta.

On 3 June, the 300-hPa low centre deepened by 10 gpm (to 9134 gpm) and moved northeast to be over the Saskatchewan-Montana border. The 500-hPa low centre deepened by 44 gpm and remained nearly stationary. Both the 850-hPa and the surface low centers deepened and tracked north to be over the Saskatchewan-Montana border. The deepening low centres at all levels reached their peak intensities and were nearly vertically stacked over each other at this time. Strengthening upslope flow due to a tightening pressure gradient of the deepening low was apparent. The time of straight superposition of the lows and strengthening upslope flow coincided with the peak rainfall episode of the event (refer to the green curve on Fig 4-5). The deep low rapidly weakened on 4 June with large scale precipitation dissipating.

In summary, Figure 4-3 shows a cutoff low coupling a blocking high at the upper levels, and an inverted trough at the surface east of southern Alberta during the event. The superposition of these two features provided synoptic forcing for heavy precipitation. The north to northeasterly wind over southern Alberta resulted in upslope flow adding to the ascending motion and orographic rainfall in the foothills region.

4.1.4 Moisture condition

Figure 4-4 shows the distribution of the 850-hPa specific humidity during the event. High specific humidity ($\geq$ 8.0 g/kg) was observed over southern Alberta and the surrounding area on 2-4 June. The peak specific humidity of 9.61 g/kg occurred at 0000 UTC 3 June, coinciding with the peak of rainfall. The distribution of the 850-hPa specific humidity suggests that vapor supply was abundant for the development of the

rainstorm during 1-5 June 2005. High moisture content over southern Alberta during the event was also indicated by the high precipitable water illustrated on Figure 4-5b.

4.1.5 Mechanisms contributing to the rainstorm

a) Contribution of PVA and PTA

Panel (a) on Figure 4-5 depicts the evolution of the 500-hPa vorticity advection and the 850-hPa temperature advection along with the time-space-averaged rainfall rate of 6 stations of southern Alberta during the event (the time-space-averaged rainfall rate is the mean rate of the 6h rainfall before and after 0000 (or 1200) UTC for 6 selected locations; selected stations are the same as those for rainstorm case 2 analysis). The figure indicates that the vorticity advection and the temperature advection were in phase and their peaks both occurred at 1200 UTC 2 June, about 6-12 hours prior to the highest rainfall. The peaks of the 500-hPa PVA and the 850-hPa PTA coincided with the occurrence of thunderstorms in southern Alberta (thunders reported between 1200 UTC 2 June and 0000 UTC 3 June at Calgary and Lethbridge). This suggests that the contributions of the 500-hPa PVA and the 850-hPa PTA were evident and in conjunction with convection at the early stage of the heavy rainfall episode.

b) Contribution of thermodynamics revealed by sounding parameters

Figure 4-5 (b, c, d) displays the time series of sounding parameters, which were derived from the Great Falls and Stony Plain soundings, along with the space-averaged 6h rainfall of 6 stations of southern Alberta during the event (methods refer to section 3.4.2, 3.5.3). Panel (b) shows that PW (green dashed curve) was relatively high (17-20 mm) during the event but had no significant peak corresponding to the peak of rainfall (green solid curve). The high PW suggests that ample antecedent water vapor allowed more latent heat to be released and high rainfall rate for convection at the early stage of the heavy rainfall episode. The curve of the tropopause height (orange dashed line) shows a local minimum in the mid course of the event right next to the peak of rainfall at 1200 UTC 3 June. The earlier high tropopause height accompanied by a high PW

implies a warm and moist antecedent condition. The subsequent lowering tropopause indicates that cooling was possibly caused by precipitation and cold advection aloft.

The sequence of ambient lapse rate $\Gamma_{850\text{-}700}$ on panel (c) indicates that the lower troposphere was mainly conditionally unstable throughout the event as it satisfied $\Gamma_{s\_850\text{-}700} < \Gamma_{850\text{-}700} < \Gamma_d$ (see section 2.1.6). The sequence of $\Gamma_{700\text{-}500}$ suggests a nearly saturated neutral to stable middle troposphere through most the event as it satisfied $\Gamma_{700\text{-}500} \leq \Gamma_{s\_700\text{-}500}$. It implies that conditional instability was limited in the lower troposphere during the event and provided buoyant force for the ascent of moist air within this layer.

The evolution of CAPE (red dashed line) on panel (d) indicates that CAPE remained relatively small during the event. It shows no CAPE peak corresponding to the rainfall peak. This implies that convective instability was unlikely a major factor triggering the heavy rainfall and convection contributed very little to the rain amount during the heaviest rainfall episode on 2-3 June. Scattered convection became relatively active when CAPE increased towards the end of the event.

4.1.6 Summary and concluding remarks for rainstorm case 1

Rainstorm case 1 during 1-5 June 2005 in southern Alberta was produced by a few southwest-moving elongated and intense rain clusters. Three large rain clusters (labeled as E1, E2 and E3 on the radar images) gave the heaviest rainfall to extreme southwest Alberta during 2-3 June. The rainstorm occurred under the combination of a favorable synoptic flow environment and orographic effects. A deep low pressure located to the east of southern Alberta produced strong north to northeasterly wind and resulted in substantial upslope flow in the southern foothills, reinforcing the ascending motion and adding to the orographic rainfall. Warm moist anteceding conditions and ample water vapor supply during the event were apparent. Contributions of the 500-hPa PVA and the 850-hPa PTA to the heavy rainfall were evident, and they were associated with convection at the early stage of the event. Free convection contributed little to the total precipitation accumulation.

4.2 Study of rainstorm case 3 (June 16-19)

4.2.1 Brief review of the case

Between 16 and 19 June 2005, the third rainstorm of the month affected southern and central Alberta. This rainstorm produced a maximum accumulated rainfall of 152 mm. It gave a highest 24-hour rainfall of 128.4 mm on 17 June at Springbank and a secondary high one of 114.9 mm on 18 June at Bow Valley. 17 June and 18 June were the heaviest rainfall days of the event (Fig. 4-6). Lightning and thunderstorms occurred at Calgary and Lethbridge on 17-18 June. Brief hailfall during lightning and thunderstorms were reported at the Medicine Hat airport on 18 June. Heavy rainfall of the rainstorm badly hit the Red Deer River and upper Bow River basins. Overflow and bank burst of the streams and rivers in the above basins caused the second extensive flood of the month.

4.2.2 Organization and evolution of precipitation

The organization and evolution of rainstorm case 3 are illustrated on the sequences of composite CAPPI radar images on Figure 4-7(I, II). On 16 June, scattered rain clusters began to bring showers to southern Alberta prior to the major precipitating system. By 0000 UTC 17 June, the major precipitating system with leading edge of convection began to develop to the south of Alberta. By 0050 UTC, convection that embedded in cluster A1 (Fig. 4-7I a) propagated north into Lethbridge and the Milk River basin when the cluster tracked northeastward (echoes peaked at 50 dBz). Lightning and thunderstorms from the convective cluster were reported at Lethbridge between 0100 and 0330 UTC 17 June. Rainfall rate of 7.5 mm/h and 19.3 mm/h were recorded at 0200 UTC 17 June (2000 LCT 16 June) at Lethbridge and the town of Milk River, respectively. Cluster A1 and the arriving A2 merged to form one large cluster by 0800 UTC 17 June (refer to Fig 4-7I d) and pushed northward for the next 6 hours. The merged cluster then weakened and separated into sections A1 and A2 again by 1500

UTC 17 June (Fig. 4-7I f). Cluster A1 tracked west towards the central Alberta foothills and remained nearly stationary over the area for the next day. In the meantime, a zonal elongated cluster B developed south of the province and tracked north. Cluster B merged into cluster A1 and enhanced over the central Alberta foothills by 2200 UTC 17 June (refer to Fig 4-7I h, i). By 2100 UTC 17 June, a large convective cluster group (labeled as "C" on Fig 4-7I h-l) with high echoes (peaking at 50 dBz) began to develop over southern Alberta giving the highest rainfall rate during the event (6h-space-averaged rainfall rate at 0000 UTC 18 June was 3.28 mm/h). The cluster group became well organized and combined to be a large cluster by 0300 UTC 18 June when it tracked further north with the embedded convection weakening. The west end of the large cluster C merged into cluster A1 early on 18 June and enhanced the precipitation in the foothills. Cluster A1 remained nearly stationary over the area until 1500 UTC 18 June. It then separated into two sections with the south one (D1) remained west of Calgary, and the north one (D2) slowly drifted north and weakened over central Alberta. Cluster D2 continued to give moderate precipitation to central Alberta until it finally weakened and turned southeast away by 0600 UTC 19 June (images omitted).

Figure 4-7II provides a closer look at the evolution of the convection within cluster group C between 2100 UTC 17 June and 0230 UTC 18 June (1500-2030 LCT on 17 June). By 2100 UTC 17 June, there were quite a few scattered convective clusters distributed between Lethbridge and Medicine Hat (station ID of YXH). A squall line also developed southwest of Milk River (station ID of MRY). When slowly moved northeast, the scattered convective clusters became well organized and formed three radial squall lines with echoes peaking at 50-60 dBz by 2300 UTC 17 June. The squall line over Medicine Hat remained nearly stationary for two and a half hours before drifting northeast away. It produced heavy thunderstorms with hailfall to the area between 2240 and 2300 UTC. Counter clockwise rotating wall cloud to the south of the station was also reported during the time of hailfall. Convection within cluster group C weakened by 0300 UTC 18 June when it moved northeast away from southeastern Alberta. Convection during the evening hours (LCT) produced locally high rainfall rates in the southern region. A rainfall rate of 15 mm/h was recorded at 2200 UTC 17 June at

Lethbridge, 23.8 mm/h at 2300 UTC 17 June and 18 mm/h at 0000 UTC 18 June were recorded at Medicine Hat, and 15 mm/h was recorded at 0200 UTC 18 June at Oyen (51.38°N 110.35°W).

In summary, rainstorm case 3 had two major intervals with the first one from 0000 to 1800 UTC 17 June and the second one from 1900 UTC 17 June to 0600 UTC 19 June. Heavy rainfall was produced by several large north-moving rain clusters with significant convection at the early stage of each span.

4.2.3 Overview of the synoptic flow pattern

Figure 4-8 depicts an overview of the synoptic circulations of typical levels over North America at 0000 UTC on 17 and 18 June 2005. On 17 June, a deep cutoff low located offshore of Oregon straightly stacked one over another. A ridge of high pressure at the upper levels (300- and 500-hPa) extended northwest over southern and central-west Alberta. Diffluence south of the ridge was presented both at the 300- and 500-hPa levels over southwest Alberta and the Northwest U.S. Another low pressure centered under the diffluence over the cross border of Idaho-Oregon-Nevada at 850 hPa (central geopotential height of 1394 gpm) and the surface (sea-level central pressure of 998 hPa). The prevailing east-southeast flow over southern Alberta was evident.

On 18 June, the cutoff low drifted east-southeast closer to the shoreline and slightly weakened. An upper trough initially trailing south from the cutoff low centre rotated north with its tail latitudinally lying just south of the Alberta-Montana border. The upper-level diffluence ahead of the trough persisted over southern Alberta. The 1394 gpm low at 850 hPa crossed to the lee of the Rocky Mountains with the centre deepened to be 1363 gpm over the cross border of Alberta-Saskatchewan-Montana. The corresponding surface centre (992 hPa) also deepened and moved to be over the Montana-Wyoming border. An inverted trough extended north then west from the surface low centre lying over southern Alberta. The inverted trough was also presented

at 850 hPa. Easterly flow north of the trough was evident in the central Alberta foothills where highest event rainfall accumulation and peak 24-hour rainfall were recorded.

In summary, the synoptic circulations during the event suggest that a deep offshore cutoff low and diffluence at upper levels, lee cyclone intensification and an inverted trough at the lower levels combined together to give an ideal synoptic environment that produced persistent convergence and the conjunctive uplift at the lower levels over central and southern Alberta for the heavy rainfall case during 16-19 June 2005. The sustained easterly wind at the lower levels over central Alberta resulted in substantial upslope flow adding to the ascending motion and orographic rainfall for the foothills.

4.2.4 Moisture condition

Figure 4-9 shows the 850-hPa specific humidity distribution during the rainstorm. It indicates that a moist tongue (specific humidity $\geq$ 8.0 g/kg) was presented from central U.S. to southeastern BC and central Alberta during 17-18 June. The highest vapor content (specific humidity $\geq$ 10.0 g/kg) was presented over southern Alberta at 0000 UTC on 18 June coinciding with the peak rainfall episode. The decreasing vapor content on 19 June corresponded with the dissipation of precipitation. This suggests that high vapor content was associated with high rainfall, and water vapor supply was abundant for the development of rainstorm case 3. With their back trajectory model, Dupilka et al (2007) identified that the vapor source for this event was from the Canadian Prairies, the Midwest U.S., and the Pacific Oceans.

4.2.5 Mechanisms contributing to the rainstorm

a) Contribution of PVA and PTA

Panel (a) on Figure 4-10 depicts the evolution of the 500-hPa vorticity advection and the 850-hPa temperature advection along with the time-space-averaged rainfall rate of 6 stations of southern Alberta during the event (method refer to section 4.1.5). The

figure indicates that there were two peaks of the 500-hPa PVA associated with the peaks of precipitation. The in-phase 500-hPa PVA with the rainfall rate implies that the 500-hPa PVA contributed to the heavy rainfall. The curve of the 850-hPa temperature advection shows one small crest in between the two rainfall peaks and no significant PTA during the heavy rainfall episode. This may suggest that the 850-hPa PTA was unlikely a factor contributed to the heavy rainfall during this event.

b) Contribution of thermodynamics revealed by sounding parameters

Figure 4-10 (b, c, d) displays the time series of sounding parameters, which were derived from the Great Falls and Stony Plain soundings, along with the space-averaged 6h rainfall of 6 stations of southern Alberta during the event (methods refer to section 3.4.2, 3.5.3). Panel (b) shows that PW (green dashed curve) was relatively high ($\geq$ 20 mm) at the early stage (1200 UTC 16 June to 0000 UTC 18 June) and decreased abruptly later in the period. This suggests an ample antecedent vapor supply allowing more latent heat to be released and high rainfall rate for convection during the heavy rainfall episode. The tropopause (orange dashed line) was also relatively high (mostly $\geq$ 10 km) throughout the event. High PW at the early stage of the event combined with high tropopause implies a warm moist antecedent condition for the heavy rainfall.

The sequence of ambient lapse rate $\Gamma_{850\text{-}700}$ on panel (c) indicates that the lower troposphere was conditionally unstable throughout the event as it satisfied $\Gamma_{s\_850\text{-}700} < \Gamma_{850\text{-}700} < \Gamma_d$ (see section 2.1.6). The sequence of $\Gamma_{700\text{-}500}$ indicates a nearly saturated neutral middle troposphere through most the event as it satisfied $\Gamma_{700\text{-}500} \approx \Gamma_{s\_700\text{-}500}$. The evolution of ambient lapse rate of the low and middle troposphere suggests that conditional instability was limited in the lower troposphere during the event and provided buoyant force for the ascent of the moist air within this layer.

The evolution of CAPE on panel (d) displays high CAPE values at the early stage of the event and it was associated with vigorous convection in southern Alberta. The figure shows a CAPE of 1043 J/kg peaked by 12 hours prior to the major crest of the space-averaged 6h rainfall and a CAPE of 556 J/kg during the peak of rainfall. This

suggests that vigorous convection was characteristic of rainstorm case 3 and convective rainfall contributed to the total accumulation of this event.

4.2.6 Summary and concluding remarks for rainstorm case 3

Rainstorm case 3 during 16-19 June 2005 in central and southern Alberta was produced by a few intense north-moving rain clusters with vigorous convection. Group clusters developed on late 17 June and early 18 June gave the heaviest rainfall. The rainstorm occurred under the combination of an ideal synoptic flow environment and orographic effects. A deep cutoff low located to the west with an upper diffluent flow to its east, and the consequent lower-level lee cyclone intensification to the southeast of Alberta resulted in persistent convergence and the conjunctive uplift at the lower levels over central and southern Alberta. Easterly wind (north of an inverted trough over southern Alberta) resulted in upslope flow, reinforcing the ascending motion and adding to the orographic rainfall in the foothills. The water vapor supply for the event was abundant. High PW plus high tropopause at the early stage of the event suggests a warm moist antecedent environment for potential convection. The 500-hPa PVA contribution was evident. Convective instability significantly contributed to the heavy rainfall.

4.3 Study of rainstorm case 4 (June 27-29)

4.3.1 Brief review of the case

Between 27 and 29 June 2005, the fourth rainstorm of the month struck southern Alberta again. A peak rainfall accumulation of 90 mm was recorded near Highwood. This rainstorm produced a highest 24-hour rainfall of 59.8 mm at Cop Upper on 28 June and a secondary high one of 57.7 mm at Beaver Mines on 27 June (Fig. 4-11). The rainstorm re-hit the lower Bow River basin and the upper Oldman River basin, which experienced the previous two floods, and induced a third flood within the month. High River and Okotoks were the towns that suffered three floods in a month.

4.3.2 Organization and evolution of precipitation

Figure 4-12 displays the organization and evolution of the major precipitation span of rainstorm case 4 with the selected composite CAPPI radar images. On 27 June, precipitation over central and southern Alberta was mainly produced by scattered cross-barrier north-moving clusters (distribution was similar to that shown on Fig. 4-12a), which stayed over the mountain ridge (pink background on the images) and along the southern foothills. These slow-moving clusters briefly gave moderate rainfall (a peak of 3.5 mm/h recorded at Milk River at 1400 UTC 27 June) to the area. On 28 June, a huge precipitating system developed in the Northwest U.S. and moved northeast into southern Alberta by 0000 UTC. The broad NW-SE oriented cluster was clearly presented at 0300 UTC along the mountain ridge (Fig. 4-12b). It slowly swung north within the next 18 hours with its west end remained nearly stationary over the southern foothills (Fig. 4-12 c to h). Echoes of 45-50 dBz occurred between 0300 and 1800 UTC in the core of the cluster where a highest rainfall rate was recorded (mean rate ranged from 2.0 to 6.4 mm/h between 0000 and 1200 UTC with a peak of 17.3 mm/h at Milk River at 0400 UTC). Lightning was briefly detected in extreme southern Alberta and isolated thunderstorm was reported at Lethbridge at 0400 UTC. After 1800 UTC, the broad cluster gradually shrank and rotated south around a weak centre about 50 km west of Medicine Hat. Precipitation gradually lessened while the cluster dissipated after 0300 UTC 29 June (images skipped).

In summary, the major high rainfall span of rainstorm case 4 occurred between 0300 UTC 28 June and 0300 UTC 29 June. The rainfall was mainly produced by a huge north-moving elongated cluster that developed south of Alberta. Scattered rainfall prior to the influence of the huge cluster also added to the total accumulation of this event.

4.3.3 Overview of the synoptic flow pattern

Figure 4-13 depicts an overview of the synoptic circulations of typical levels over North America at 1200 UTC on 27 and 28 June 2005. On 27 June, a deep long

wave trough with a few embedded short wave troughs was presented at both the 300- and 500-hPa levels over western North America. A low centre of 5621 gpm at 500 hPa was located over Washington and a closed low of 1432 gpm at 850 hPa was positioned well beneath the 500-hPa low. A high pressure area at the surface covered the Northwest Territories and the Canadian Prairies. Easterly flow south of the high pressure prevailed over southern Alberta. On 28 June, a cutoff low developed in the long wave trough at 300 hPa over the cross-border of Idaho-Washington-Oregon, and stacked well above the 500-hPa low. A diffluent flow at 300 hPa east of the cutoff low was presented over southern Alberta and Montana. The 850-hPa low centre tracked east to be lying over the Alberta-Montana border. In the meantime, a surface lee cyclone developed underneath the 850-hPa low centre and the 300-hPa diffluent region, reinforcing the lower-level upward motion and the consequent rainfall. Strengthening easterly wind north of the developing cyclone resulted in upslope flow adding to the upward motion for orographic rainfall in the southern Alberta foothills. The occurrence of lee cyclogenesis coincided with the heaviest rainfall episode of the event.

The synoptic circulation pattern during the event suggests that a deep long wave trough with development of a cutoff low and presence of diffluence at the upper levels, combined with surface lee cyclogenesis was the synoptic environment for the development of rainstorm case 4. Easterly wind enhanced the upward motion over the southern Alberta foothills adding orographic rainfall to the total precipitation.

4.3.4 Moisture condition

Distribution of specific humidity at 850 hPa at 0000 UTC during rainstorm case 4 is displayed on Figure 4-14. It indicates that a moist tongue (specific humidity $\geq$ 6.0 g/kg) extended from the Northwest U.S. to Yukon covering central and southern Alberta during 27-29 June. Higher vapor content (specific humidity $\geq$ 8.0 g/kg) persisted over central and southern Alberta on 28-29 June. The persistence of higher vapor content coincided with the high rainfall span (0000 UTC 28 June - 0000 UTC 29 June). The 8.0 g/kg contour retreated southeast of Alberta later on 29 June (1200 UTC), and this was

corresponding to the dissipation of precipitation. High specific humidity over most regions of Alberta and the surrounding areas during the event indicates that vapor supply was abundant for the development of this rainstorm.

4.3.5 Mechanisms contributing to the rainstorm

a) Contribution of PVA and PTA

Panel (a) on Figure 4-15 depicts the evolution of the 500-hPa vorticity advection and the 850-hPa temperature advection along with the time-space-averaged rainfall rate of 6 stations of southern Alberta during the event (method refer to section 4.1.5). It indicates that the 500-hPa vorticity advection and 850-hPa temperature advection were in phase and their peaks both occurred at 0000 UTC 28 June, about 6 hours prior to the peak of rainfall (which was at 0600 UTC 28 June). The peaks of the 500-hPa PVA and the 850-hPa PTA were also corresponding to the time of isolated convection in extreme southern Alberta. It is evident that the 500-hPa PVA and the 850-hPa PTA were associated with isolated convection at the early stage of the event and contributed to the heavy rainfall to some extent.

b) Contribution of thermodynamics revealed by sounding parameters

Figure 4-15 (b, c, d) displays the time series of sounding parameters, which were derived from the Great Falls and Stony Plain soundings, along with the space-averaged 6h rainfall of 6 stations of southern Alberta during the event (methods refer to section 3.4.2, 3.5.3). Panel (b) shows that PW was high at the early stage of the event ($\geq$ 20 mm) with a peak about 6 hours before the rainfall crest. This suggests that antecedent water vapor supply was ample allowing high latent heat to be released for convection and high rainfall rate. Panel (b) also indicates a higher tropopause ($\geq$ 10.5 km) prior to and at the early stage of the event, with lowering height ($<$ 10 km) following the rainfall peak. The evolution of PW and tropopause height suggests there was a warm moist antecedent condition for the development of rainstorm case 4.

The sequence of ambient lapse rate $\Gamma_{850\text{-}700}$ on panel (c) indicates that the lower troposphere was mainly conditionally unstable throughout the event as it satisfied $\Gamma_{s\_850\text{-}700} < \Gamma_{850\text{-}700} < \Gamma_d$ (see section 2.1.6). The sequence of $\Gamma_{700\text{-}500}$ suggests a nearly saturated neutral middle troposphere through most the event as it satisfied $\Gamma_{700\text{-}500} \approx \Gamma_{s\_700\text{-}500}$. The evolution of the ambient lapse rate of the lower and middle troposphere suggests that conditional instability was limited in the lower troposphere during the event and provided buoyant force for the ascent of the moist air within this layer.

The evolution of CAPE on panel (d) indicates that there was a peak CAPE value (423 J/kg) about 6 hours prior to the rainfall crest. This coincided with the occurrence of isolated lightning and a thunderstorm in extreme southern Alberta. It suggests that convective instability contributed little to the heavy rainfall and convection was localized and unimportant except at the early stage of the high rainfall span.

4.3.6 Summary and concluding remarks for rainstorm case 4

Rainstorm case 4 during 27-29 June 2005 in southern Alberta was mainly produced by a huge and intense north-moving elongated rain cluster. The rainstorm occurred under the combination of a favorable synoptic flow environment and orographic effects. A deep long wave upper trough with development of a cutoff low, presence of upper-level diffluence and surface lee cyclogenesis to the south all together comprised the synoptic background for the development of the rainstorm. Strengthening easterly wind north of the lee cyclone resulted in upslope flow, reinforcing the ascending motion and adding to the orographic rainfall in the southern foothills. There was a warm moist antecedent condition and ample water vapor supply for the development of the heavy rainfall. Contributions of the 500-hPa PVA and the 850-hPa PTA were apparent and were in connection with isolated convection at the early stage of the event. Convective instability contributed little to the total precipitation accumulation.

Chapter 5: Comparison of the four rainstorms

5.1 Introduction

It is of interest to identify similarities and differences between the four successive Alberta rainstorms of June 2005, as regards the regional meteorological setting and the local details. Three of the four influencing precipitating systems came from the Northwest U.S., one from central Saskatchewan. The peak event rainfalls of the four rainstorms all occurred along the Alberta foothills. Warm moist antecedent condition and embedded convection at the early stage of or during each event were the common features of the four rainstorms. Table 5-1 summarizes some of the meteorological parameters of the four heavy rainfall cases.

5.2 Comparison of the surface weather systems

All four heavy rainfall cases had occurrence of lee cyclone genesis or intensification at the surface that extended to 700 hPa (Table 5-1). Figure 5-1 depicts the characterized sea-level circulations of the highest rainfall days of the four rainstorms. Four intensified or developed cyclones were all located to the east or southeast of southern Alberta. All inverted troughs of these lows extended west or northwest across southern Alberta. The lee cyclone centers of case 2 and case 4 were close and the peak event rainfall regions of these two cases were close too. East, or north to northeast low-level wind over central and southern Alberta was apparent for all four cases. By comparing the total event rainfall distribution (Fig. 1-1), it is evident that the peak event rainfall of each case occurred in the region where upslope flow was presented in the northwest quadrant of the lee cyclone.

5.3 Comparison of the upper air circulations

By comparing the upper air circulations of the four rainstorms, we find some common characteristics as follow: cutoff cold lows at 500 hPa were presented in all four

cases, diffluent flow at 300 hPa over southern Alberta occurred in three of the four cases (cases 2, 3, 4); blocking-highs were presented at both the 300- and 500-hPa levels over northern Alberta in the first two cases that had longer duration. However, the origins, tracks and the central minimum geopotential heights of the four 500-hPa cutoff cold lows were distinctive (Fig. 5-2). The cutoff lows of the later three cases originated from the southwest or northwest of Alberta at different distances, and the one of case 1 originated from the southeast. The track of the cutoff low of case 1 was mostly northward, the one of case 3 was mostly southward, and the ones of case 2 and case 4 were mostly from west to east, touching the southern edge of Alberta.

In case 1, the cold low developed in the Midwest U.S. and drifted north then remained nearly stationary over southern Saskatchewan during the peak rainfall episode. The low reached its maximum intensity (with a min. height of 550 dam) at 1200 UTC 2 June, about 12 hours prior to the rainfall crest. The low weakened on 4 June and tracked northeast away from the area with rain lessening. The peak event rainfall area was located about 450 km west of the cold low.

In case 2, a primary cold low developed offshore of BC and tracked southeast to be over Oregon. The primary low reached its maximum intensity (with a min. height of 543 dam) at 1200 UTC 5 June, about 48 hours prior to the rainfall crest. A secondary split-off low developed in the lee of the Rocky Mountains over western Montana late on 7 June, associating with the peak rainfall episode. The secondary low tracked southeast and then northeast away on 8-9 June after briefly staying near the southern Alberta foothills. The primary low crossed the mountains and weakened east of Alberta with precipitation dissipating on 9 June. The peak event rainfall area was located about 800 km northeast of the primary cold low.

In case 3, a primary cold low developed further offshore of BC and tracked southeast then south to stay offshore of the middle U.S. west coast. The primary low reached its maximum intensity (with a min. height of 542 dam) between 1200 UTC 16 June and 0000 UTC 17 June, about 24 hours prior to the rainfall crest. A secondary split-

off low developed in the lee of the Rocky Mountains over southern Alberta late on 18 June, associating with the peak rainfall episode. The secondary low tracked northeast away on 19 June after briefly staying near the southern Alberta foothills. The peak event rainfall area was located about 1200 km northeast of the primary cold low.

In case 4, the cold low originated in Alaska. It tracked southeast along the BC coast to Washington, and then moved east-northeast across the Rocky Mountains to southern Alberta during the heavy rainfall episode. The low reached its maximum intensity (with a min. height of 561 dam) at 1200 UTC 27 June, about 18 hours prior to the rainfall crest. The low finally moved rapidly southeast then northeast away from Alberta with precipitation dissipating late on 29 June. The peak event rainfall area was located about 600 km northeast of the cold low.

It is interesting to note that there were occurrences of a split-off secondary low in case 2 and case 3, in which the primary low had lower central geopotential height associating with higher event rainfall; the similar tracks of case 2 and case 4 associated with similar locations of the peak event rainfalls (Fig. 1-1).

5.4 Water vapor supply for the four rainstorms

By comparing the distributions of the 850-hPa specific humidity of the four rainstorms (Fig. 3-12, 4-4, 4-9, 4-14), we find that moist centers or tongues of high specific humidity ($\geq$ 8.0 g/kg) were presented over central and southern Alberta on the peak rainfall days in all four cases. The highest specific humidity ($\geq$ 10.0 g/kg) presented over southern Alberta in case 3 at 0000 UTC 18 June was associated with the extreme 6h-space-averaged rainfall rate of 3.28 mm/h (see Table 5-1 and its footnote), which is the highest rainfall rate among the four cases. A common feature of the moisture distributions of the four cases is that there existed a major high vapor content center located in the Midwest U.S. with a tongue ($\geq$ 6.0 g/kg) extended into BC and the Canadian Prairies, sometimes even further north to Yukon. There also existed a secondary high vapor center over the Northwest U.S. in the Idaho-Montana-Wyoming

area in the later three cases. The distributions of the 850-hPa specific humidity indicate that moisture supply for the four rainstorms was abundant, and the source region was likely mainly from the Midwest U.S.

5.5 Contributions of PVA and PTA

Figure 5-3 shows the evolution of the 500-hPa vorticity advection and the 850-hPa temperature advection of the four rainfall cases. The peak values of the 500-hPa PVA and the 850-hPa PTA and their occurrence time in each case are summarized in Table 5-1. One common feature of the four cases is that the 500-hPa PVA were in phase with (cases 2 and 3) or peaked about 6-12 hours prior to (cases 1 and 4) the rainfall crests. It is evident that the 500-hPa PVA contributed to all four rainfall cases, but had no significant linear correlation. The time series of the 850-hPa temperature advection of the four cases indicates that the 850-hPa PTA peaked about 6-12 hours prior to the rainfall crests except in case 2. This suggests that contribution of the 850-hPa PTA to the heavy rainfall was not guaranteed to be high.

5.6 Contribution of thermodynamics

To see the overall contribution of thermodynamics to the four rainstorms in June 2005, we plotted the time histories of the previously discussed sounding parameters along with the sequence of the space-averaged 6h rainfall of the month on Figure 5-4 (a, b, c). Panel (a) shows that all rainfall cases occurred within the crests of PW, with the first two cases occurring within the same crest. A period of no or least rainfall associated with very high PW can be identified during 21-23 June. By comparing the mean PW of the four cases (Table 5-1), it shows that the higher the PW was presented, the lesser the rainfall recorded, and vice versa. This interesting result suggests that high PW was an essential condition for heavy rainfall but not sufficient to determine the rainfall amount. Higher rainfall with lower PW implies that rain water were likely contributed by moisture advection from distance sources.

Panel (b) shows the sequence of the ambient lapse rate of June 2005. It suggests that the lower troposphere (850 to 700 hPa) was mainly conditionally unstable through out the month ($\Gamma_{s\_850\text{-}700} < \Gamma_{850\text{-}700} < \Gamma_d$), while the middle troposphere (700 to 500 hPa) was mostly moist neutral to nearly stable ($\Gamma_{850\text{-}700} \leq \Gamma_{s\_850\text{-}700}$) through out the month. Four heavy rainfall cases all occurred on the days when the middle troposphere was nearly moist neutral and the lower troposphere was conditionally unstable.

Panel (c) shows the sequence of CAPE during June 2005. Four major crests can be identified. The peak values of CAPE and their occurrence time during each event are summarized in Table 5-1. It shows that three of the four heavy rainfall cases were associated with higher CAPE (of 423 J/kg or larger), and CAPE peaked about 6 to 24 hours prior to the peak rainfall episodes. Though the CAPE value (of 556 J/kg) in the third rainstorm was not the highest one among the four cases, vigorous convection during the heavy rainfall episode produced a highest extreme 6h-space-averaged rain rate (Table 5-1) of the four rainstorms. High CAPE (of 1511 J/kg) was associated with high PW during 21-23 June but accompanied by no or least precipitation. The time history of CAPE implies that CAPE contributed to heavy rainfall to some extent in the four Alberta rainstorms, but it is not the only criterion to determine the uplift for producing high rainfall.

Chapter 6: Summary and Conclusions

6.1 Summary of the cases and research project

The four consecutive heavy rainfall cases occurring in Alberta during June 2005 were synoptic scale precipitation events, with three of them causing floods in central and southern Alberta. Case 2 was the extreme one in terms of its rainfall accumulation and flood damage. Three of the four events were produced by rainstorms developed south of the U.S. border, while one developed east of Alberta. Embedded convection was characteristic of all four rainfall cases, but contributed little to the total rain amount of each case. Convection in rainstorm case 3 was vigorous, producing the highest extreme 6h-space-averaged rainfall rate, brief hailfall and rotating wall clouds.

In the light of the destructive capability of flood-producing rainstorms, it is important to understand the potential of the occurrence of heavy rainfall and issue timely warnings to the public. The principal objectives of this study were twofold: 1) to find out the main mechanisms contributing to the extreme rainfall that caused severe flooding in Alberta on 5-9 June 2005, and 2) to attempt to discover the similarities and differences of meteorological conditions for the development of the four Alberta rainstorms during June 2005. In addition, to document the synoptic flow pattern and the associated dynamical/physical mechanisms of the four characteristic rainstorms is useful for improving our scientific understanding of the development environment and mechanisms of the flood-producing rainstorms. The result of this investigation will likely provide a valuable reference for preparing weather predictions for future potential flood-producing rainfall events in Alberta.

In this study, detailed analyses of the organization and evolution of the precipitating system, synoptic flow environment and the associated dynamics, thermodynamics, orographic effects on precipitating systems, and moisture condition of the four Alberta rainstorms were carried out to achieve our objectives. Employing radar and satellite images, weather maps, soundings and available reanalysis data, I analyzed

these rainstorms in 3 dimensions: time evolution of the systems, horizontal flow circulation, state and instability of the atmosphere. Particularly detailed analyses of synoptic circulations and estimates of orographic rainfall were made for the extreme rainfall case which occurred during 5-9 June 2005 in southern Alberta. A comprehensive review was made to exhibit the similarities and differences of the four rainstorms.

6.2 Conclusion

6.2.1 Flow environment

The weather map analysis shows that a sea-level quasi-stationary inverted trough or trowal lying lee of the Rocky Mountains was a common feature for the four events. Despite of the differences in location and intensity, lee cyclone genesis or intensification occurred in all four cases at the surface in the inverted trough or trowal, and extended into the 700-hPa level. It was evident that east, or north to northeast low-level wind over central and southern Alberta resulted in upslope flow, reinforcing the ascending motion and adding to the orographic rainfall in all four cases.

The weather map analysis also indicates that short wave troughs and cutoff cold lows at 500 hPa were associated with the four rainstorms. A cutoff low coupling a blocking high at 500 hPa and the levels above was presented over western North America in case 1 and case 2 which had longer event durations. The origins, intensities, and paths of the primary cold lows of the four cases were distinctive. The intensity of the cold low was interrelated to the extreme 6h-space-averaged rainfall rate of each case. The deeper the cold low, the higher the extreme 6h-space-averaged rainfall rate recorded. The paths of the cold lows of case 2 and case 4 that had close peak event rainfall locations were similarly from west to east. The moving speed of the cold low was correlated to the event duration and rainfall accumulation. A slower moving cold low was associated with longer event duration and a higher accumulation, and vice versa. A split-off secondary low at 500 hPa on the lee of the Rocky Mountains was characteristic of case 2 and case 3 that produced the highest and secondary highest event rainfall.

Upper tropospheric diffluence (at 300 hPa and above) over southern Alberta and the Northwest U.S. was significant in three of the four cases (cases 2, 3, 4), which had the 500-hPa primary cold lows originating from the southwest or northwest of Alberta.

Although there were various characteristics, the synoptic flow environments of the four rainstorms provided favorable conditions that dynamically supported the lifting required for heavy precipitation.

6.2.2 Dynamics, thermodynamics and physical mechanisms

The upper level (300 hPa) diffluence provided dynamic support for the vertical motion required for heavy precipitation in three of the four events (cases 2, 3, 4). Detailed analysis of extreme rainstorm case 2 suggests that horizontal cyclonic wind shear and convergence near the trough lines in the lower to middle troposphere (below 500 hPa) also provided strong dynamic support for the heavy rainfall. Vertical wind shear in the lower troposphere dynamically enhanced the precipitation.

Discussion in previous chapters indicates that the 500-hPa PVA contributed to lee cyclogenesis and vertical motion reinforcing the precipitating system. In all four cases, the peaks of the 500-hPa PVA were presented either during the heaviest rainfall episode or about 6-12 hours earlier. This suggests that the 500-hPa PVA provided dynamic supports to different extent for the four heavy rainfall events. The dynamic support of the 500-hPa PVA was clearly exhibited in case 2 and case 3 as the evolution of the vorticity advection was in phase with the rainfall evolution.

The presence of baroclinic instability represented by the co-existing WAA and CAA in the middle troposphere was a signature of lee cyclogenesis, which was clearly exhibited in the analysis of the 700-hPa flow pattern of extreme rainstorm case 2. In addition to the contribution to lee cyclogenesis, lower-level PTA resulting in vertical motion and enhancing the rainfall was apparent in cases 1, 3 and 4 as the 850-hPa PTA

peaked about 6-12 hours prior to the heaviest rainfall episode. Contribution of the 850-hPa PTA to extreme rainstorm case 2 was not significant throughout the event.

Conditionally instability of the lower troposphere during the four rainfall events provided buoyancy for the vertical motion of moisture-bearing air. Saturated neutrality of the middle troposphere limited the vertical development of the precipitating cloud system. Consequently precipitation remained mostly uniform during the major span of the four cases. CAPE was instantaneous energy released during each event and contributed little to the total rainfall accumulation. For these synoptic-scale precipitation events, convection was unlikely a major cause for the heavy rainfall despite that embedded convection was common. Also, analysis of the time history of the CAPE of June 2005 suggests that large CAPE was not necessarily associated with high rainfall and small CAPE was not necessarily associated with low rainfall.

The influence of orography on precipitation of the four Alberta rainstorms occurred in two ways: lee cyclogenesis and orographic lifting. It was evident that the east or north to northeasterly wind over central or southern Alberta resulted in upslope flow, reinforcing the updraft and adding to the orographic rainfall in the foothills in all four cases. Rainfall contributed by orographic lifting was sustained. For case 2, about half of the observed rainfall came from orographic lifting.

6.2.3 Water vapor supply

Ample water vapor supply in the lower troposphere was evident in four rainfall cases. A moisture tongue of high specific humidity at 850 hPa was common during each event. Transport of water vapor by southerly and easterly flow from the nearby regions of the heavy rainfall area was apparent during the four events. The major source region of moisture for the four rainstorms was likely the Midwest U.S. Study by Dupilka et al. (2007) indicates that the additional source regions of moisture for rainstorms during 5-9, and 16-19 June 2005 likely included the Canadian Prairies and the Pacific Oceans. On the other hand, high vapor content (e.g. high PW) prior or during the event allowed more

latent heat to be released for vertical development for convection and precipitation in all four cases.

Our analyses for the four Alberta heavy rainfall events during June 2005 were from the viewpoint of synoptic scale. Mechanisms for the occurrence of the four cases involved interaction and superposition of atmospheric dynamics, thermodynamics, and physical processes that concern the exchanges of kinematic, potential and thermal energies. Updraft for moisture-bearing air to produce heavy precipitation was the outcome of the synergistic contributions of PVA, PTA (WAA), NTA (CAA), CAPE, underlying surface, and other mesoscale or microscale mechanisms. The degree of contribution of individual mechanisms had great variability from case to case. The extreme case during 5-9 June 2005 was the result of a combination of an ideal synoptic flow environment and orographic effects.

6.3 Comments and suggestions for future work

The behavior of weather systems interacting with topography is a challenging issue for synoptic-scale as well as mesoscale weather analysis and forecasting research. As discussed in Chapters 1 and 2, topography of the mountain terrain provides some preferred regions of severe weather, such as convective development caused by differential slope heating, thermally-driven upslope winds and topographically forced convergence; lee cyclogenesis caused by vertical stretching; as well as orographic rainfall due to mechanical terrain forcing. The influence of orography ranges from microscale to synoptic scale.

Mechanical orographic forcing and its dynamics for lee cyclogenesis, mountain waves and orographic rainfall over a smooth terrain can be approached in theory and observationally. However, progress in understanding the different mesoscale processes associated with terrain characteristics, flow blocking, diversion, roughness variation, elevated heat source and sink, has been rather slow. Further study on the lee upslope

precipitation in Alberta affected by mesoscale disturbances under differential terrain heating and the consequent thermal-driven upslope wind should be addressed.

As discussed in Chapters 1 and 2, water vapor supply for heavy rainfall comes from two feedings: local moisture recycling through evapotranspiration and vapor transport from remote sources. Detailed study of the local moisture recycling and remote sources has been carried out by many scholars (Szeto 2002, Liu and Stewart 2003, Brimelow and Reuter 2005, Dupilka et al. 2007). However, study on the moisture balance over Alberta during the successive rainstorms and the vapor recycling over this region has yet to be addressed. Addressing this subject will give us a better understanding of the amount of vapor feedings from local evaporation/ evapotranspiration, vapor transportation from remote source regions, and the amount of vapor transportation out off the area, as well as the amount of water precipitated out over the area. The result will provide us a better comprehension on the contribution extent of the local vapor supply separated from that of the remote sources. .

In addition to the support of synoptic-scale dynamics and thermodynamics, the occurrence of heavy precipitation involves some other mesoscale dynamics and physical processes that may not be readily demonstrated. Latent heat release contributed to heavy rainfall development is among these un-quantified factors. Many scholars (e.g. Hoskins 1990, Uccellini 1990) had demonstrated that latent heat release plays important role in the self-development of extratropical cyclones that are responsible for large scale precipitation. Due to the difficulty of the accurate measurement of local rate of change of latent heat release within a precipitating system, the progress in demonstrating the extent of latent heat release contributed to the precipitating system and its outcome rainfall has been rather slow. In-depth study on latent heat release to exhibit the degree of direct contribution to the development or intensification of lee cyclones, and the consequent reinforcement of precipitation during Alberta's heavy rainfall event may be carried out should the accurate measurement of local rate of change of latent heat release becomes achievable.

Table 1-1 Rainstorms with rainfall of 200 mm or more during their life time in southern Alberta for the period 1921 to 2006

Year	Start Date	End Date	Amount* (mm)	Location of heaviest rainfall
1964	Jun 7	Jun 8	252	Waterton Lakes Red Rock (49.13N 114.03W) in the Oldman River Basin
1969	Jun 19	Jun 29	229	Pekisko (50.37N 114.42W) in the lower Bow River Basin
1973	Jun 14	Jun 17	218	Sedalia (51.6N 111.95W) in the southeastern North Saskatchewan River Basin
1975	Jun 17	Jun 20	356	Waterton Lakes Red Rock (49.13N 114.03W) in the Oldman River Basin
1995	Jun 6	Jun 7	310	Spionkop Creek (49.22N 114.08W) in the Oldman River Basin
2005	Jun 5	Jun 9	248	Pekisko (50.37N 114.42W) in the lower Bow River Basin

* Data between 1921 and 1973 were adopted from Verschuren and Wojtiw (1980). Data after 1973 were originated from the available sources of Alberta Environment and Environment Canada.

Table 2-1 Summary of the four rainstorms during the June 2005 Alberta flood

Rainstorm Case	Case 1	Case 2	Case 3	Case 4
Started time	0600 UTC 1 Jun	0600 UTC 5 Jun	1200 UTC 16 Jun	0600 UTC 27 Jun
Ended time	0600 UTC 5 Jun	0600 UTC 9 Jun	1800 UTC 19 Jun	1200 UTC 29 Jun
Duration (hour)	96	96	78	54
Max. rainfall accumulation * (mm)	140	248	152	90
Max. rainfall accumulation location	Cardston	Pekisko	Springbank	Highwood
Max. 24h rainfall * (mm)	49.5	131.8	128.4	59.8
Max. 24h rainfall date	Jun 2	Jun 7	Jun 17	Jun 28
Max. 24h rainfall location	Milk River	Pekisko	Springbank	Cop Upper
Area in Alberta received $\geq$ 50 mm of rain (km^2)	$\approx$ 32,000	$\approx$ 62,500	$\approx$ 50,500	$\approx$ 10,500
Central affected basin	Oldman River Basin	Lower Bow River and upper Oldman River Basins	Red Deer River and upper Bow River Basins	Lower Bow River and upper Oldman River Basins
Flood occurrence	No	Yes	Yes	Yes

* Max. rainfall accumulation of each case calculated for the same periods shown on Figure 1-1. Max. 24h rainfall accumulated from 0600 UTC (0000 MST) to 0600 UTC (0000 MST) on the next day.

Table 2-2 Summary of the record high stream flow during the June 2005 Alberta flood

Basin Name	Station Name	Peak water flow* (m^3/s)	Highest or next highest peak water flow on record (m^3/s)	% chance of this flood occurring in any given year	Peak in the event
North Saskatchewan River Basin	Clearwater River near Dovercourt	938	341	Less than 1%	Case 3
	North Ram River near Forestry Road	75	72	2%	Case 3
	Prairie Creek near Rocky Mountain House	212	131	Less than 1%	Case 3
Red Deer River Basin	Bearberry Creek near Sundre	227	123	1 - 2%	Case 3
	James River near Sundre	685	237	Less than 1%	Case 3
	Little Red Deer River near the Mouth	452	173	Less than 1%	Case 3
	Raven River near Raven	91	39	Less than 1%	Case 3
	Red Deer River at Drumheller	1450	1260	2 - 5%	Case 3
	Red Deer River below Burnt Timber Ck.	1220	693	Less than 1%	Case 3
Bow River Basin	Bow River below Carseland Dam	1980	1690	Less than 1%	Case 2
	Bow River near the Mouth	1640	1570	Less than 1%	Case 2
	Fish Creek near Priddis	482	200	Less than 1%	Case 2
	Highwood River near the Mouth	1340	1120	Less than 1%	Case 3
	Pekisko Creek near Longview	119	100	1%	Case 2
	Sheep River at Black Diamond	380	366	4%	Case 3
	Stimson Creek near Pekisko	135	99	Less than 1%	Case 2
	Threepoint Creek near Millarville	389	283	Less than 1%	Case 2
Oldman River Basin	Willow Creek at Oxly Ranch	700	504	Less than 1%	Case 2
	Willow Creek near Claresholm	694	498	Less than 1%	Case 2
	Willow Creek at Highway 811	761	592	Less than 1%	Case 2
	Prairie Blood Coulee near Lethbridge	63	32	Less than 1%	Case 2
	Mosquito Creek near the Mouth	66	60	Less than 1%	Case 2

* Stream flow data originated from the Alberta Environment flood estimates through their website: http://www3.gov.ab.ca/env/water/ws/advisories/summaryJune2005Detailed.html.

Table 3-1 Relation of vorticity advection, temperature advection and vertical wind shear to measured mean rain rate of extreme rainstorm case 2

Date	Time (UTC)	Vorticity Advection at 500 hPa (10^{-9} s^{-2})	Temperature Advection at 850 hPa (10^{-4}K/s)	Speed shear from surface to 850 hPa * ($m\ s^{-1}km^{-1}$)	Measured mean rain rate * (mm/h)
5 Jun, 2005	0000	-0.20	0.05	-1.48	0.51
	1200	-0.20	0.00	5.33	0.86
6 Jun, 2005	0000	-0.10	0.20	3.84	0.88
	1200	-0.15	-0.15	8.43	0.70
7 Jun, 2005	0000	0.10	0.15	11.22	1.86
	1200	0.75	0.05	8.94	2.41
8 Jun, 2005	0000	0.05	0.02	-3.80	0.87
	1200	-0.15	0.00	-6.06	0.28

* Wind shears were derived from the sounding of Stony Plain (Alberta). Positive value is cyclonic shear (veering), negative is anticyclonic shear (backing). Measured mean rain rate is the time-space-averaged rainfall rate taken the mean rate of 6h rainfall before and after 0000 or 1200 UTC for 6 selected locations of southern Alberta.

Table 3-2 Updrafts contributing to extreme rainstorm case 2

Date	Time (UTC)	850hPa PTA induced updraft (m/s)	850hPa PTA induced rain rate (mm/h)	Orographic updraft (at 925 hPa) (m/s)	Orographic rain rate (at 925 hPa) (mm/h)	Measured mean rain rate * (mm/h)
5 Jun, 2005	0000	0.002	0.09	0.003	0.13	0.51
	1200	0.000	0.00	0.018	0.61	0.86
6 Jun, 2005	0000	0.012	0.50	0.022	1.00	0.88
	1200	-0.006	0.00	0.004	0.12	0.70
7 Jun, 2005	0000	0.004	0.17	0.026	1.08	1.86
	1200	0.001	0.04	0.008	0.25	2.41
8 Jun, 2005	0000	0.004	0.12	0.012	0.49	0.87
	1200	0.000	0.00	0.004	0.11	0.28

* See notes of Table 3-1.

Table 5-1 Summary of the meteorological parameters of the four rainstorms during the June 2005 Alberta flood

Rainstorm Case	**Case 1** (Jun 1-5)	**Case 2** (Jun 5-9)	**Case 3** (Jun 16-19)	**Case 4** (Jun 27-29)
Extreme 6h-space-averaged rain rate * (mm/h)	1.7	2.65	3.28	1.27
Extreme 6h-space-averaged rain rate occurrence time	18 Z * 2 Jun - 00 Z 3 Jun	12-18 Z 7 Jun	18 Z 17 Jun - 00 Z 18 Jun	06-12 Z 28 Jun
Min. pressure of sea-level closed low (hPa)	994	995	992	1008
Min. pressure of sea-level closed low occurrence time	18 Z 2 Jun	00 Z 7 Jun	00 Z 18 Jun	12 Z 28 Jun
Min. geopotential height of 500-hPa cutoff low (dam)	550	545	542	562
Min. geopotential height at 500 hPa occurrence time	12 Z 2 Jun	00-12 Z 6 Jun	12 Z 16 Jun	12 Z 27 Jun
Max. PVA (10^{-9} s^{-2})	1.0	0.75	0.55	0.55
Max. PVA occurrence time	12 Z 2 Jun	12 Z 7 Jun	00 Z 18 Jun	00Z 28 Jun
Max. PTA (10^{-4} K/s)	0.7	0.2	0.6	0.35
Max. PTA occurrence time	12 Z 2 Jun	00 Z 6 Jun	12 Z 17 Jun	00 Z 28 Jun
Max. CAPE * (J/kg)	113	1057	784	423
Max. CAPE occurred time	00 Z 5 Jun	00 Z 6 Jun	00 Z 17 Jun	00 Z 28 Jun
Mean PW * (mm)	18.9	17.7	20.9	23.0
Lee cyclone development at 700 hPa	Lee cyclone intensification	Lee cyclone genesis	Lee cyclone intensification	Lee cyclone genesis
Existence of blocking-high at 300 hPa	Omega-shaped blocking-high	Closed blocking-high	No	No
Existence of diffluence at 300 hPa over Alberta	-	Diffluence	Diffluence	Diffluence

* Extreme 6h-space-averaged rain rate is the peak value of the mean rainfall rate in a 6h period of 6 selected locations of southern Alberta during the event. CAPE was computed from the sounding data of Great Falls (Montana). Mean PW was computed from the sounding data of three stations: Stony Plain (Alberta), Great Falls and Glasgow (Montana). "Z" denotes the universal time.

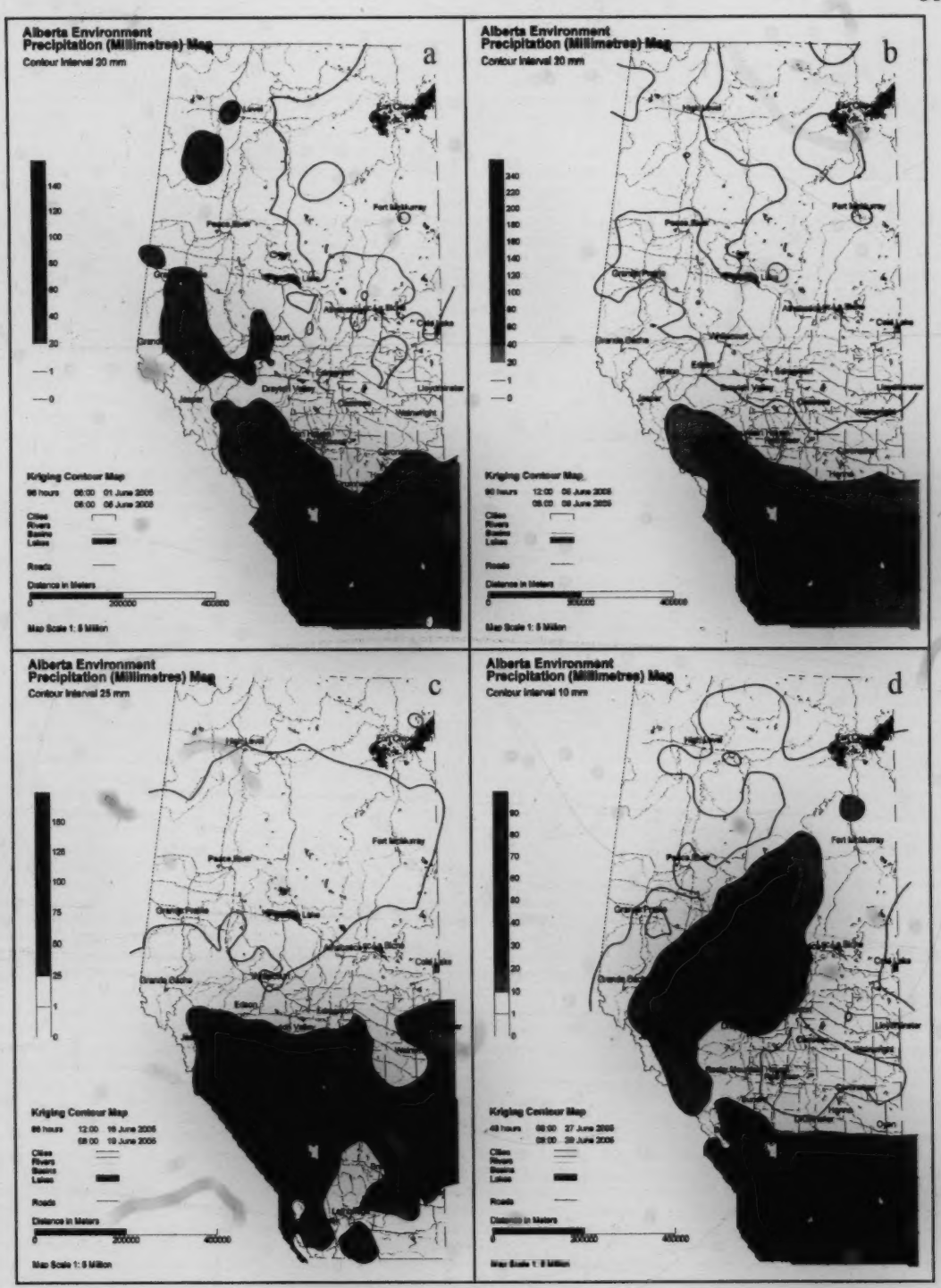

Figure 1-1. Precipitation accumulation of the four rainstorms during the June 2005 Alberta flood. (Maps provided by Alberta Environment.)

Figure 1-2. Major Alberta river basins.

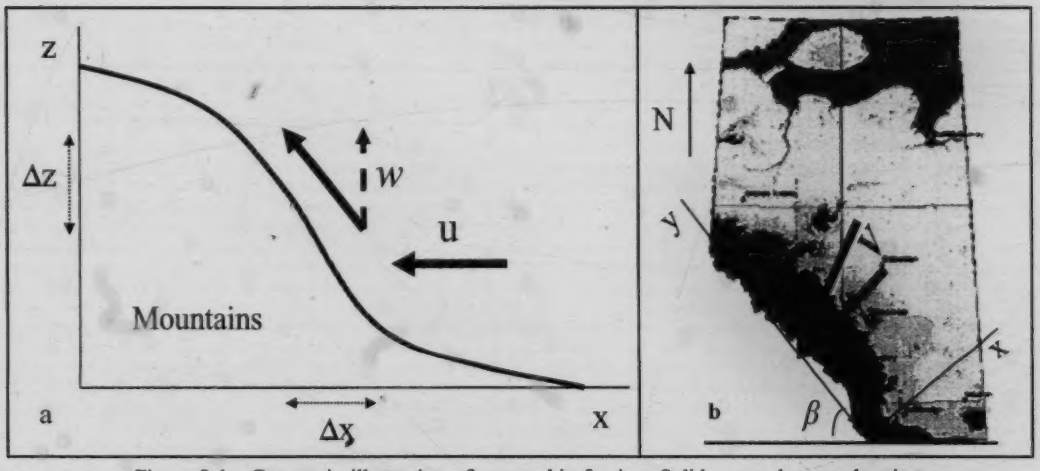

Figure 2-1. Geometric illustration of orographic forcing. Solid arrow denotes the air flow, dash arrow denotes the vertical component of the flow. (See text for other details.)

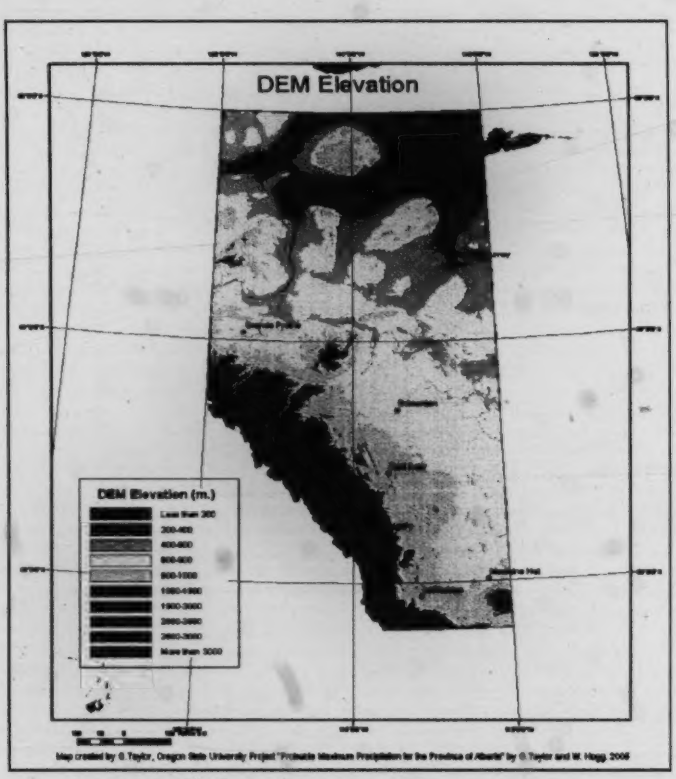

Figure 2-2. Digital Alberta terrain elevation in meter above sea-level. (Created by Taylor and Hogg, 2005.)

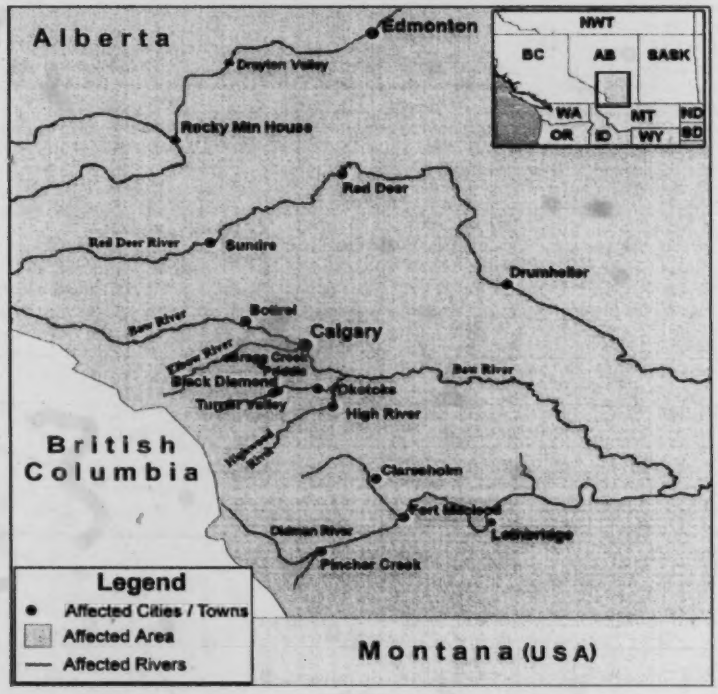

Figure 2-3. Central affected area of the June 2005 Alberta flood.

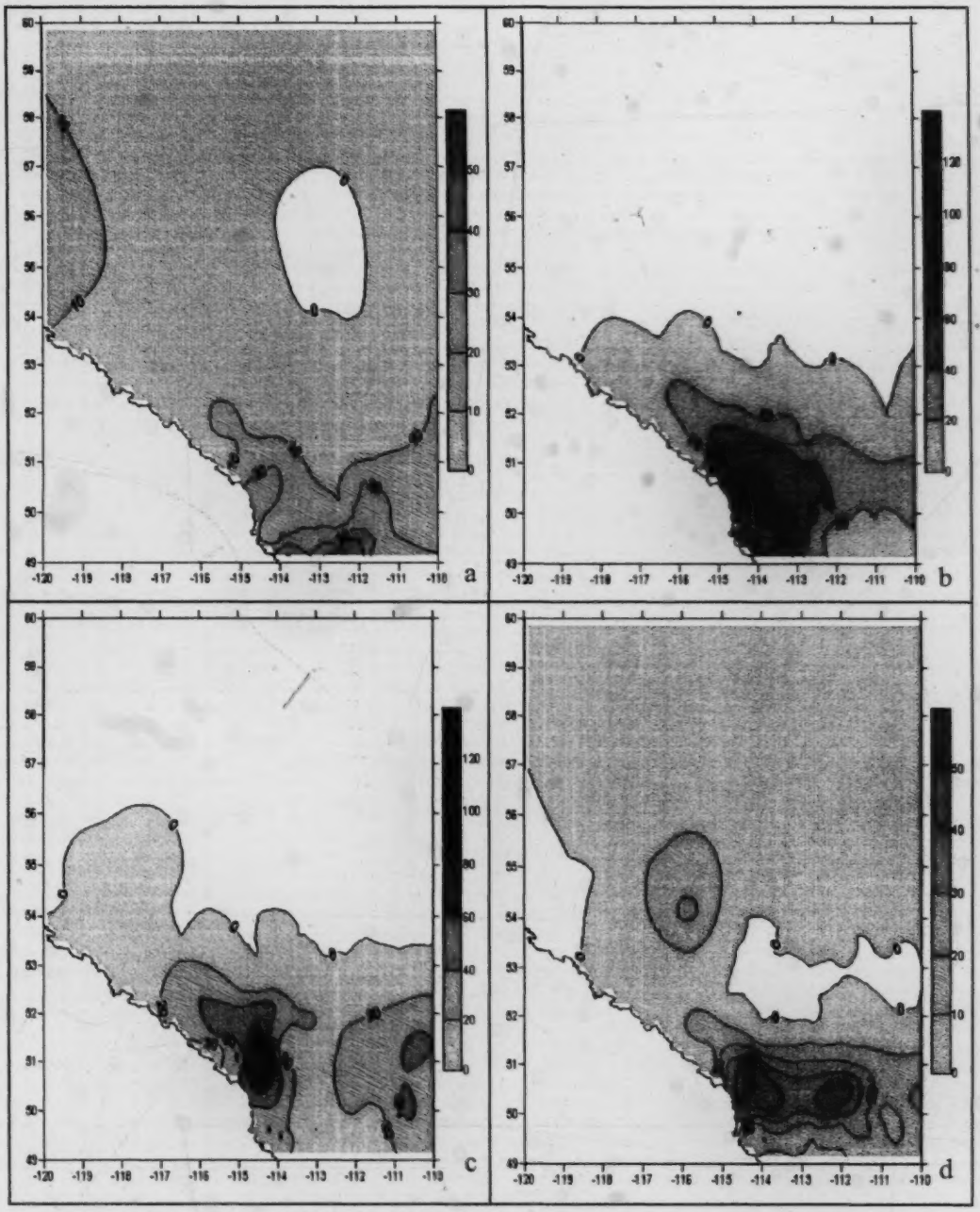

Figure 2-4. Maximum 24-hour rainfall distribution of the four rainstorms during the June 2005 Alberta flood (accumulation ending at 0600 UTC daily). (a) June 2; (b) June 7; (c) June 17; (d) June 28. Units in millimeter.

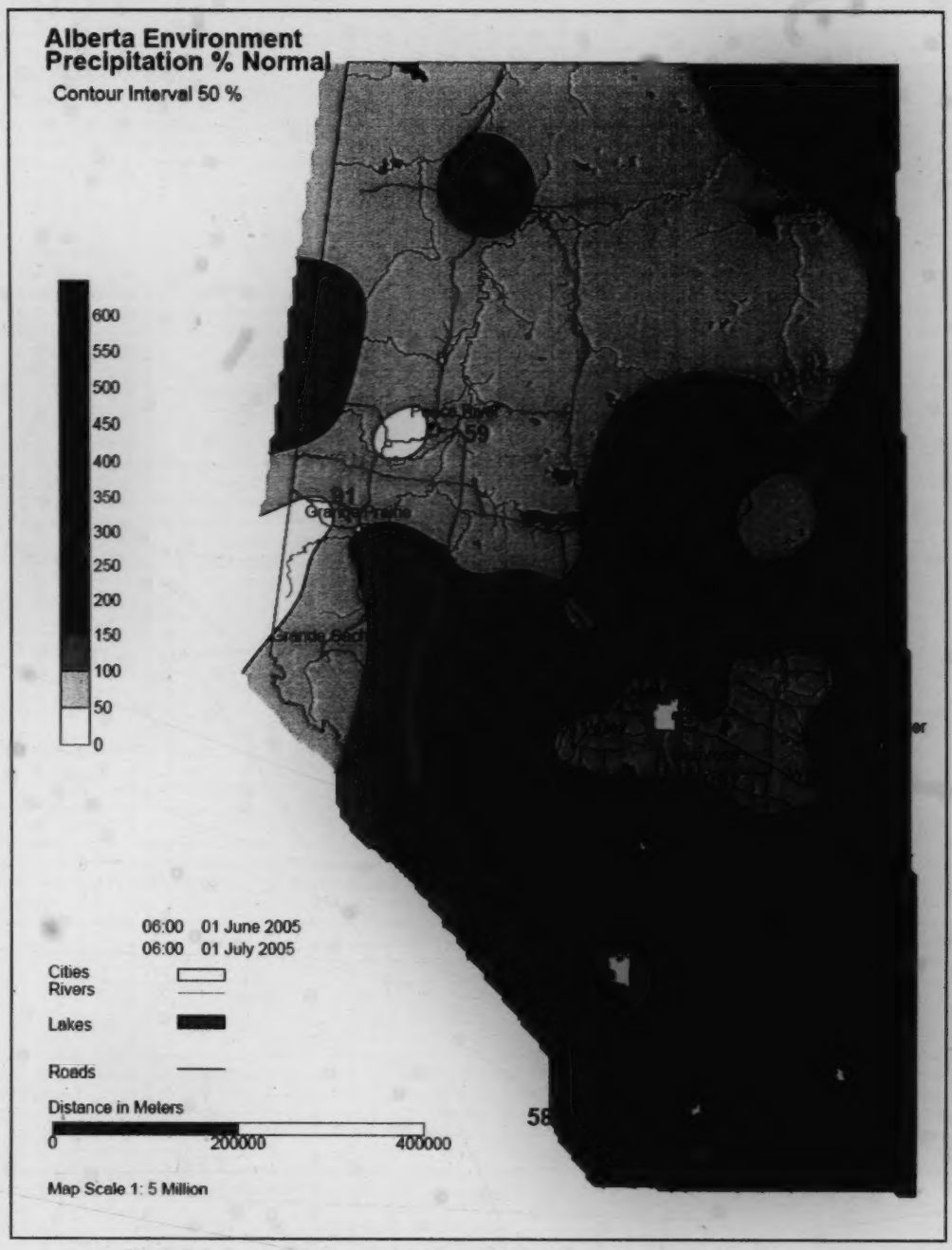

Figure 2-5. Precipitation anomaly of June 2005 in Alberta (based on Alberta's precipitation climatology). (Map provided by Alberta Environment.)

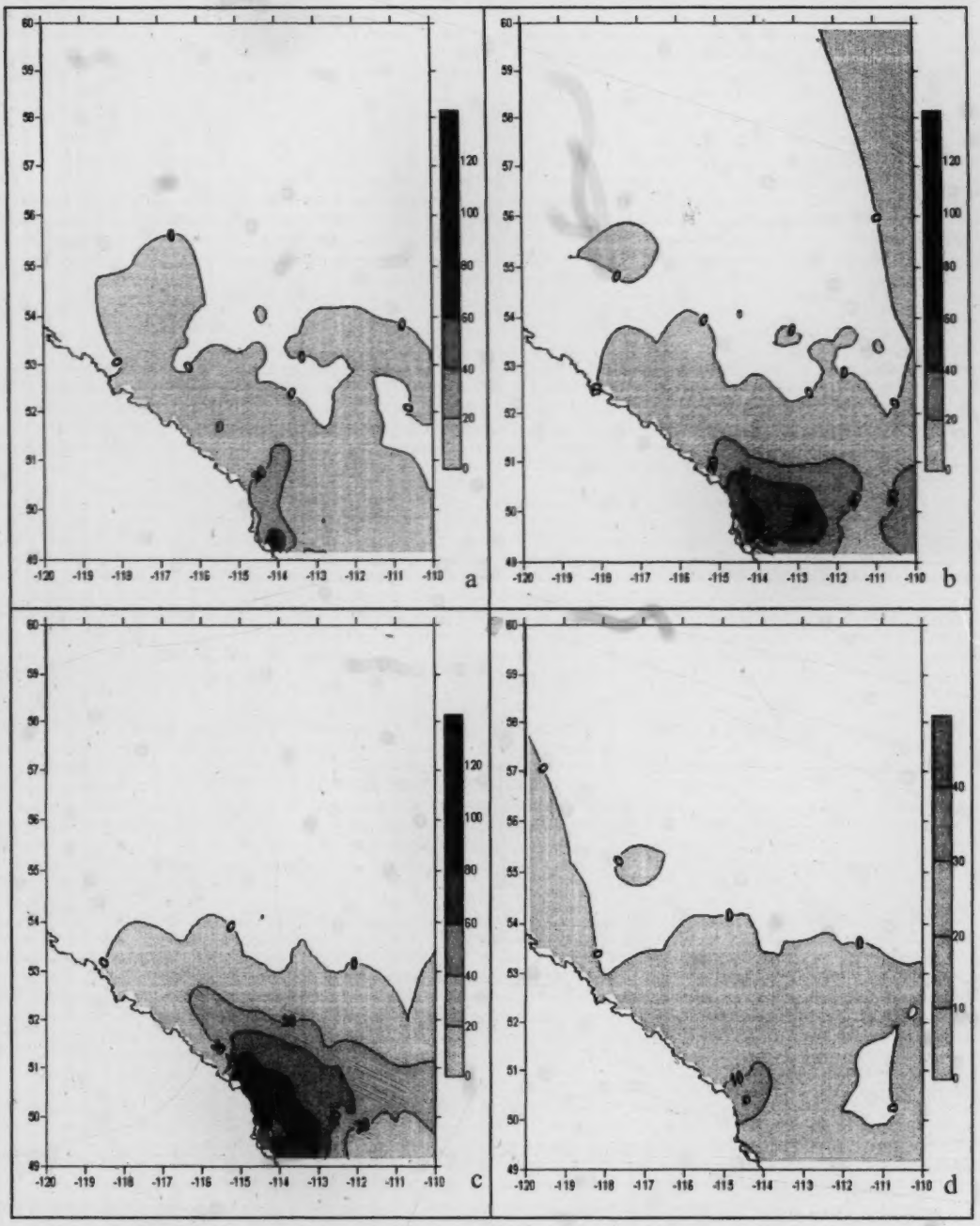

Figure 3-1. 24-hour precipitation distribution of rainstorm case 2 during 5-8 June 2005 (accumulation ending at 0600 UTC). (a) June 5, (b) June 6, (c) June 7, (d) June 8. Units in millimeter.

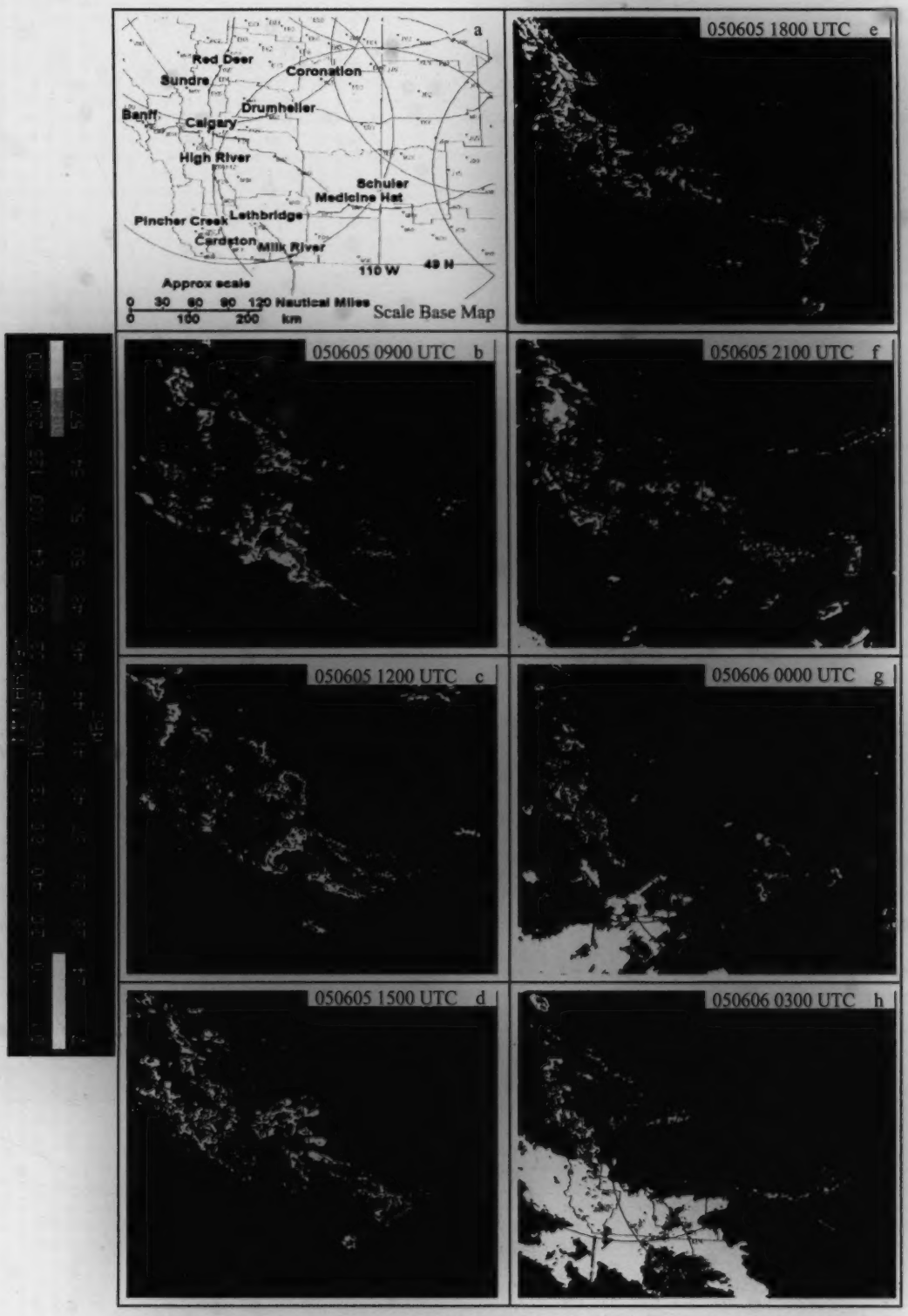

Figure 3-2I. Evolution of composite CAPPI radar echoes of rainstorm case 2 during 5-6 June 2005, interval: 3 hours. (Images provided by Environment Canada, hereafter EC.)

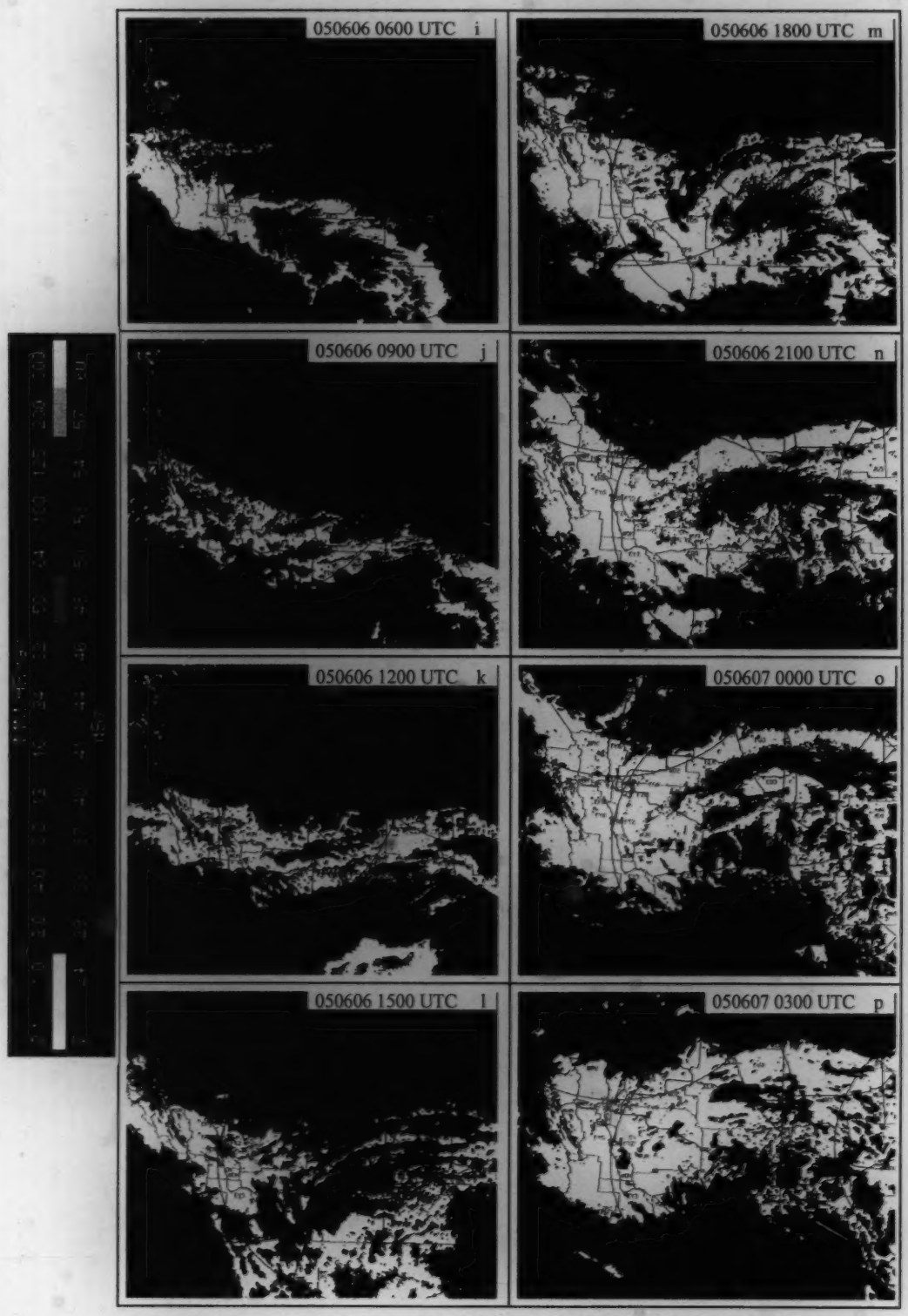

Figure 3-2II. Evolution of composite CAPPI radar echoes of rainstorm case 2 during 6-7 June 2005, interval: 3 hours.

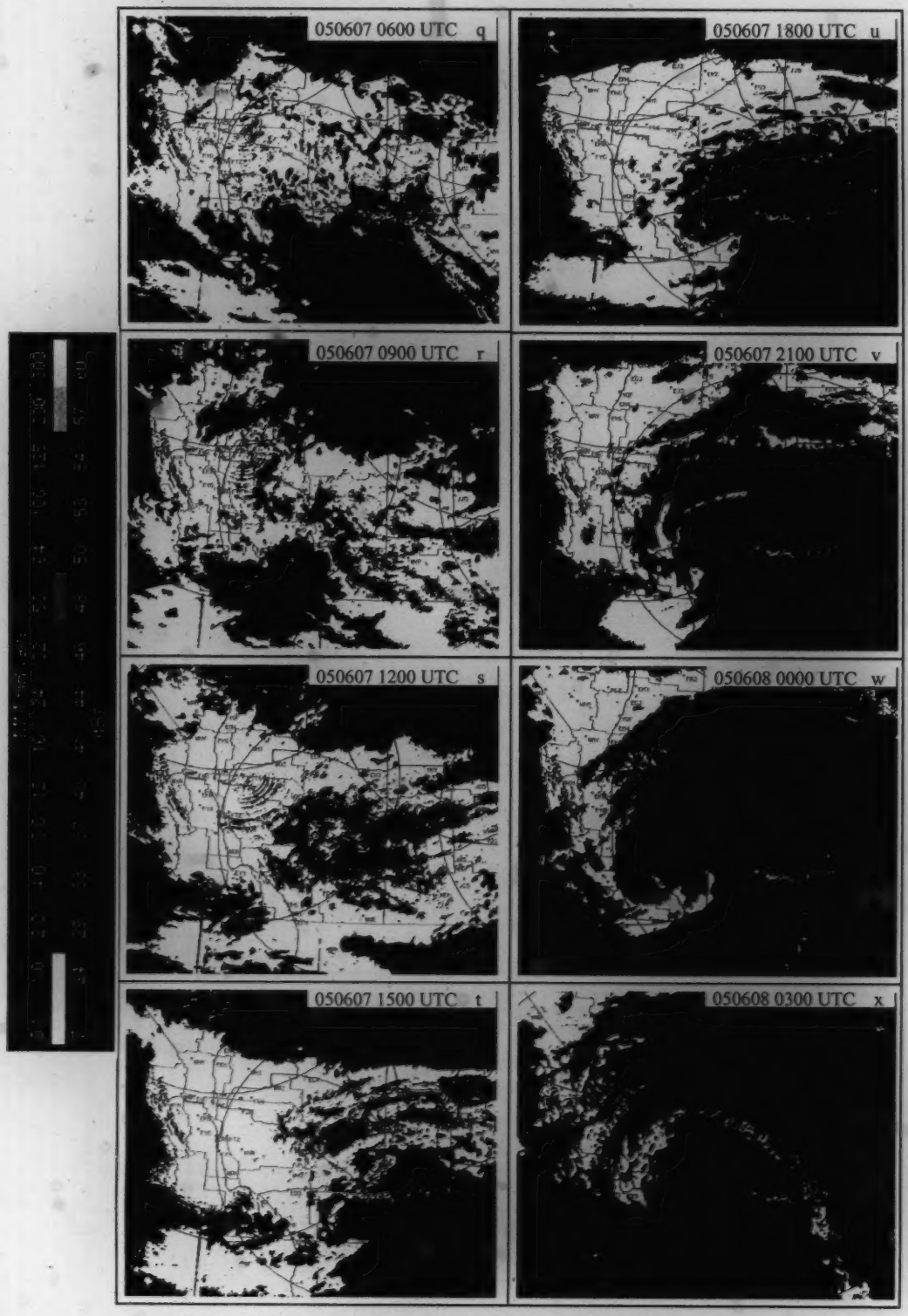

Figure 3-2III. Evolution of composite CAPPI radar echoes of rainstorm case 2 during 7-8 June 2005, interval: 3 hours. The solid red circle in panel (t) denotes the cyclonic centre of the echoes.

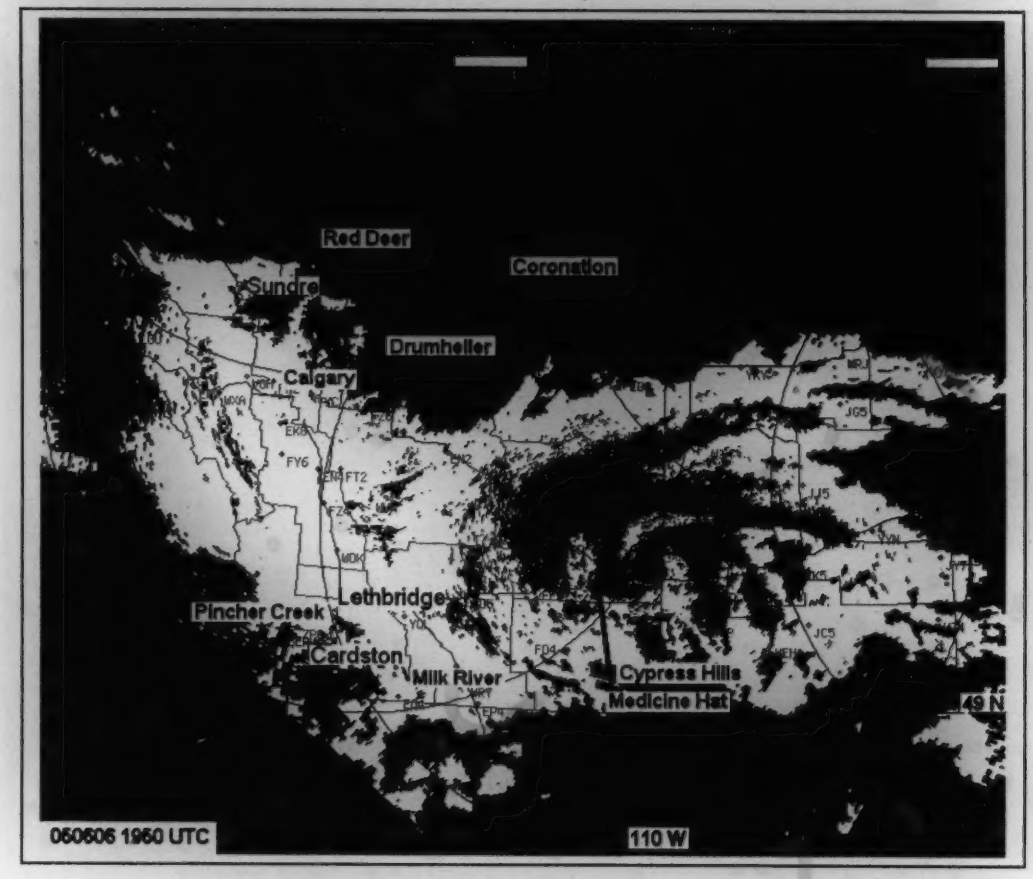

Figure 3-3. Snapshot composite CAPPI image of rainstorm case 2 at 1950 UTC 6 June 2005 (Brown arrows indicate the locations of Medicine Hat and Cypress Hills).

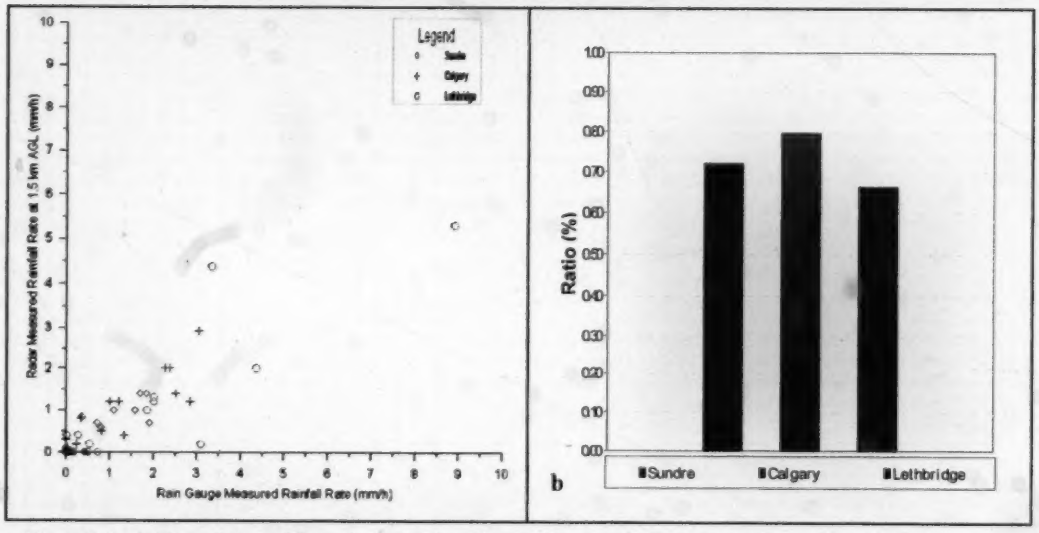

Figure 3-4. (a) Correlation of the estimated radar rain rate (at synoptic hour) to the observed rain rate during 5-9 June 2005. (b) Ratio of the estimated radar rainfall accumulation to the observed rainfall accumulation.

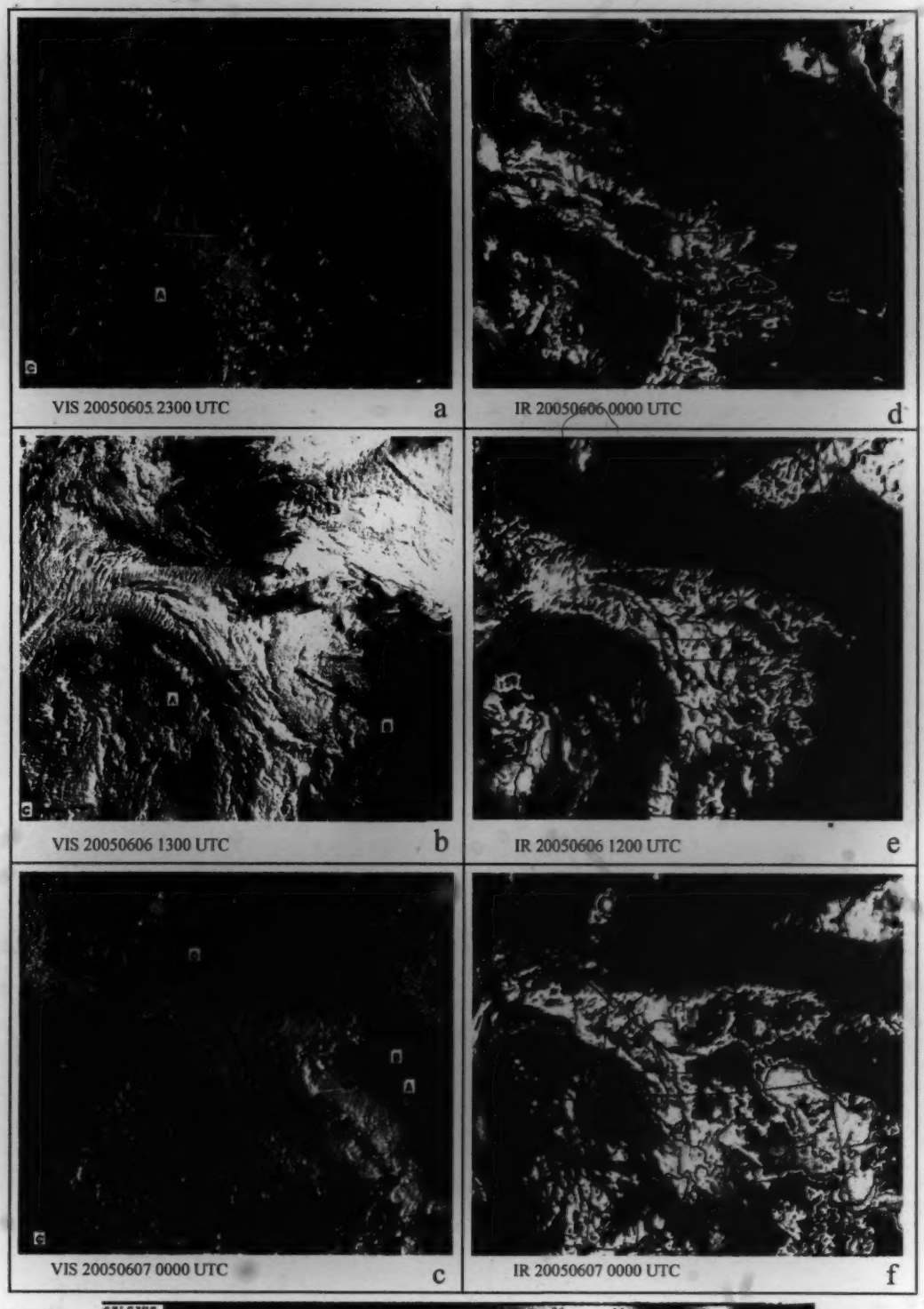

Figure 3-5I. Sequence of visible and infrared GOES satellite images of rainstorm case 2 during 5-7 June 2005. (Images provided by EC.)

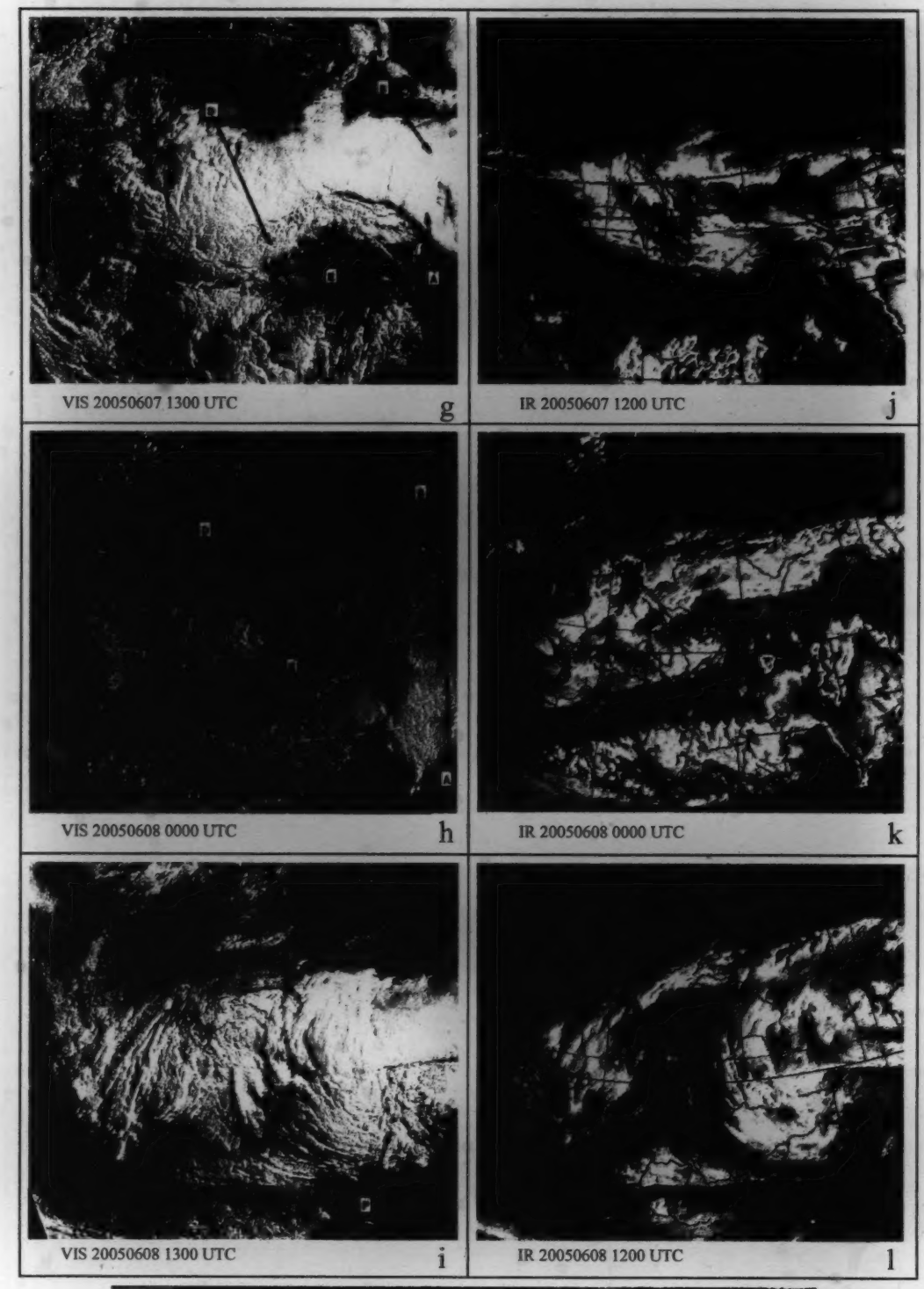

Figure 3-5II. Sequence of visible and infrared GOES satellite images of rainstorm case 2 during 7-8 June 2005.

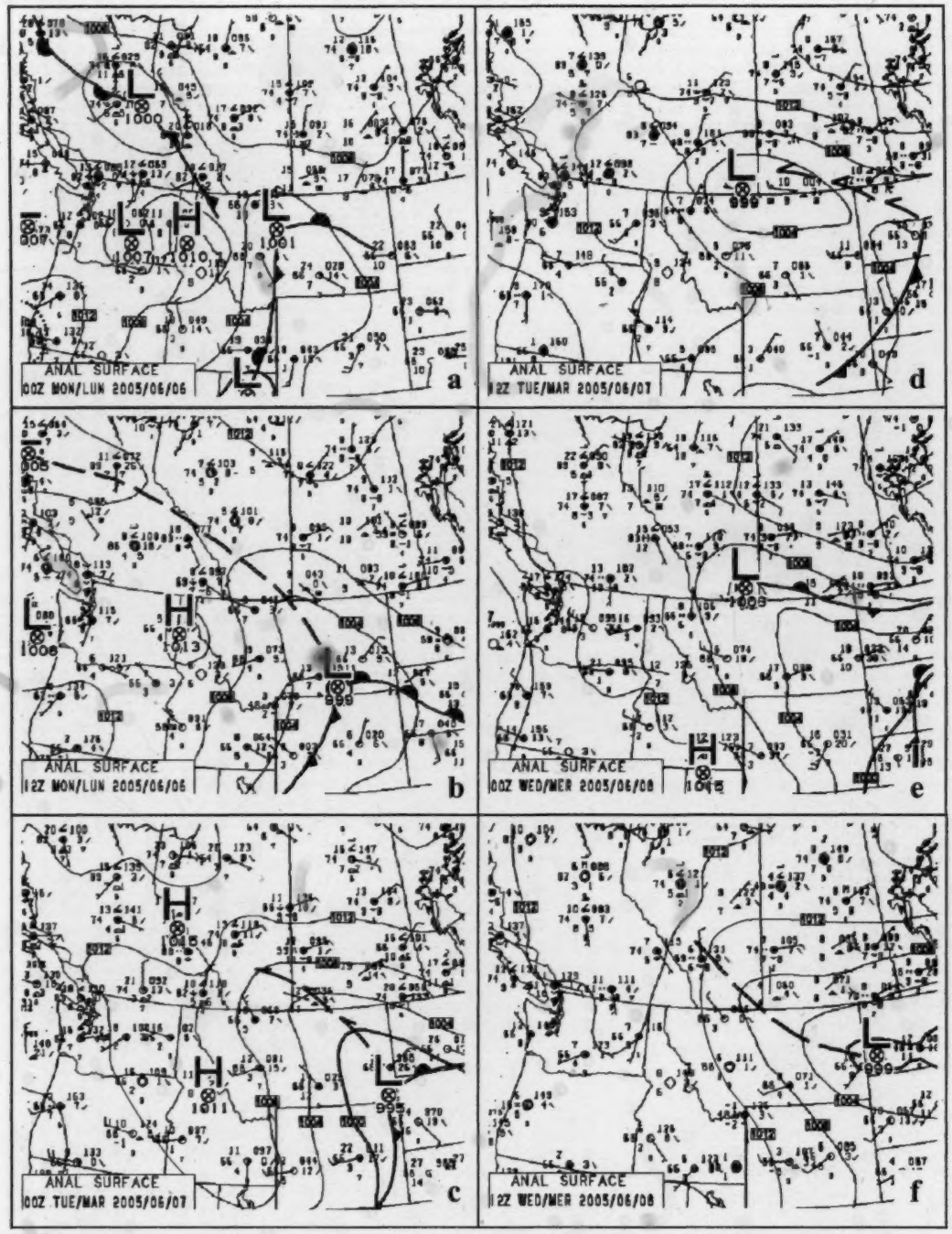

Figure 3-6. Sequence of surface analysis during 6-8 June 2005. Thin solid lines: isobars at intervals of 4 hPa; 1008: label of isobar; dashed lines: surface trough lines; dashed arrows: trowals; thick lines with rounded tips: warm fronts; thick lines with pointed tips: cold fronts. ⊗: center of the high or low pressure with the central mean-sea-level pressure underneath it; H and L denote high pressure and low pressure, respectively. (Maps modified from EC operational analysis charts.)

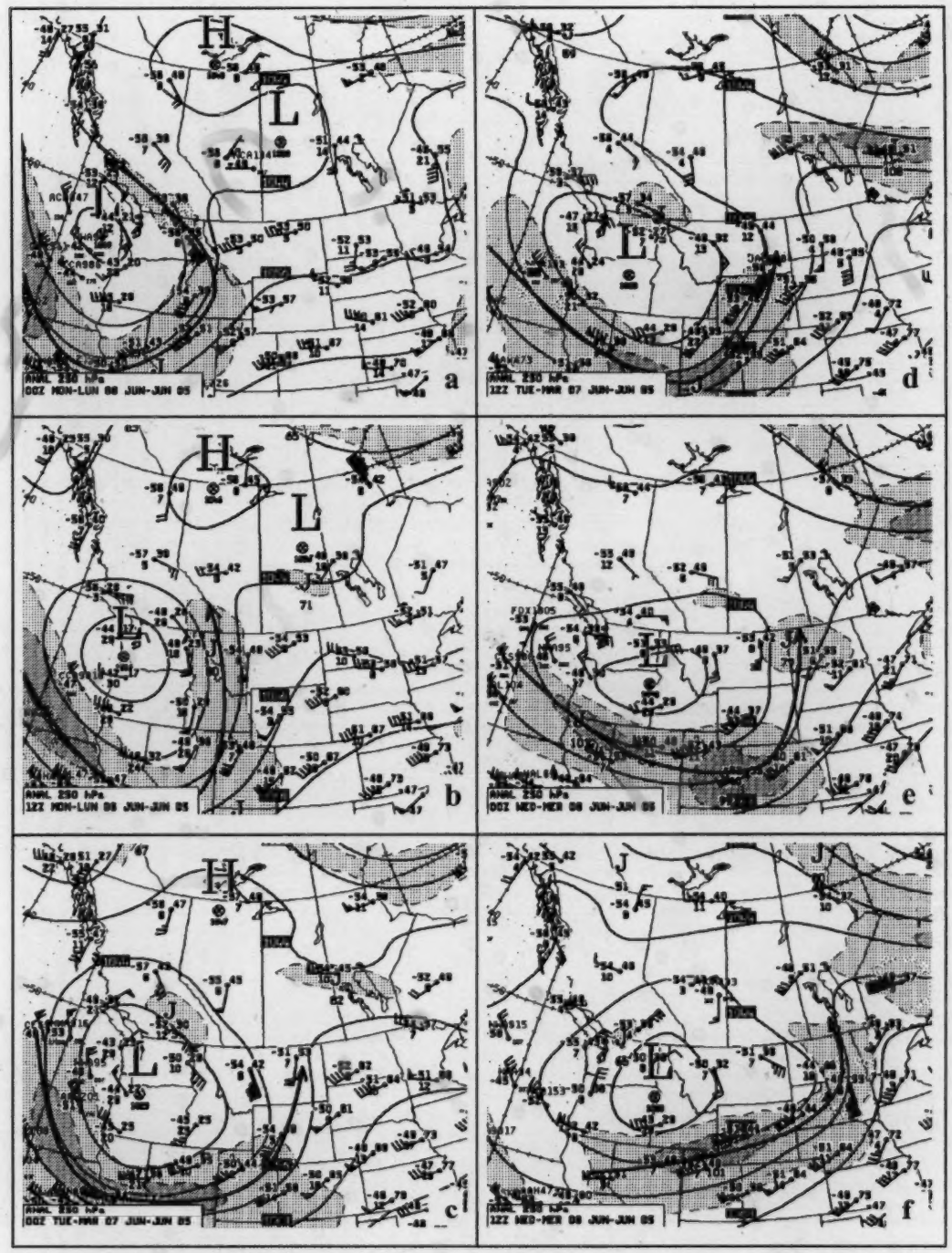

Figure 3-7. Sequence of 250-hPa analysis during 6-8 June 2005. Solid lines: contours of geopotential height at intervals of 12 decameters (dam); shaded gray areas: jet streams where wind speed is larger than 60 knots shading at intervals of 30 knots; red long arrows: axes of jet streams. Wind bar follows the conventional meteorological data plot (one bar is 10 knots). 1044 : contour label. ⊗ : center of the high or low pressure with the central geopotential height beneath it. H and L denote high pressure and low pressure, respectively. Bolded numbers or wind bars are doubted data. (Map modified from EC operational analysis charts.)

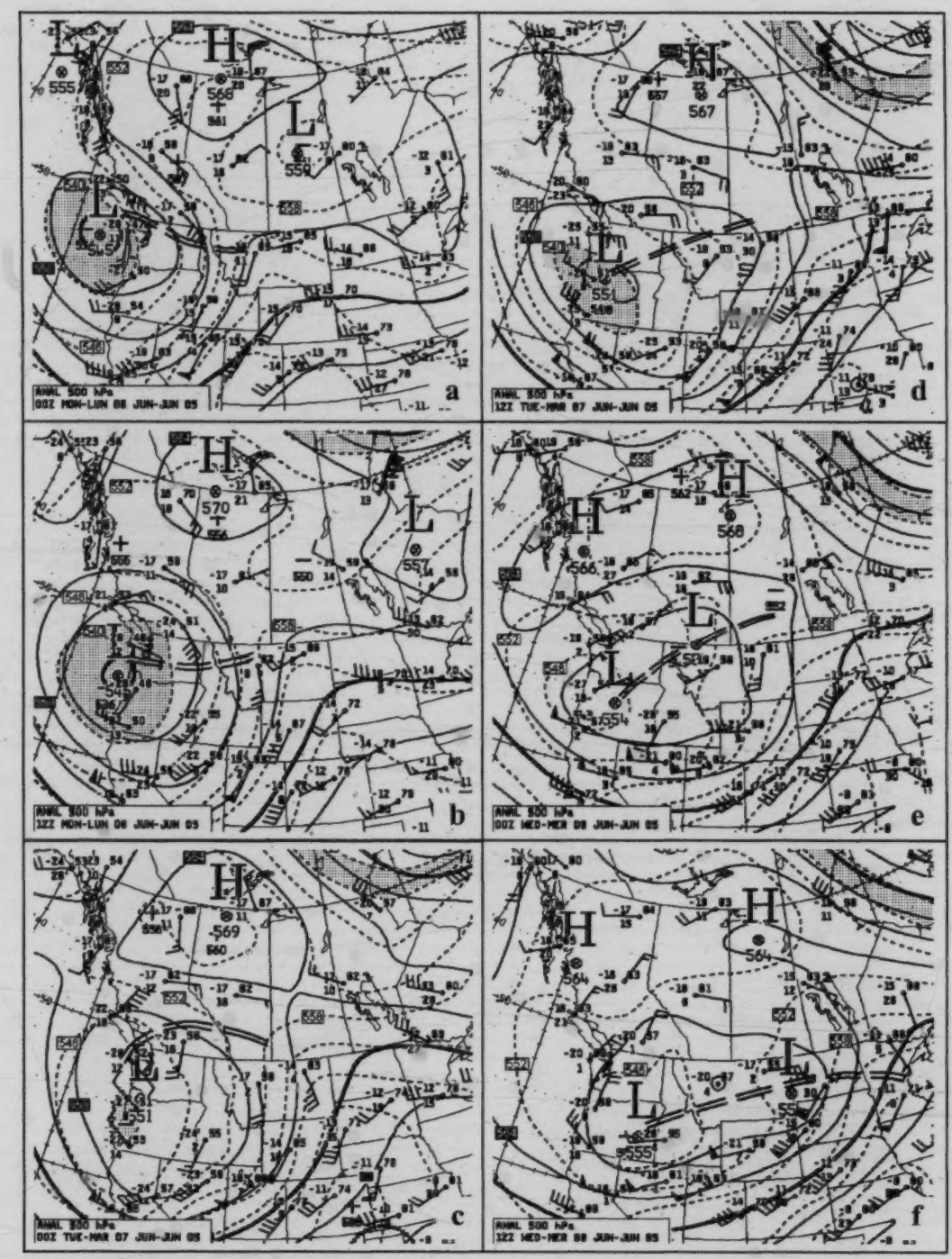

Figure 3-8. Sequence of 500-hPa analysis during 6-8 June 2005. Brown double dashed lines: subjectively analyzed trough axes; solid lines: contours of geopotential height (dam); heavy solid lines: 546 dam and 570 dam; short dashed lines: thicknesses (dam) between 1000 and 500 hPa; shaped gray areas: thicknesses between 534 and 540 dam. Contour interval: 6 dam; 564: label of height contour; 546: label of thickness; + and – denote warm and cold core with the max. or min. thickness value underneath it, respectively. Other legends are the same as those indicated on Figure 3-7. (Maps modified from EC operational analysis charts.)

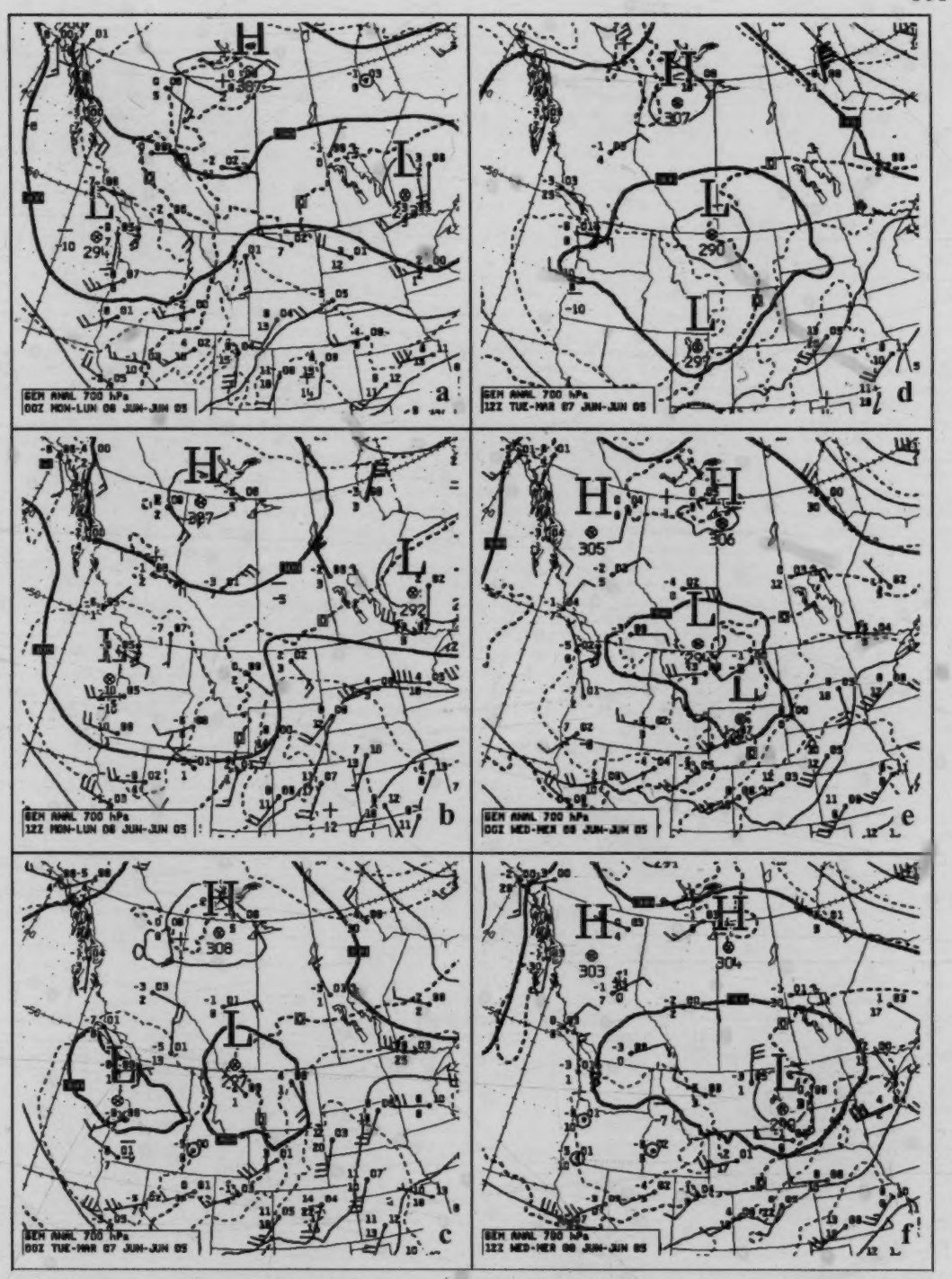

Figure 3-9. Sequence of 700-hPa analysis during 6-8 June 2005. Solid lines: contours of geopotential height at intervals of 6 dam; short dashed lines: isotherms at intervals of 5 C. 300 : label of geopotential contour; 0 : label of isotherm; + and – denote warm and cold core with the max. or min. temperature value underneath it, respectively. Other legends are the same as those indicated on Figure 3-7. (Maps modified from EC operational analysis charts.)

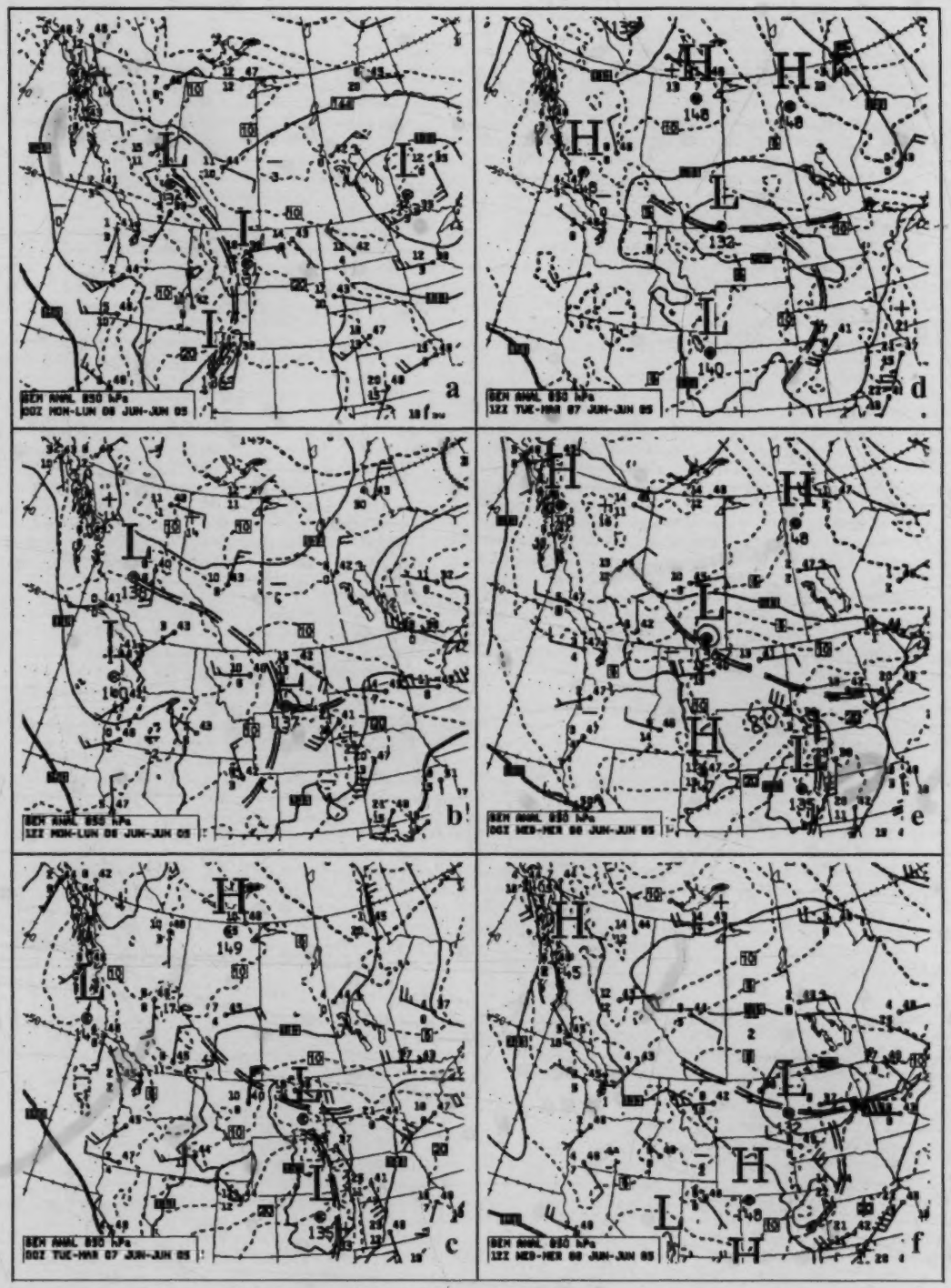

Figure 3-10. Sequence of 850-hPa analysis during 6-8 June 2005. Brown double dashed lines: subjectively analyzed trough axes; solid lines: contours of geopotential height at intervals of 6 dam; short dashed lines: isotherms at intervals of 5 C. [144] : label of geopotential contour; [5] : label of isotherm. Other legends are the same as those indicated on Figure 3-9. (Maps modified from EC operational analysis charts.)

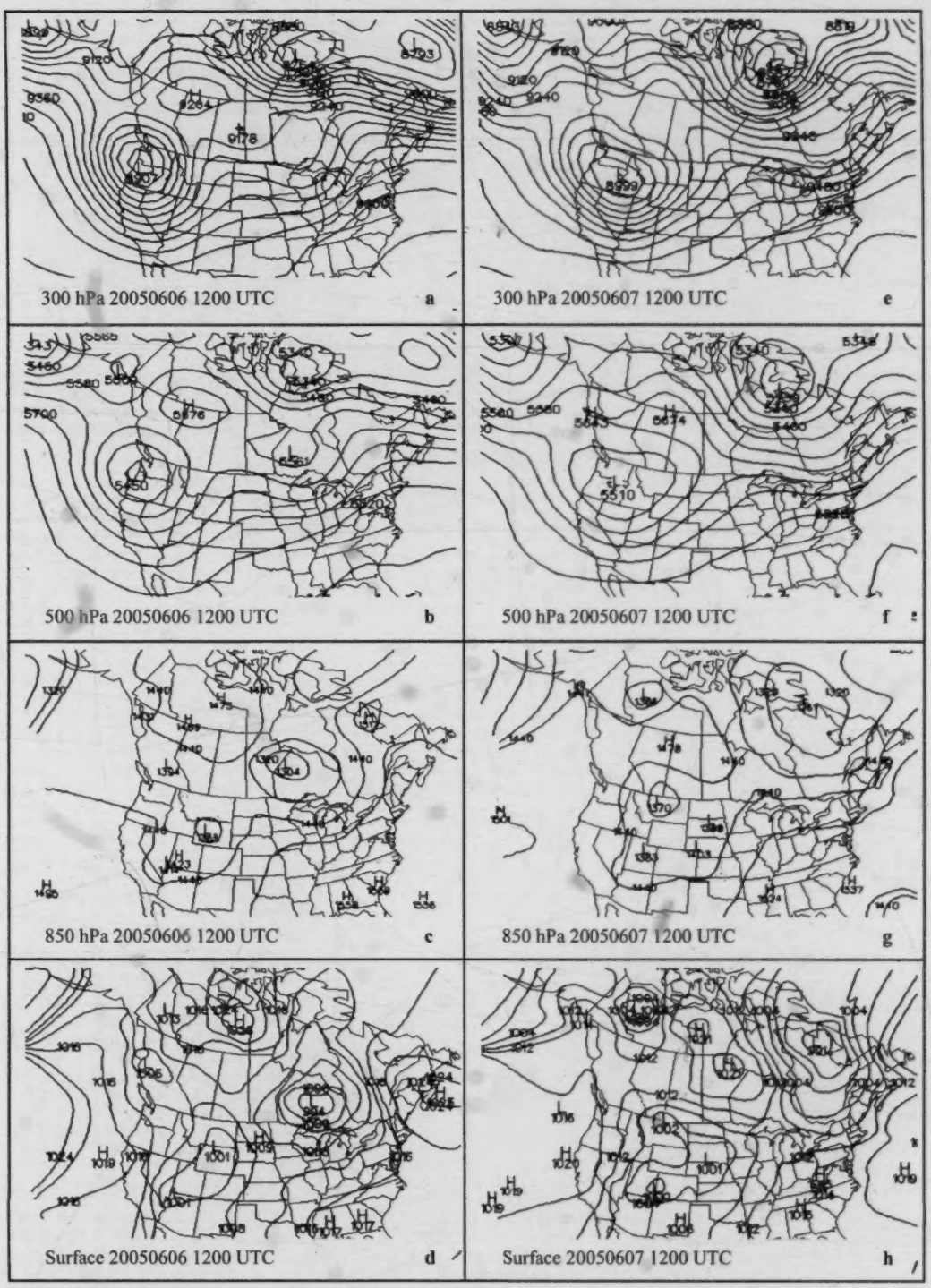

Figure 3-11. Superimposition of the synoptic circulations at typical levels at 1200 UTC 6 June (left) and 7 June 2005 (right). Unit at upper levels is geopotential meter (gpm) at intervals of 60 gpm; unit at sea-level is hectopascal (hPa) at intervals of 4 hPa. H and L denote high pressure and low pressure with the central value beneath it, respectively. (Maps from PSWC.)

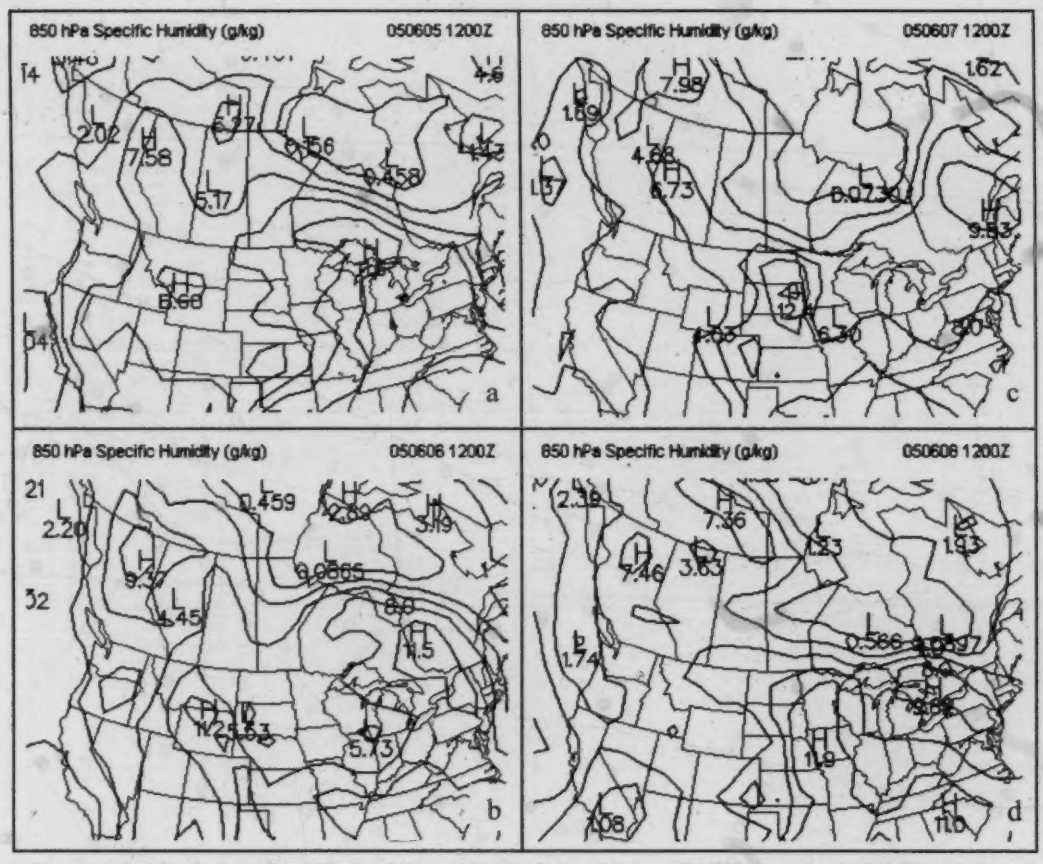
850 hPa Specific Humidity (g/kg) 050605 1200Z
850 hPa Specific Humidity (g/kg) 050607 1200Z
850 hPa Specific Humidity (g/kg) 050606 1200Z
850 hPa Specific Humidity (g/kg) 050608 1200Z
a
b
c
d

Figure 3-12. Distribution of specific humidity at 850 hPa during 5-8 June 2005. Contour interval is 2.0 (g/kg). H and L denote the maximum and minimum with the central value beneath it, respectively. (Maps from PSWC).

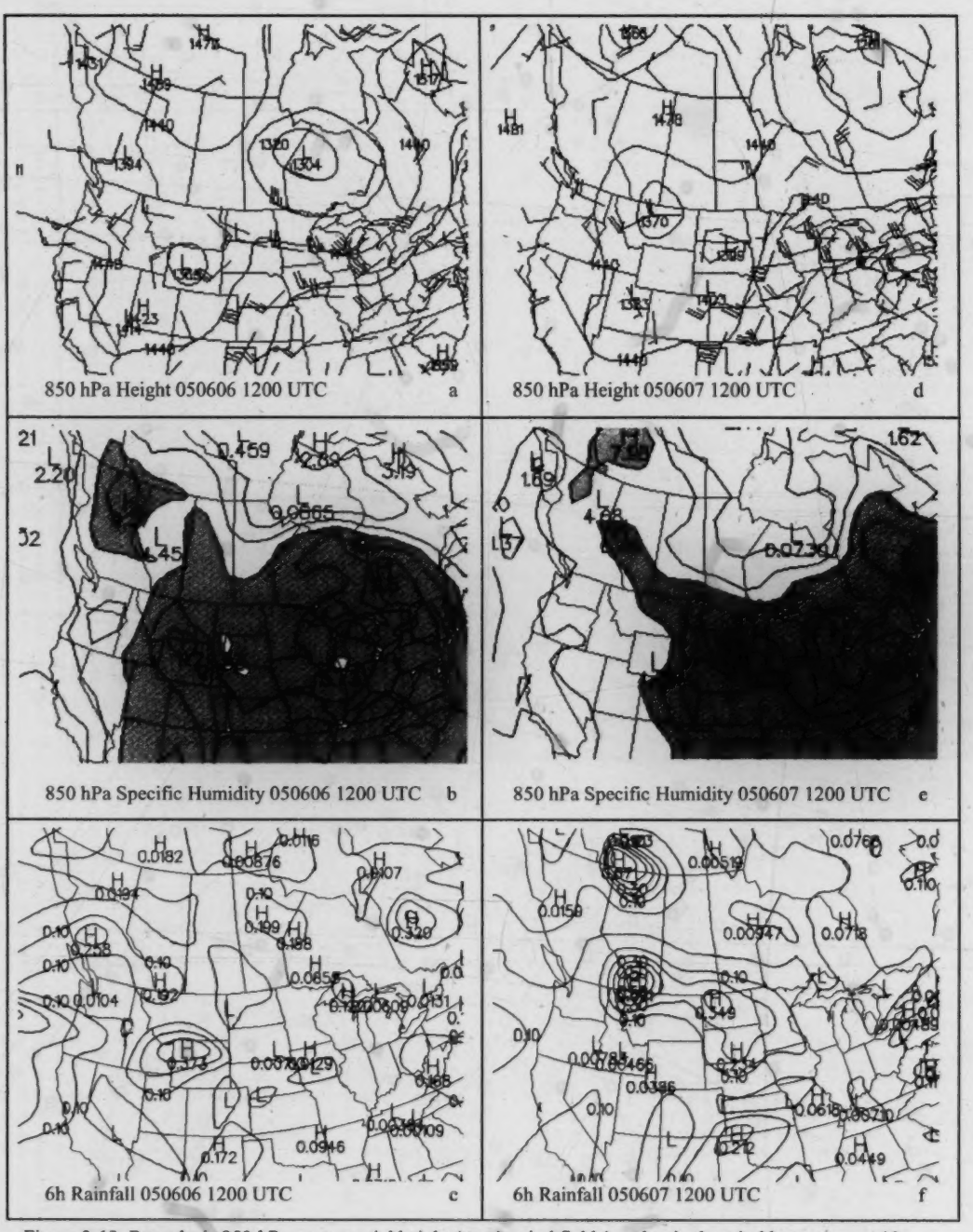
850 hPa Height 050606 1200 UTC a
850 hPa Height 050607 1200 UTC d
850 hPa Specific Humidity 050606 1200 UTC b
850 hPa Specific Humidity 050607 1200 UTC e
6h Rainfall 050606 1200 UTC c
6h Rainfall 050607 1200 UTC f

Figure 3-13. Reanalysis 850-hPa geopotential height (gpm), wind field (one bar in the wind bar represent 10 knots), specific humidity (g/kg), and observed 6h rainfall (inch/6h) during 6-7 June 2005. (Maps from PSWC.)

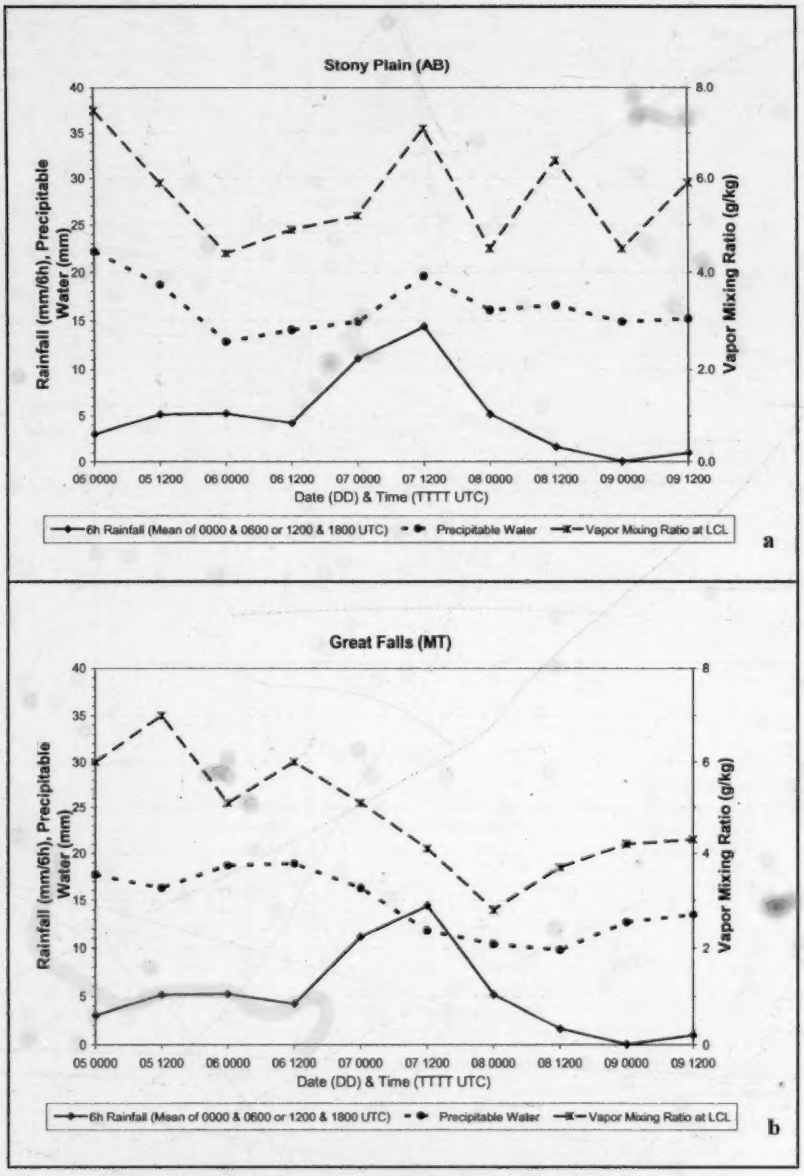

Figure 3-14. Evolution of precipitable water and vapor mixing ratio at Stony Plain (Alberta) and Great Falls (Montana), along with space-averaged 6h rainfall in southern Alberta during 5-9 June 2005.

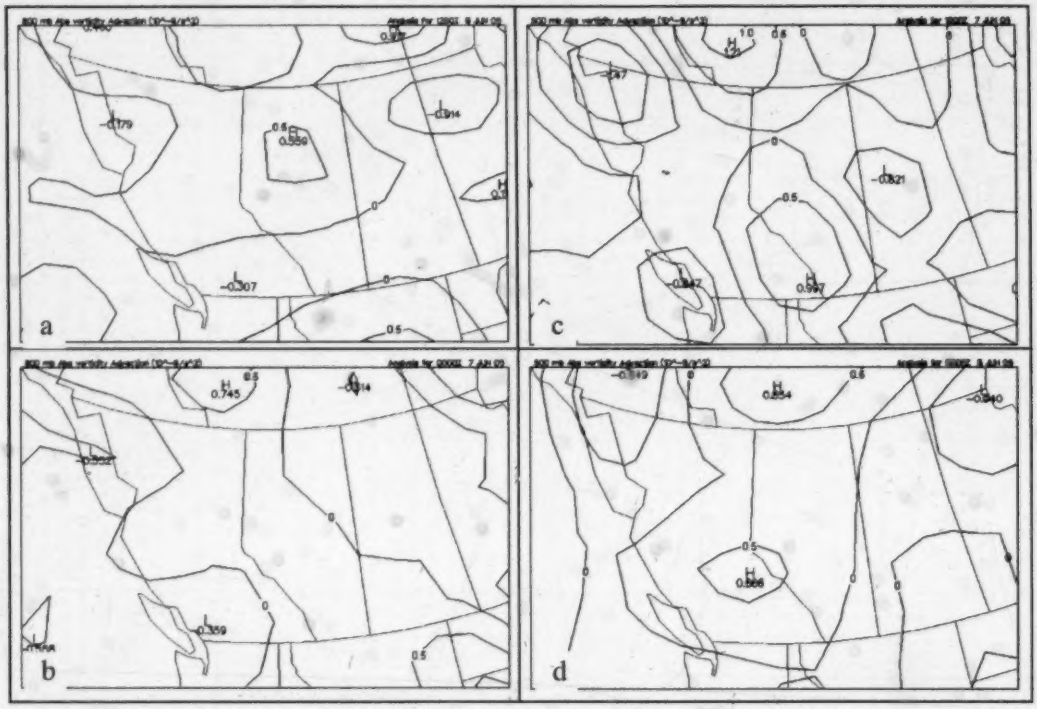

Figure 3-15. Sequence of absolute vorticity advection at 500 hPa during 6-8 June 2005. Contour interval is 0.5×10^{-9} s^{-2}. H and L denote max. PVA and min. NVA with the central value beneath it, respectively. (Maps from PSWC.)

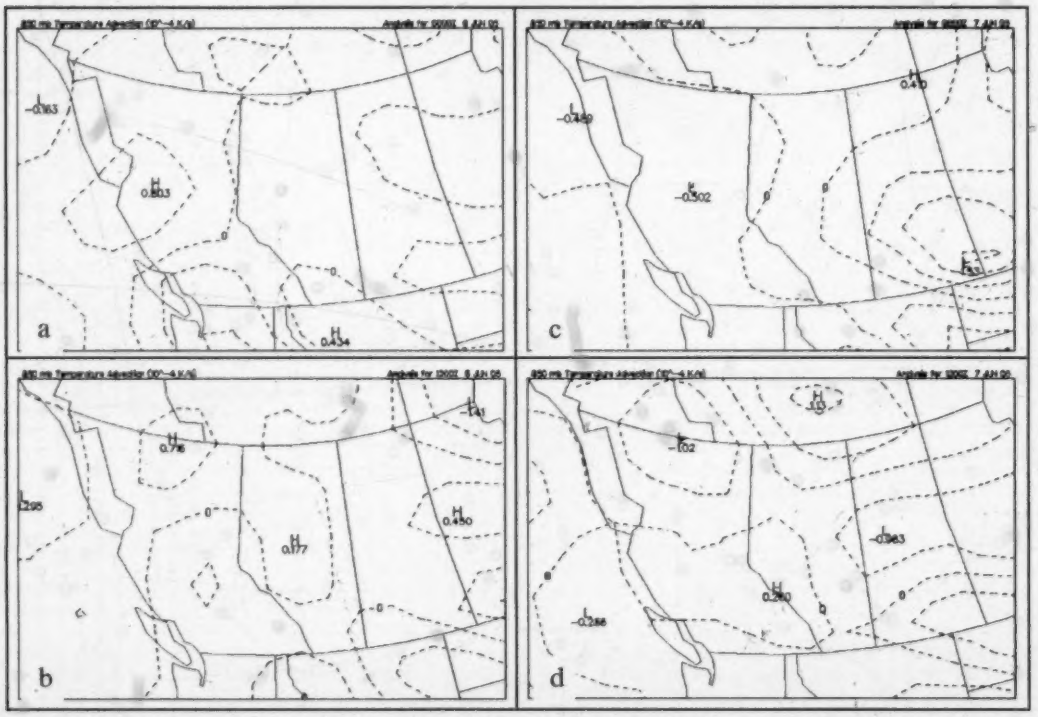

Figure 3-16. Sequence of temperature advection at 850 hPa during 6-7 June 2005. Contour interval is 0.5 (10^{-4} K/s), H and L denote max. PTA and min. NTA with the central value beneath it, respectively. (Maps from PSWC.)

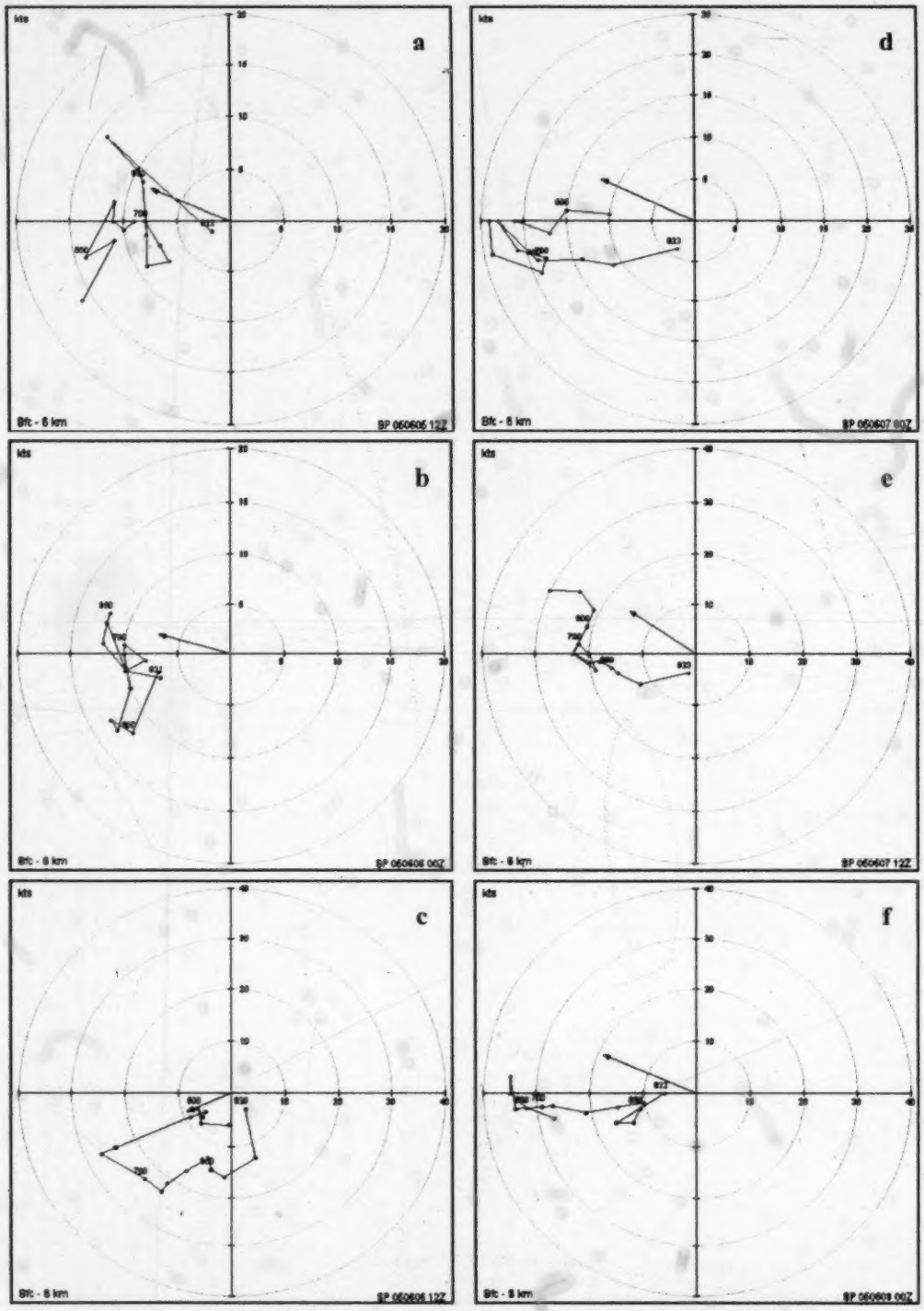

Figure 3-17. Sequence of hodographs of Stony Plain (Alberta) during 5-8 June 2005. Brown arrows: storm motion vectors; red lines: connections of the wind vector points at neighboring levels.

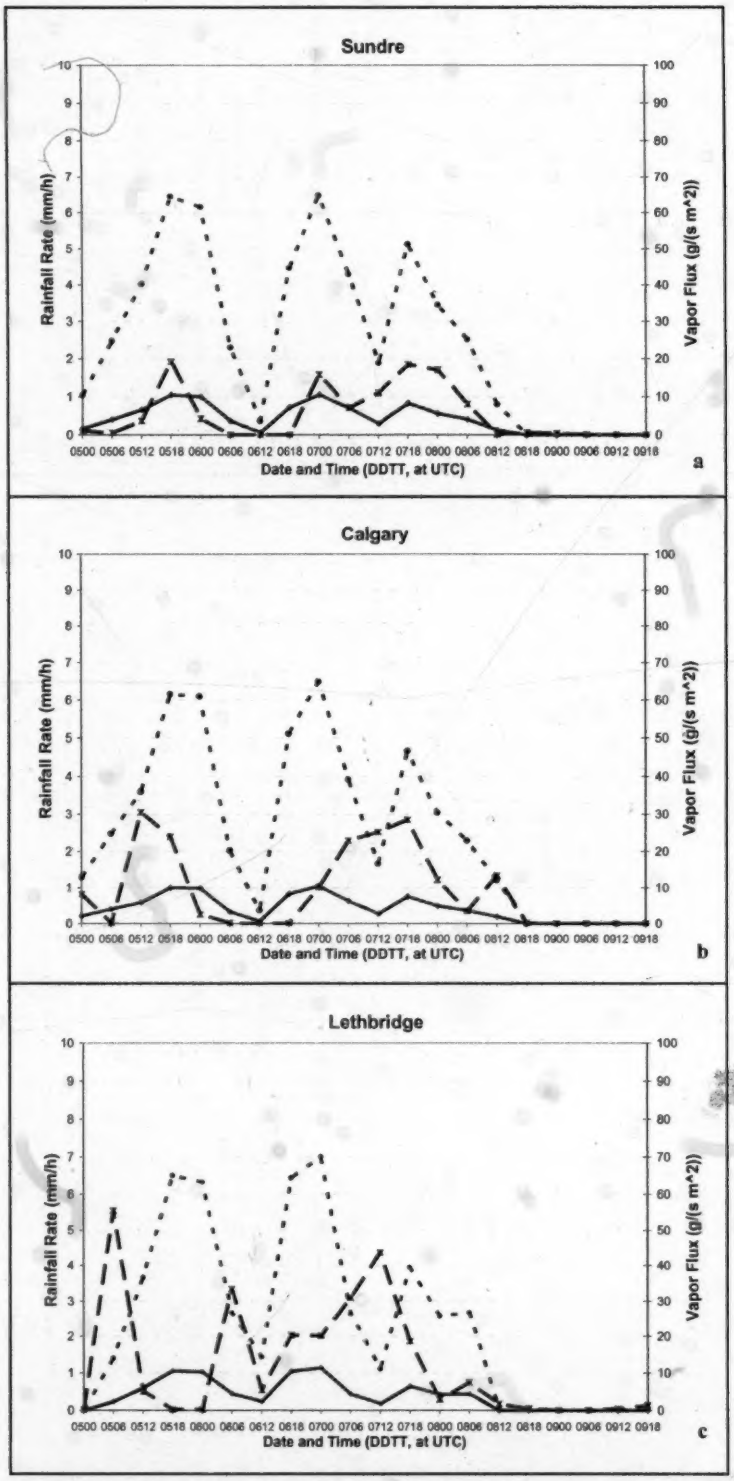

Figure 3-18. Time series of horizontal vapor flux (brown stippled), estimated orographic rainfall rate (green solid) and rain gauge measured rainfall rate (blue dashed) for Sundre, Calgary, and Lethbridge during 5-9 June 2005.

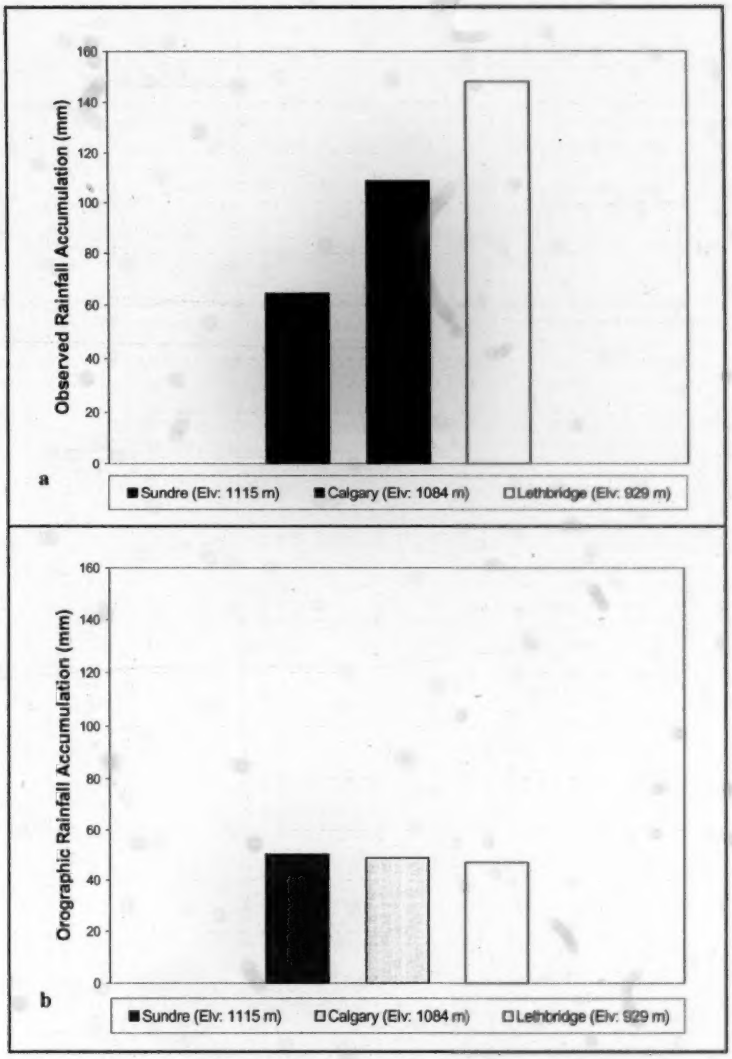

Figure 3-19. (a) Accumulated observed rainfall and, (b) Accumulated estimated orographic rainfall of 3 locations during 5-9 June 2005.

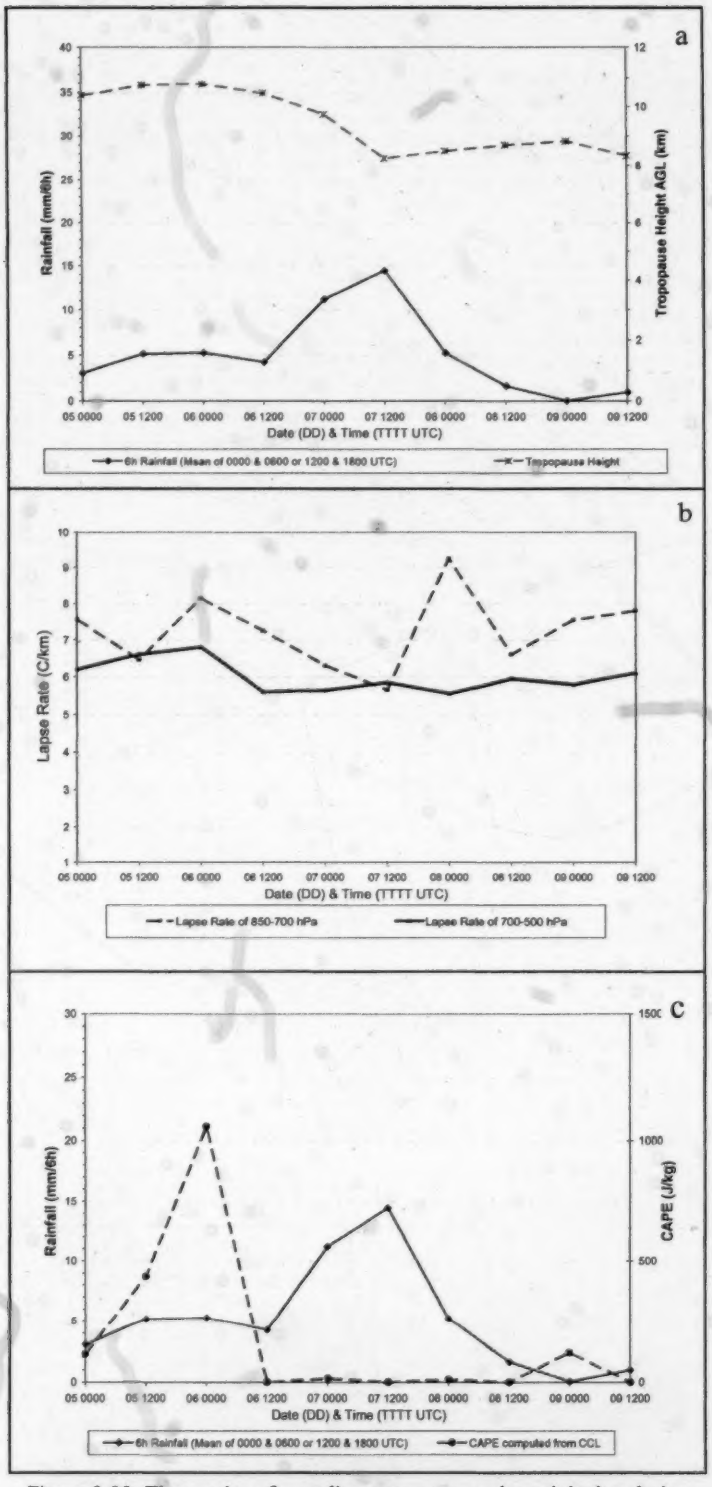
a
Rainfall (mm/6h)
Tropopause Height AGL (km)
Date (DD) & Time (TTTT UTC)
6h Rainfall (Mean of 0000 & 0600 or 1200 & 1800 UTC)
Tropopause Height
b
Lapse Rate (C/km)
Date (DD) & Time (TTTT UTC)
Lapse Rate of 850-700 hPa
Lapse Rate of 700-500 hPa
c
Rainfall (mm/6h)
CAPE (J/kg)
Date (DD) & Time (TTTT UTC)
6h Rainfall (Mean of 0000 & 0600 or 1200 & 1800 UTC)
CAPE computed from CCL

Figure 3-20. Time series of sounding parameters and precipitation during 5-9 June 2005. (a) Tropopause height and space-averaged 6h rainfall; (b) Ambient lapse rate; (c) CAPE and space-averaged 6h rainfall.

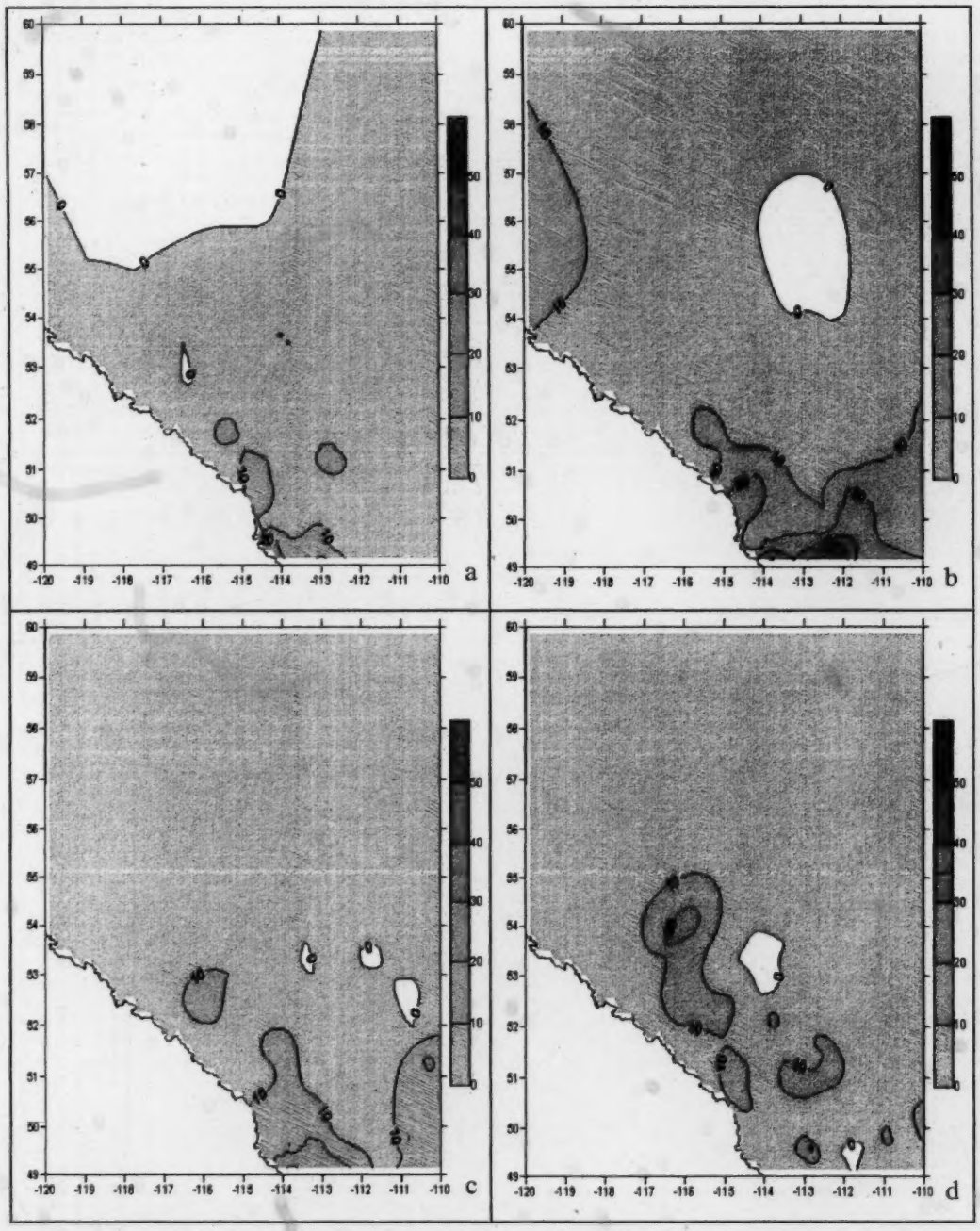

Figure 4-1. 24-hour precipitation distribution of rainstorm case 1 during 1-4 June 2005 (accumulation ending at 0600 UTC). (a) June 1, (b) June 2, (c) June 3, (d) June 4. Units in millimeter.

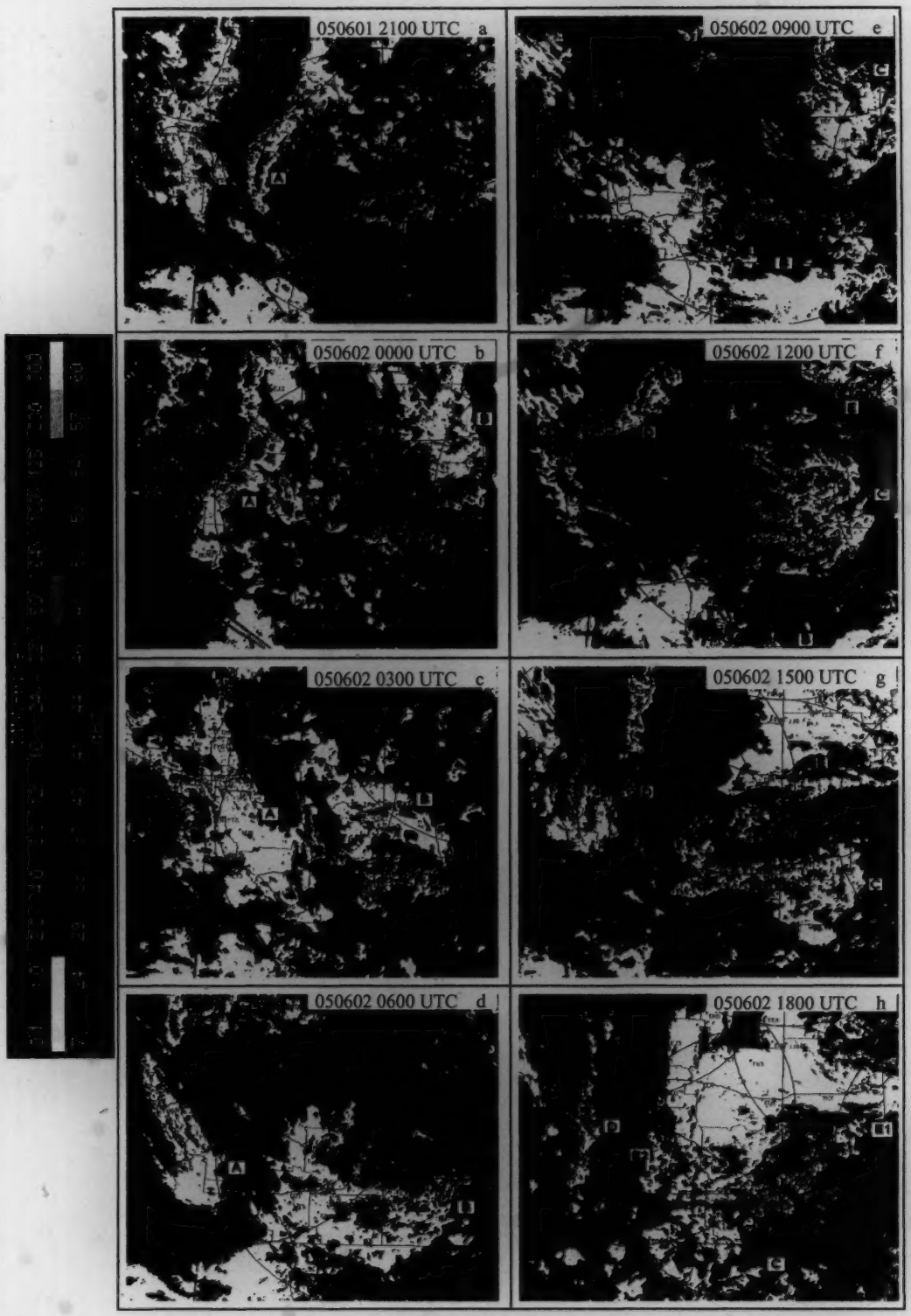

Figure 4-2I. Evolution of composite CAPPI radar echoes of rainstorm case 1 during 1-2 June 2005 at intervals of 3 hours. (Same scale as shown on Figure 3-2I.)

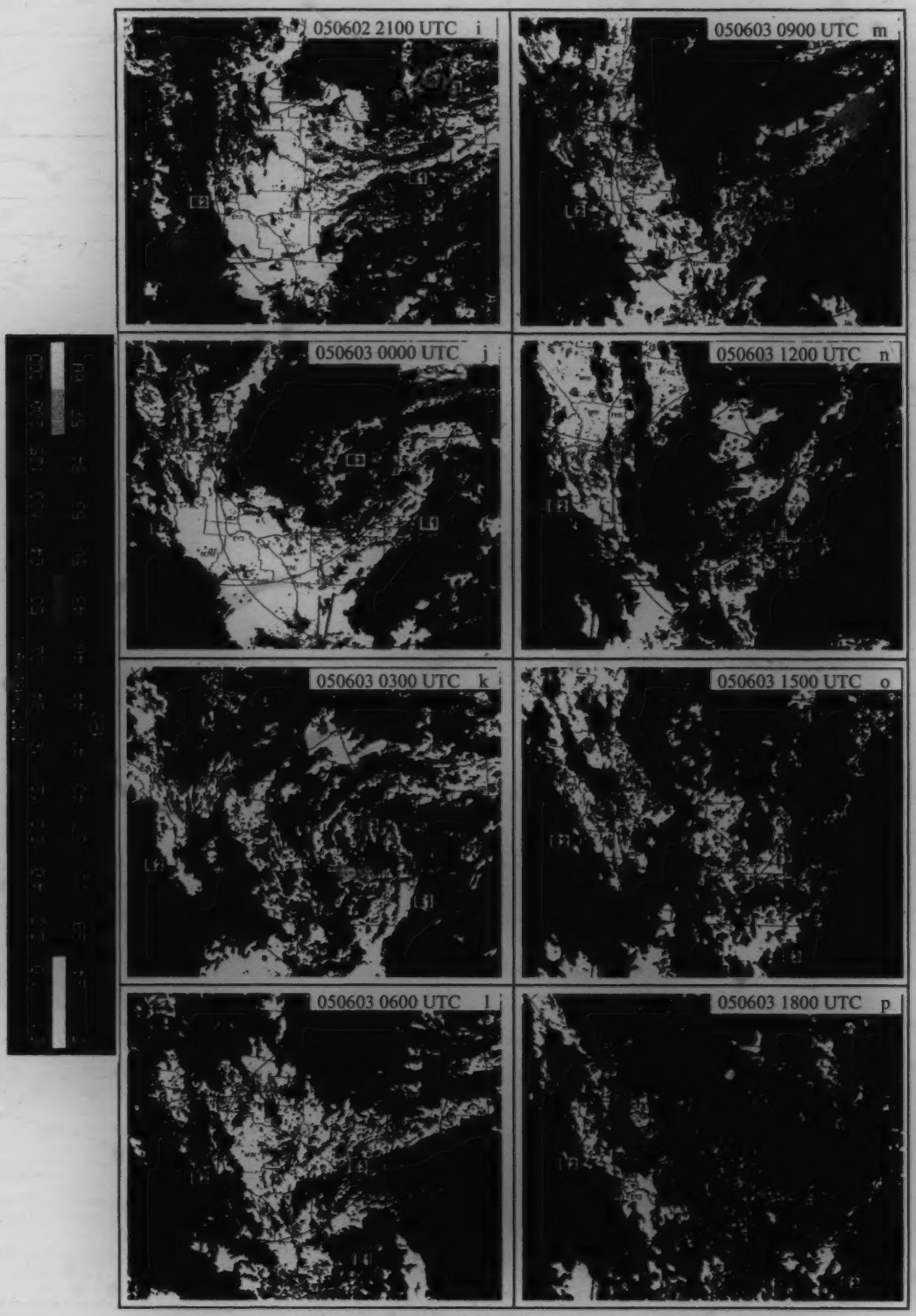

Figure 4-2I (continue). Evolution of composite CAPPI radar echoes of rainstorm case 1 during 2-3 June 2005 at intervals of 3 hours. (Same scale as shown on Figure 3-2I.)

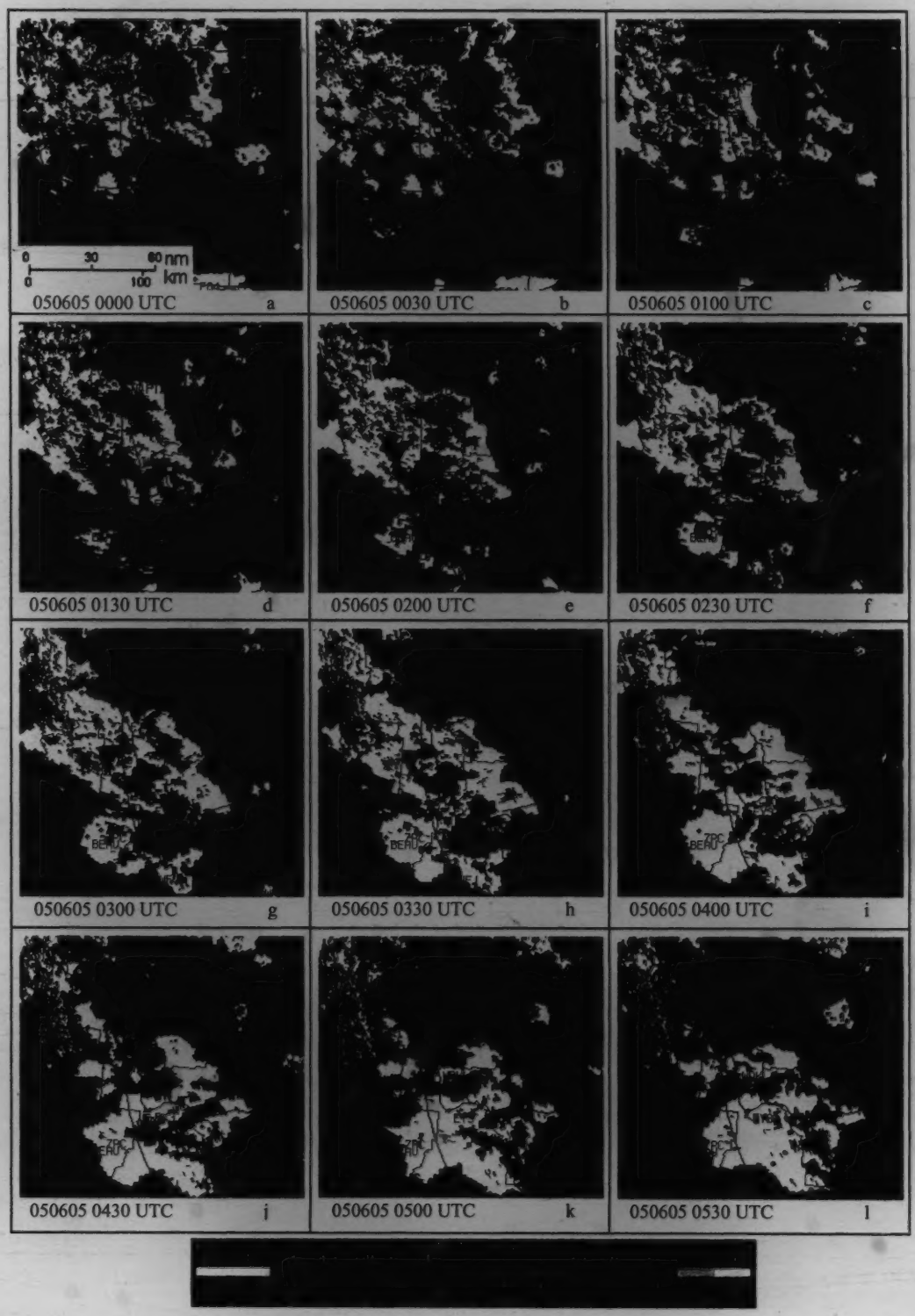

Figure 4-2II. Evolution of the zoom-in CAPPI radar echoes over southwestern Alberta during the early hours on 5 June 2005 at intervals of 30 minutes.

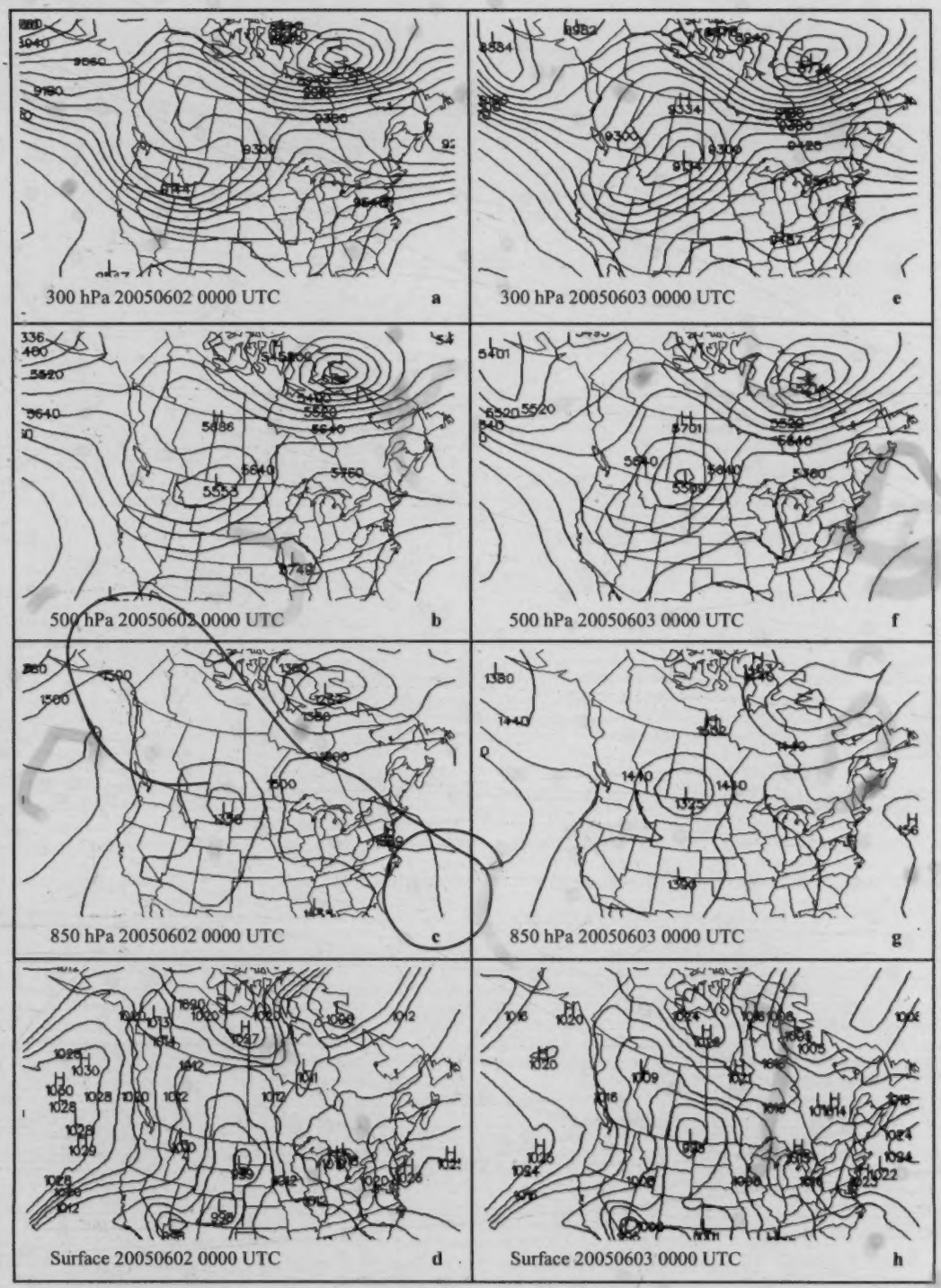

Figure 4-3. Superimposition of the synoptic circulations at typical levels at 0000 UTC 2 June (left) and 3 June 2005 (right). Unit at upper levels is geopotential meter (gpm) at intervals of 60 gpm; unit at sea-level is hecto-pascal (hPa) at intervals of 4 hPa. H and L denote high pressure and low pressure with the central value beneath it, respectively. (Maps from PSWC.)

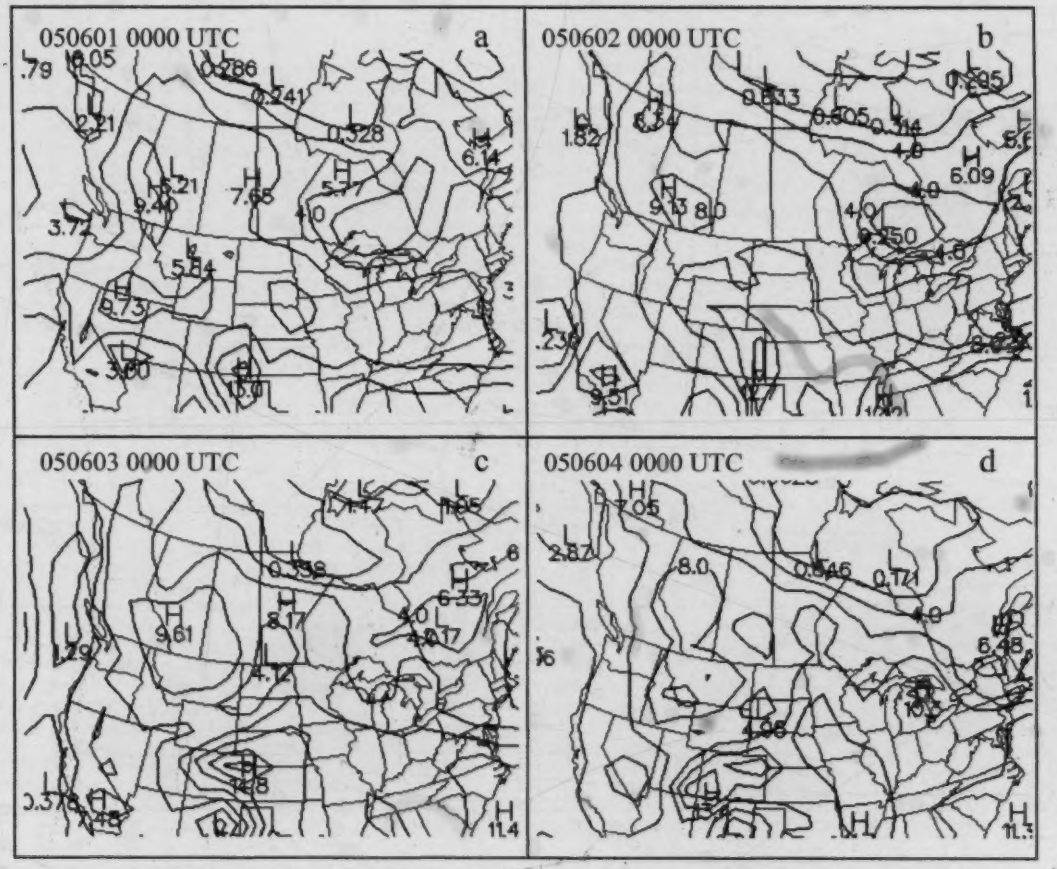

Figure 4-4. Distribution of specific humidity at 850 hPa during 1-4 June 2005. Contour interval is 2.0 (g/kg). H and L denote the maximum and minimum with the central value beneath it, respectively. (Maps from PSWC.)

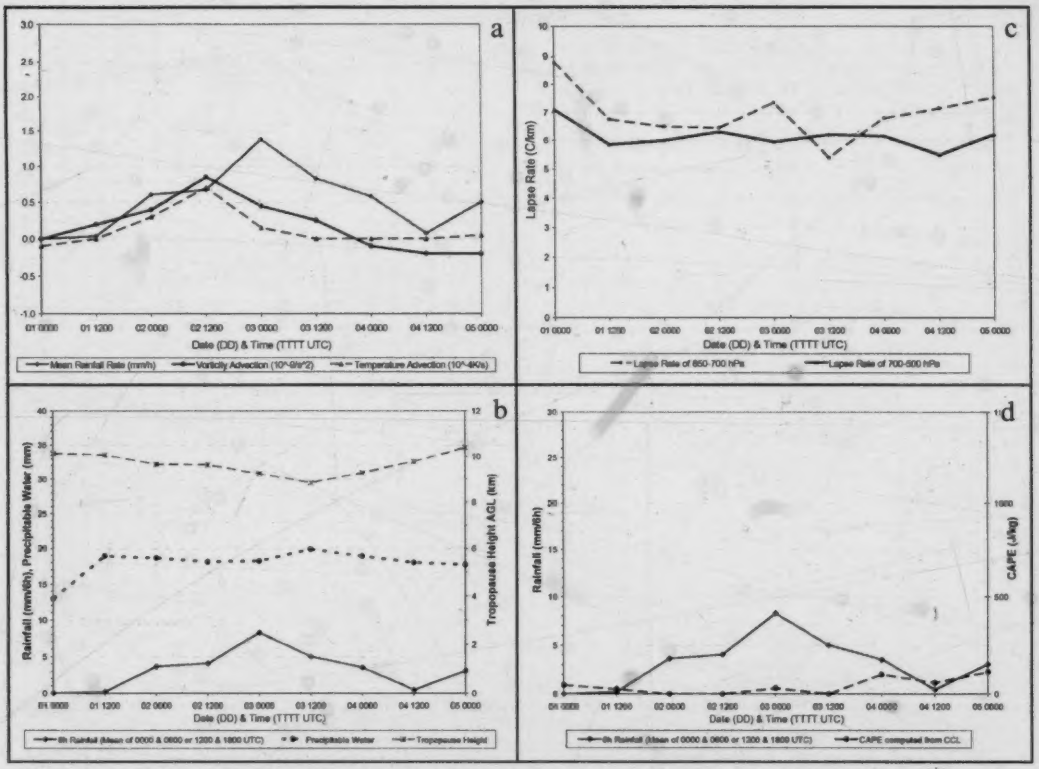

Figure 4-5. Time series of dynamic and thermodynamic parameters and precipitation during 1-5 June 2005. (a) Vorticity advection (10^{-9} s^{-2}), temperature advection (10^{-4}K/s) and time-space-averaged rainfall rate (mm/h); (b) Precipitable water (mm), tropopause height (km) and space-averaged 6h rainfall (mm/6h); (c) Ambient lapse rate (C/km); (d) CAPE (J/kg) and space-averaged 6h rainfall (mm/6h).

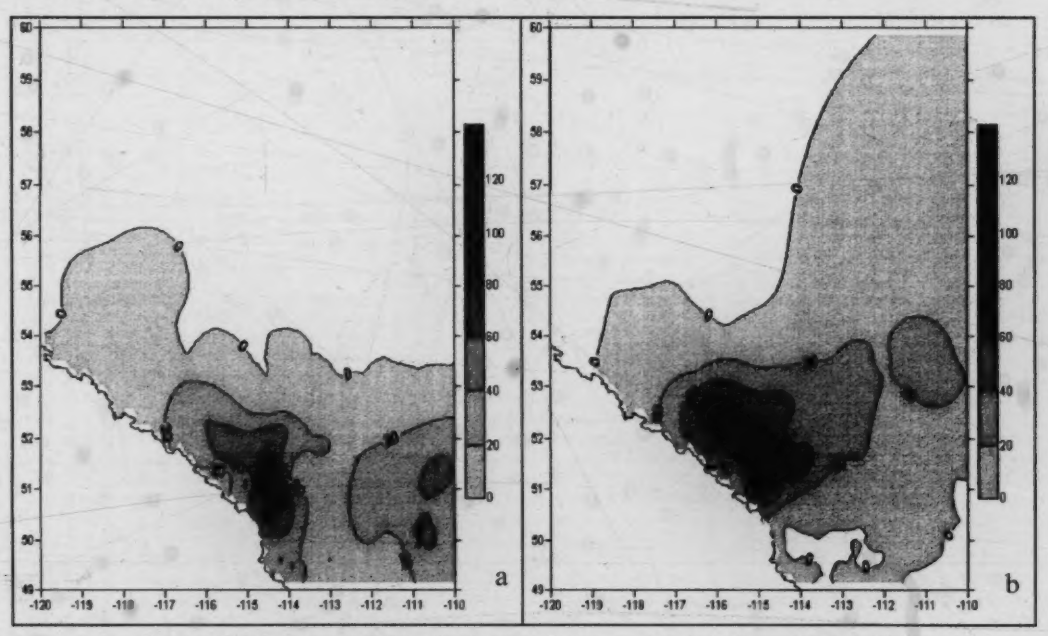

Figure 4-6. 24-hour precipitation distribution of rainstorm case 3 during 17-18 June 2005 (accumulation ending at 0600 UTC). (a) June 17, (b) June 18. Units in millimeter.

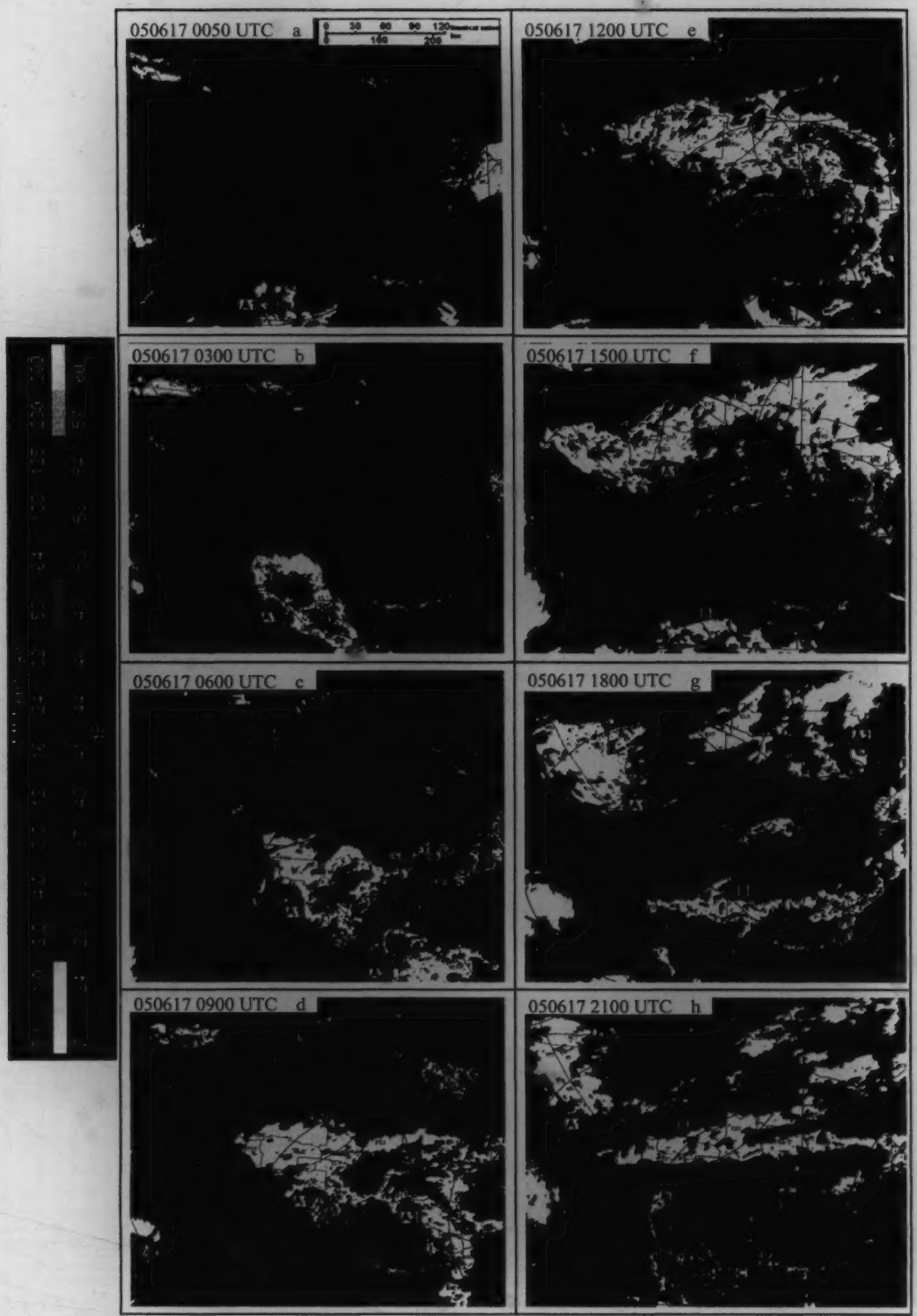

Figure 4-7I. Evolution of composite CAPPI radar echoes of rainstorm case 3 on 17 June 2005 at intervals of 3 hours except between the first and second images. (Strathmore radar was not available and labeled as N/A.)

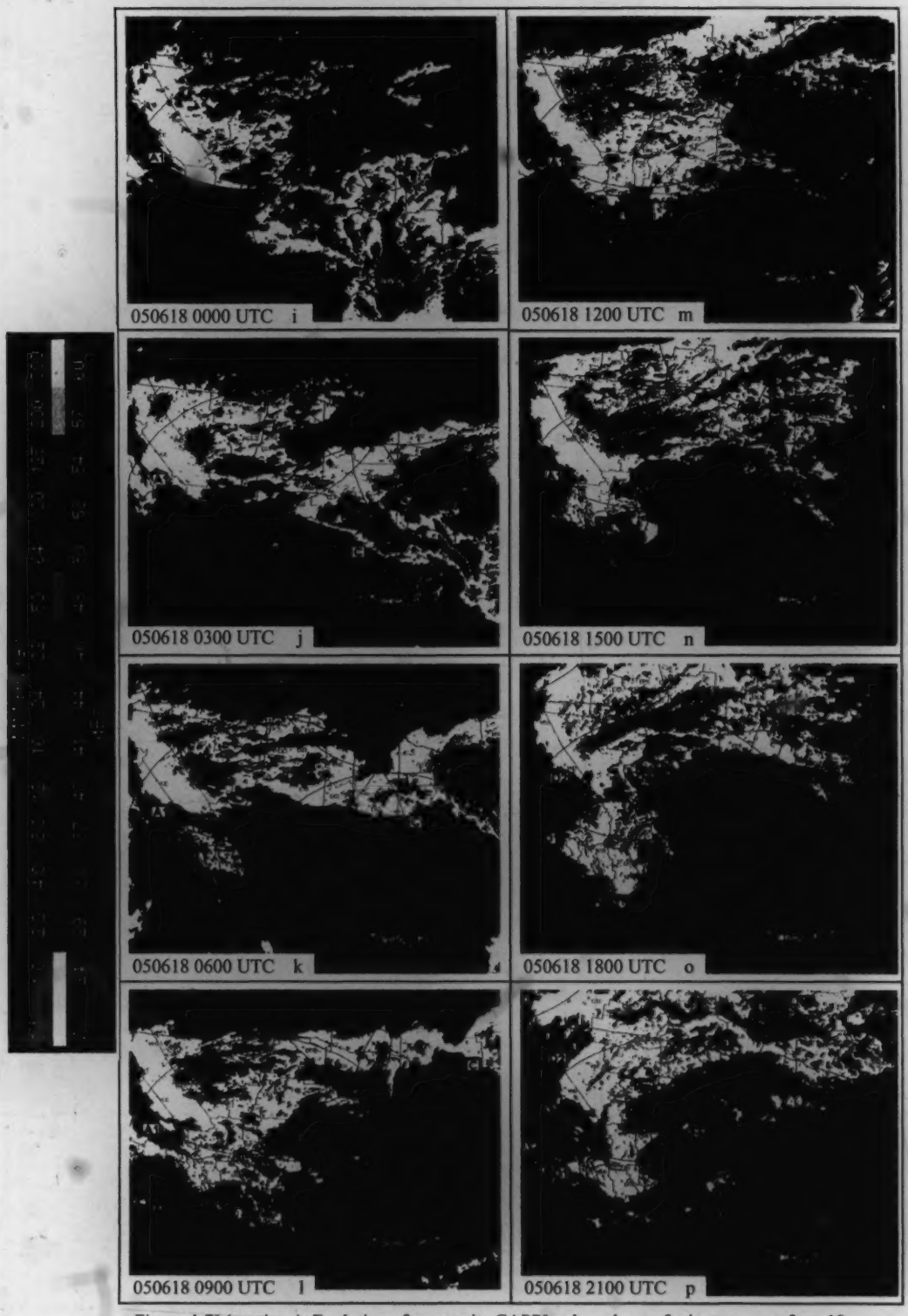

Figure 4-7l (continue). Evolution of composite CAPPI radar echoes of rainstorm case 3 on 18 June 2005 at intervals of 3 hours. (Strathmore radar was not available and labeled as N/A.)

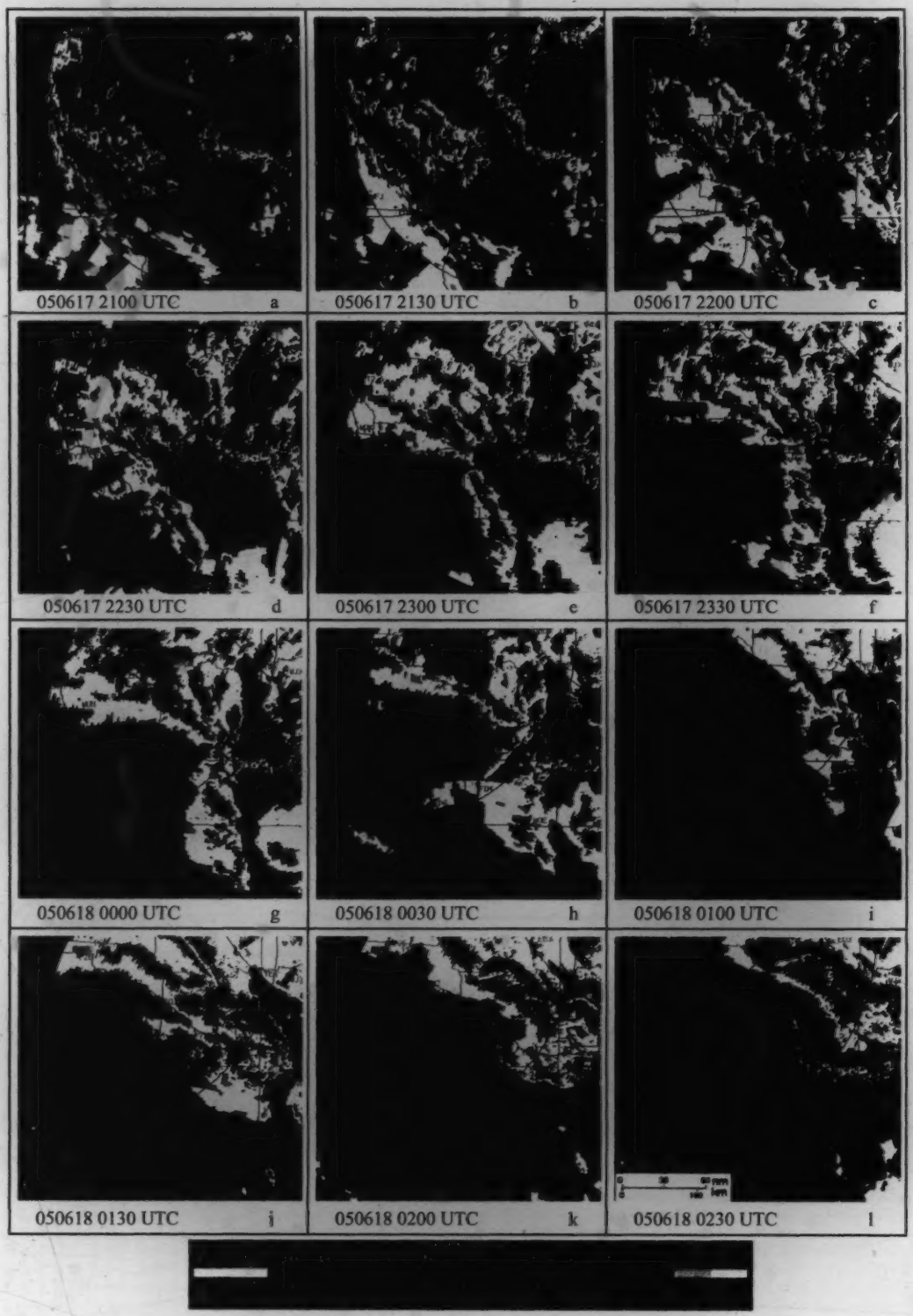

Figure 4-7II. Evolution of the zoom-in CAPPI radar echoes over southeastern Alberta from 2100 UTC 17 June to 0230 UTC 18 June 2005 at intervals of 30 minutes. (Strathmore radar was not available and labeled as N/A.)

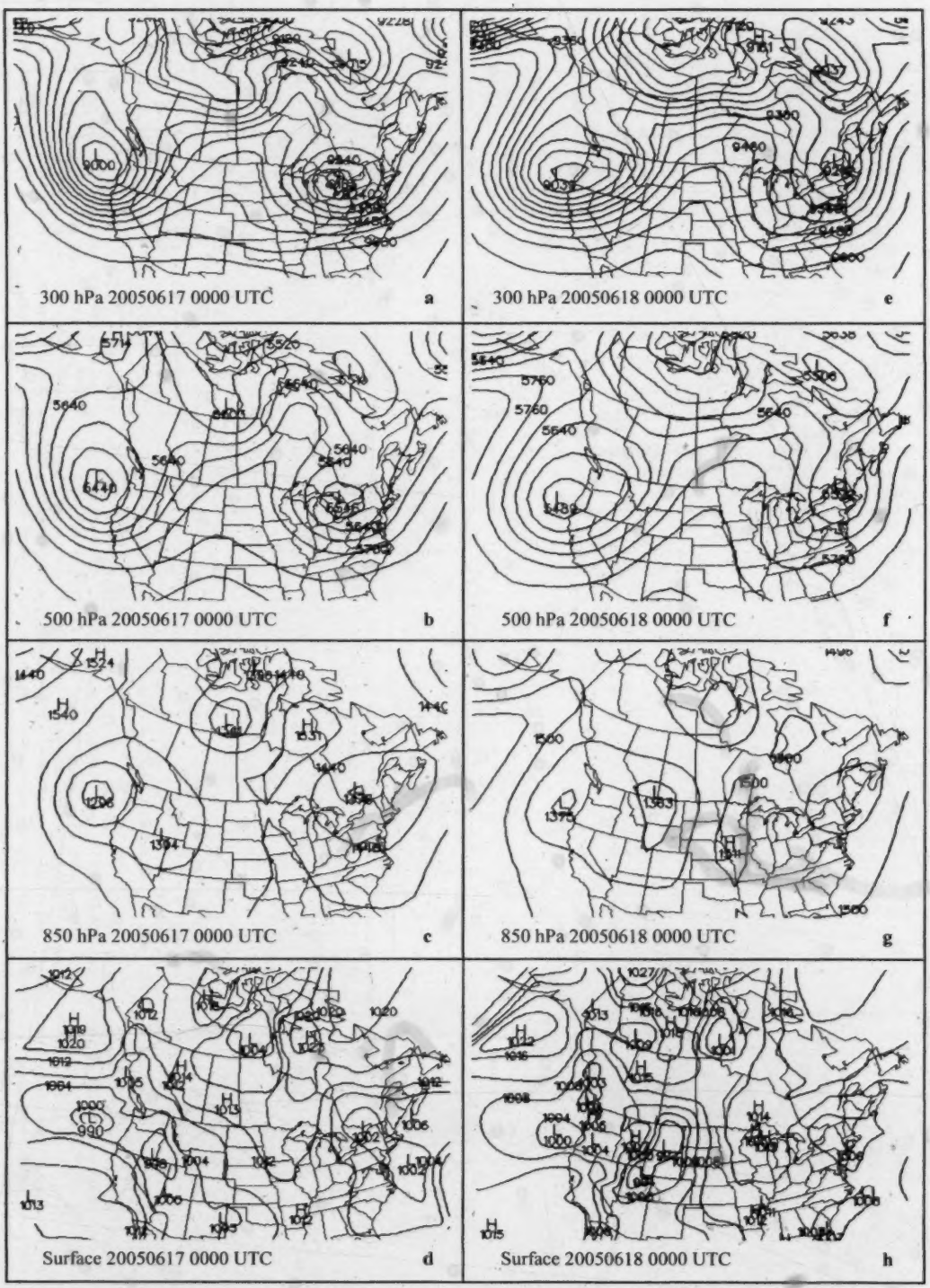

Figure 4-8. Superimposition of the synoptic circulations at typical levels at 0000 UTC 17 June (left) and 18 June 2005 (right). Unit at upper levels is geopotential meter (gpm) at interval of 60 gpm; unit at sea-level is hecto-pascal (hPa) at interval of 4 hPa. H and L denote high pressure and low pressure with the central value beneath it, respectively. (Maps from PSWC.)

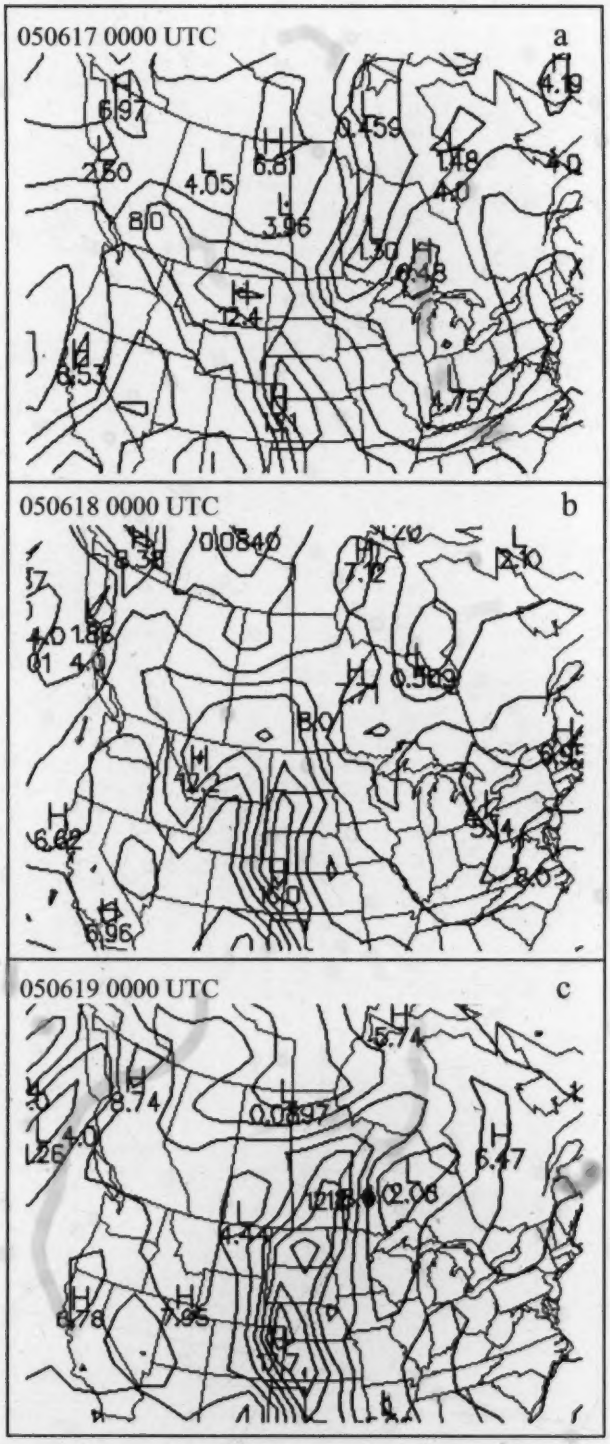

Figure 4-9. Distribution of specific humidity at 850 hPa during 17-19 June 2005. Contour interval is 2.0 (g/kg). H and L denote the maximum and minimum with the central value beneath it, respectively. (Maps from PSWC.)

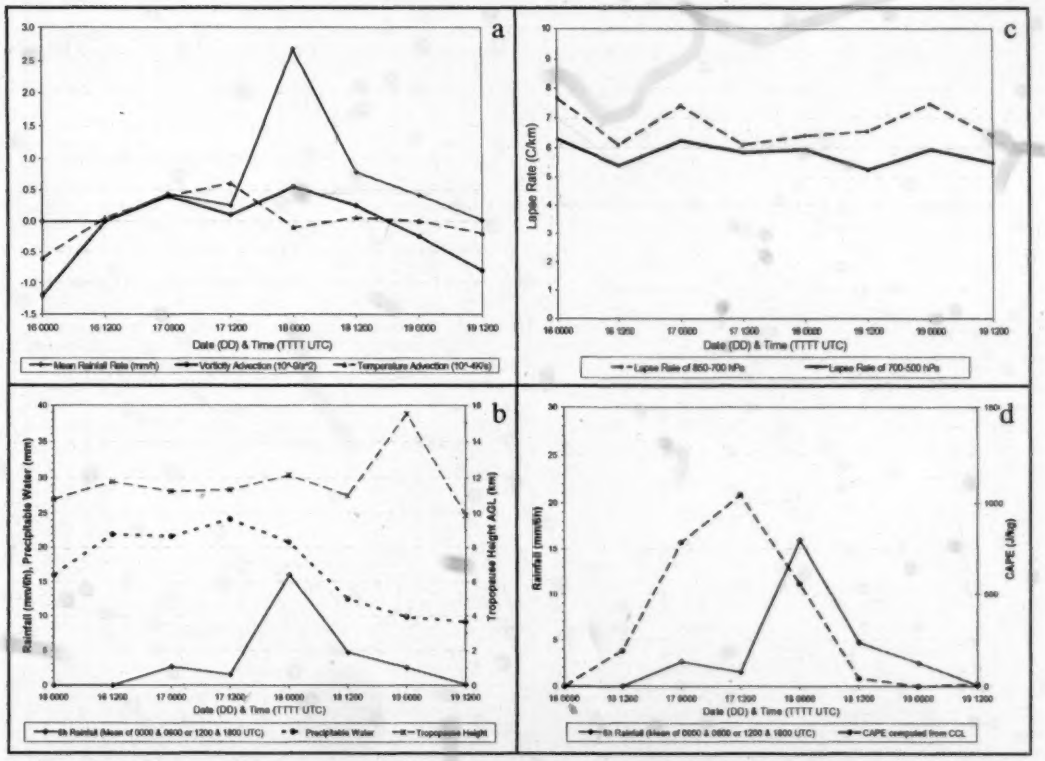

Figure 4-10. Time series of dynamic and thermodynamic parameters and precipitation during 16-19 June 2005. (a) Vorticity advection (10^{-9} s^{-2}), temperature advection (10^{-4}K/s) and time-space-averaged rainfall rate (mm/h); (b) Precipitable water (mm), tropopause height (km) and space-averaged 6h rainfall (mm/6h); (c) Ambient lapse rate (C/km); (d) CAPE (J/kg) and space-averaged 6h rainfall (mm/6h).

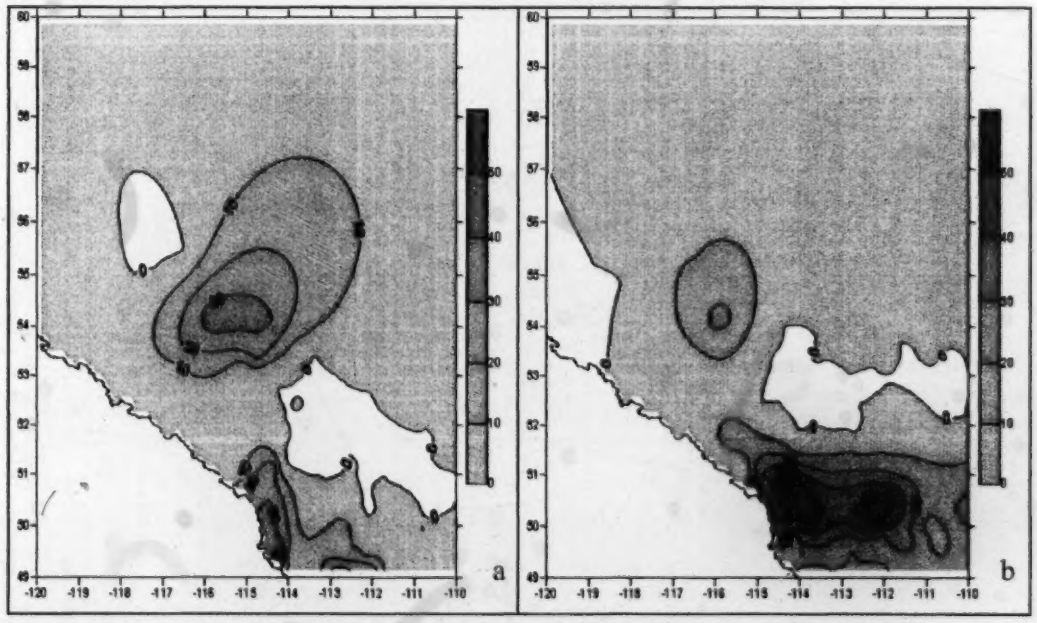

Figure 4-11. 24-hour precipitation distribution of rainstorm case 4 during 27-28 June 2005 (accumulation ending at 0600 UTC). (a) June 27, (b) June 28. Units in millimeter.

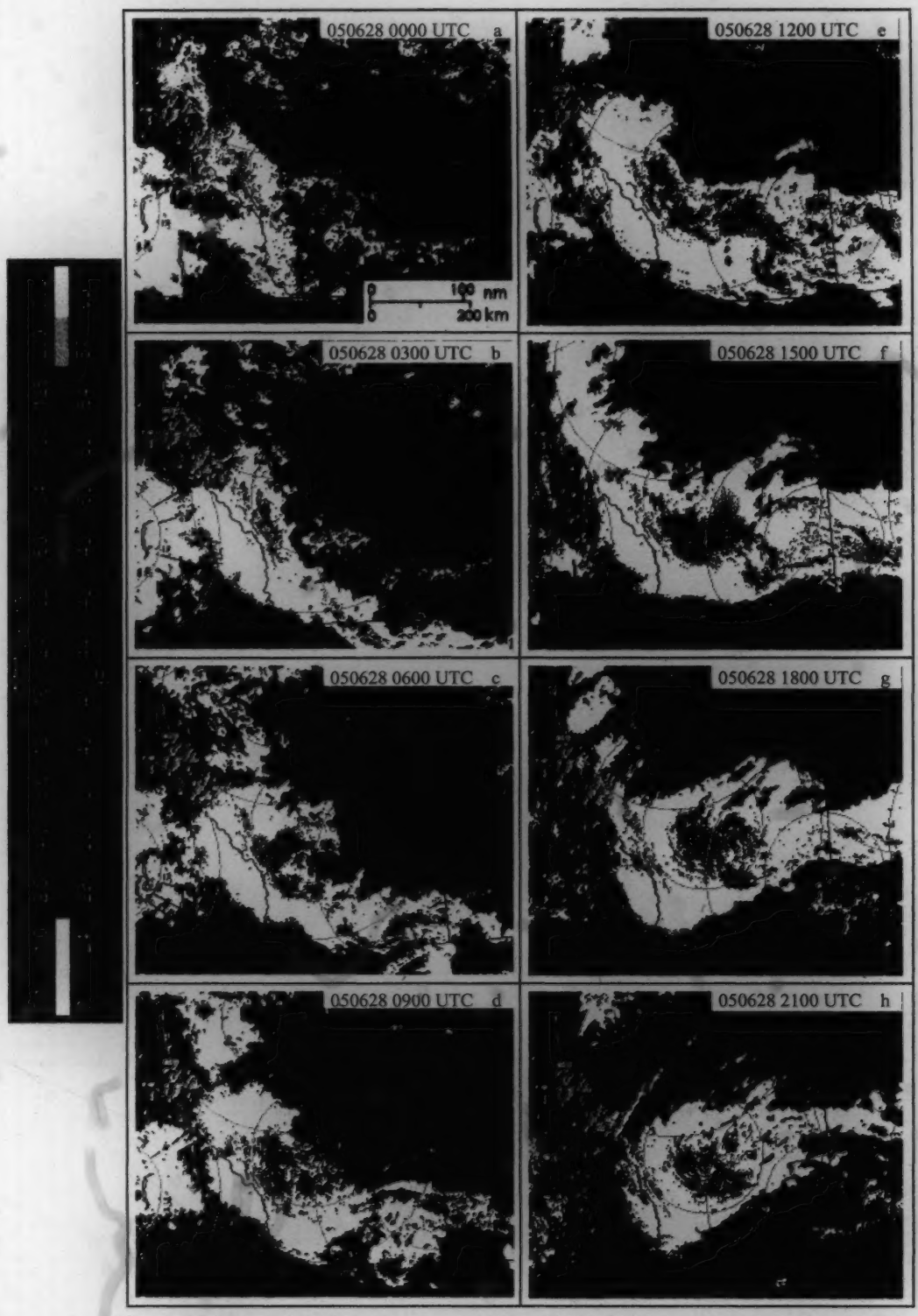

Figure 4-12: Composite CAPPI radar echoes on 28 June 2005, with topographic background, at intervals of 3 hours. (XSM, XBU, WHK are radar stations at Strathmore, Schuler and Carvel, respectively.)

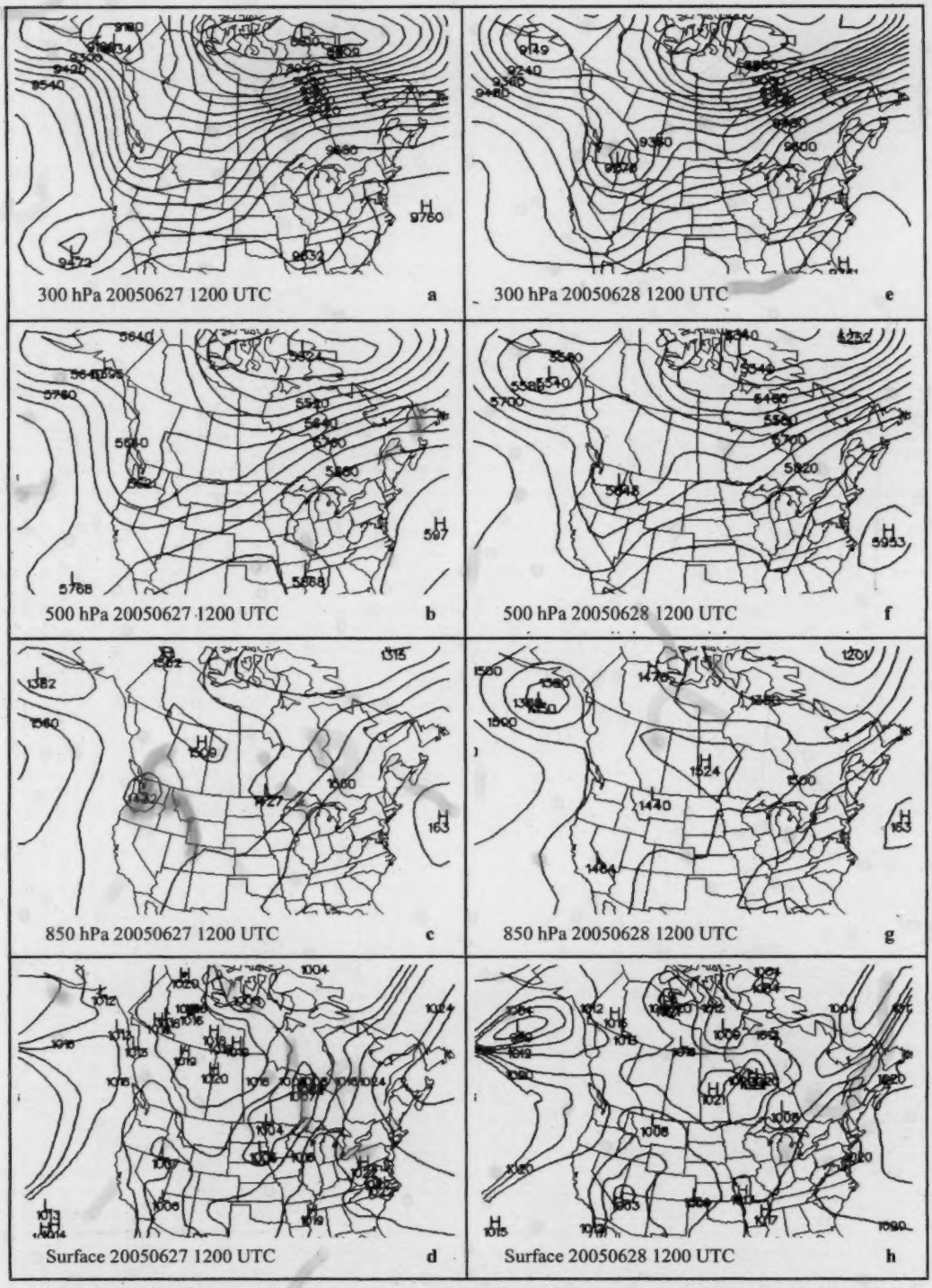

Figure 4-13. Superimposition of the synoptic circulations at typical levels at 1200 UTC 27 June (left) and 28 June 2005 (right). Unit at upper levels is geopotential meter (gpm) at intervals of 60 gpm; unit at sea-level is hecto-pascal (hPa) at intervals of 4 hPa. H and L denote high pressure and low pressure with the central value beneath it, respectively. (Maps from PSWC.)

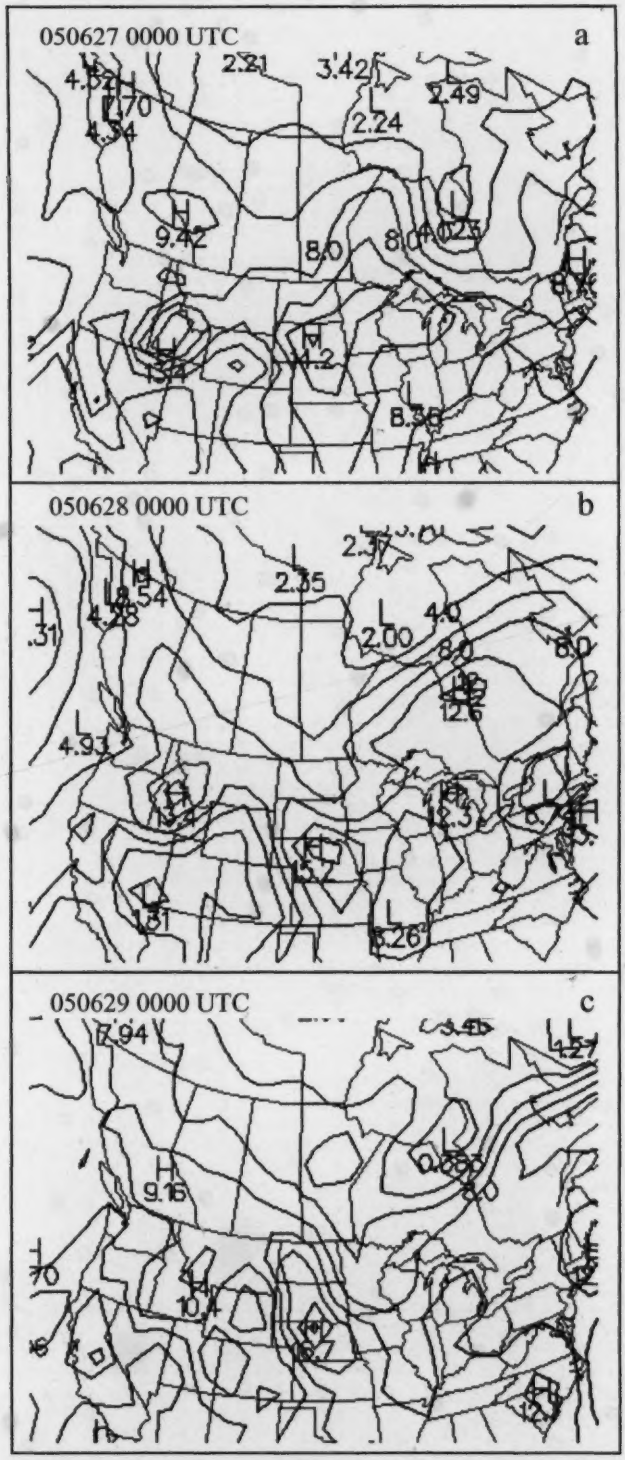

Figure 4-14. Distribution of specific humidity at 850 hPa during 27-29 June 2005. Contour interval is 2.0 (g/kg). H and L denote the maximum and minimum with the central value beneath it, respectively. (Maps from PSWC.)

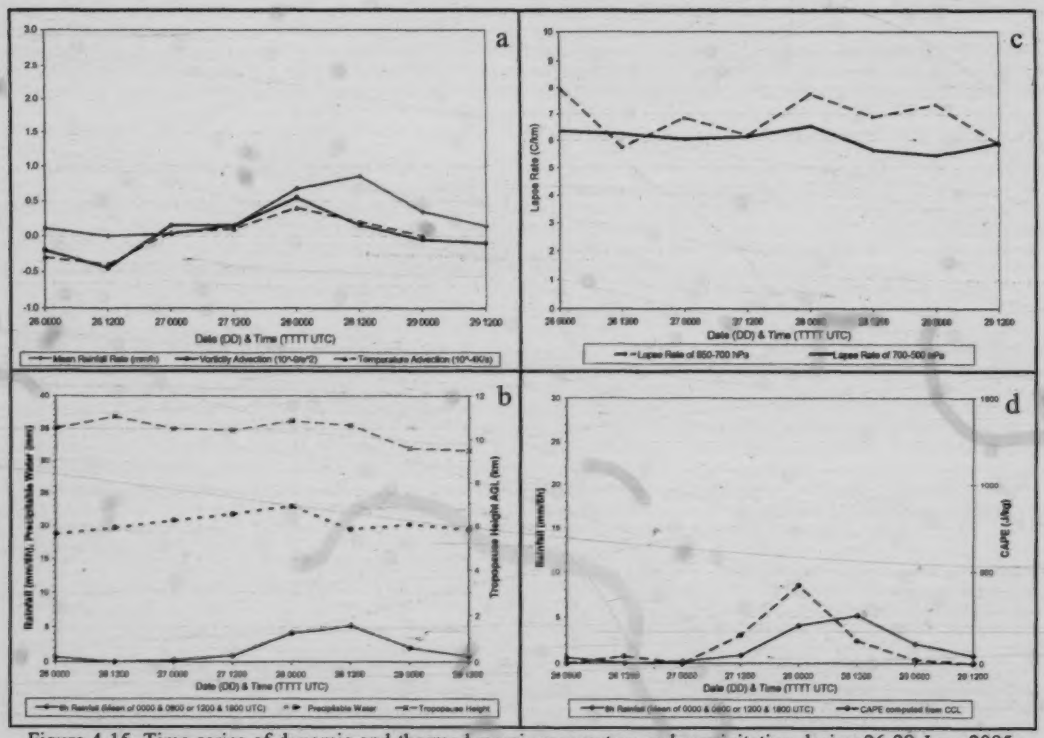

Figure 4-15. Time series of dynamic and thermodynamic parameters and precipitation during 26-29 June 2005. (a) Vorticity advection (10^{-9} s^{-2}), temperature advection (10^{-4}K/s) and time-space-averaged rainfall rate (mm/h); (b) Precipitable water (mm), tropopause height (km) and space-averaged 6h rainfall (mm/6h); (c) Ambient lapse rate (C/km); (d) CAPE (J/kg) and space-averaged 6h rainfall (mm/6h).

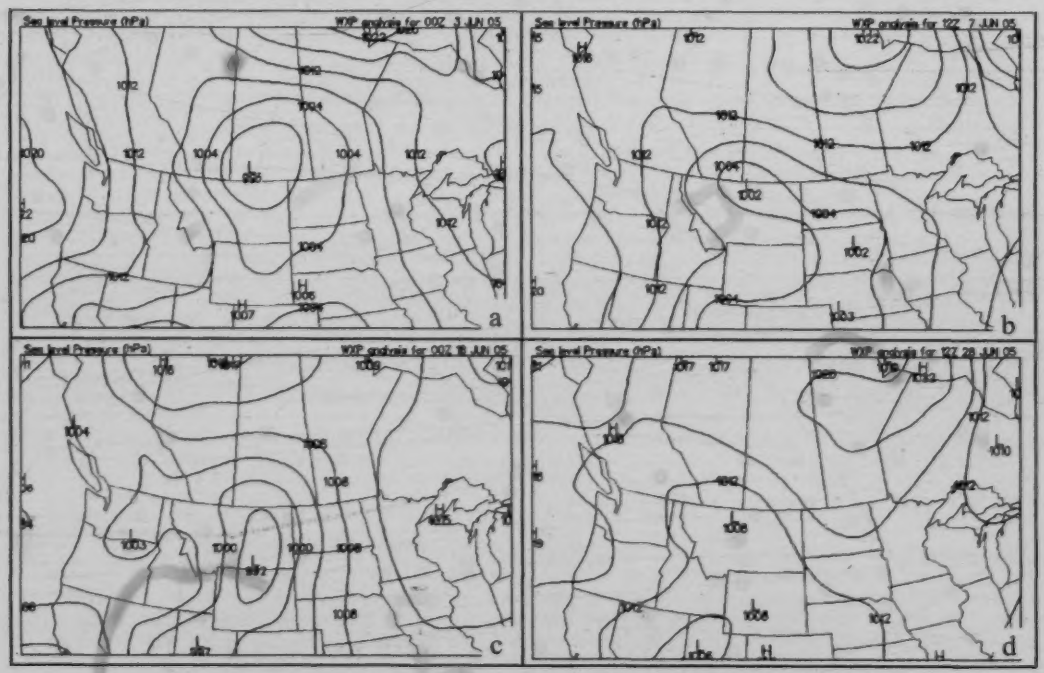

Figure 5-1. Characterized sea-level synoptic flow patterns of the four rainstorms. (a) June 2, (b) June 7, (c) June 18, (d) June 28. (Maps from PSWC)

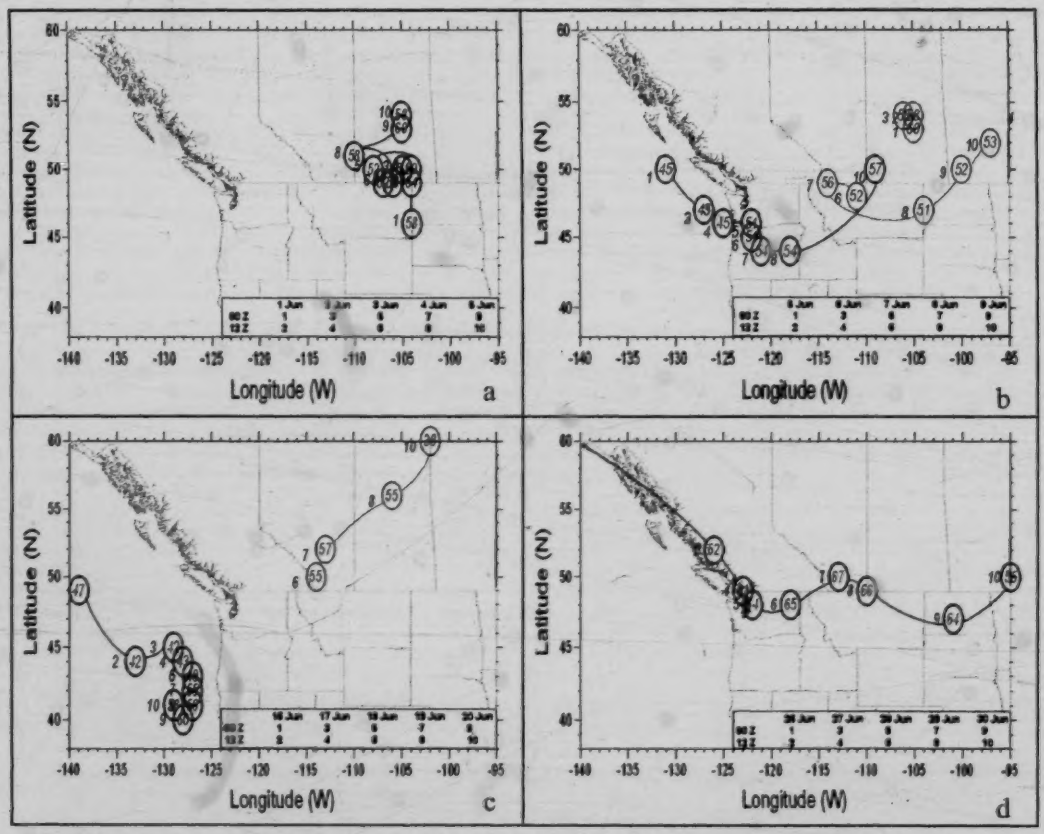

Figure 5-2. Evolution of the 500-hPa lows of the four rainstorms. (a) June 1-5, (b) June 5-9, (c) June 16-20, (d) June 26-30. Black circles are the primarily lows, green circles are the secondary lows. The tracks of the lows are indicated by the dark and light brown curves for the primarily lows and secondary lows, respectively. The numbers inside the circles are the last two digits of minimum geopotential height. The numbers to the left of the circles indicate the time steps beginning with 1 as of 0000 UTC on the first day of each event, at intervals of 12 hours (refer to the table on the lower right corner of each plot).

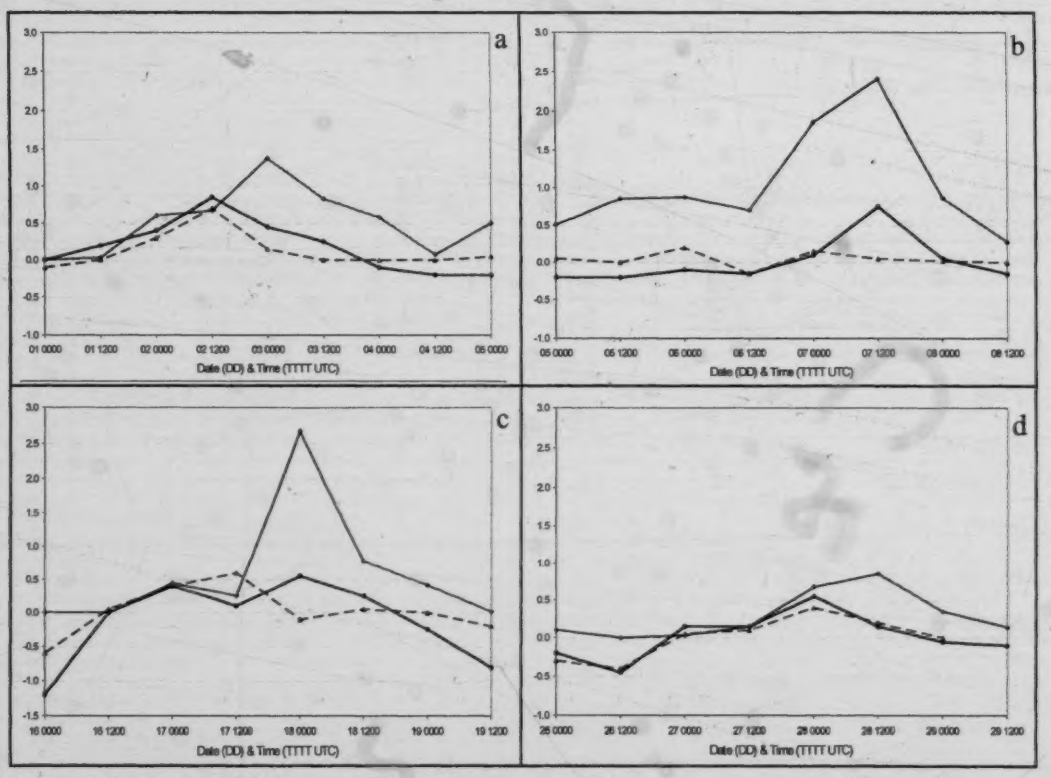

Figure 5-3. Evolution of vorticity advection (10^{-9} s^{-2}, brown solid), temperature advection (10^{-4}K/s, pink dashed) and time-space-averaged rainfall rate (mm/h, green solid) of the four rainstorms. (a) June 1-5, (b) June 5-9, (c) June 16-19, (d) June 27-29.

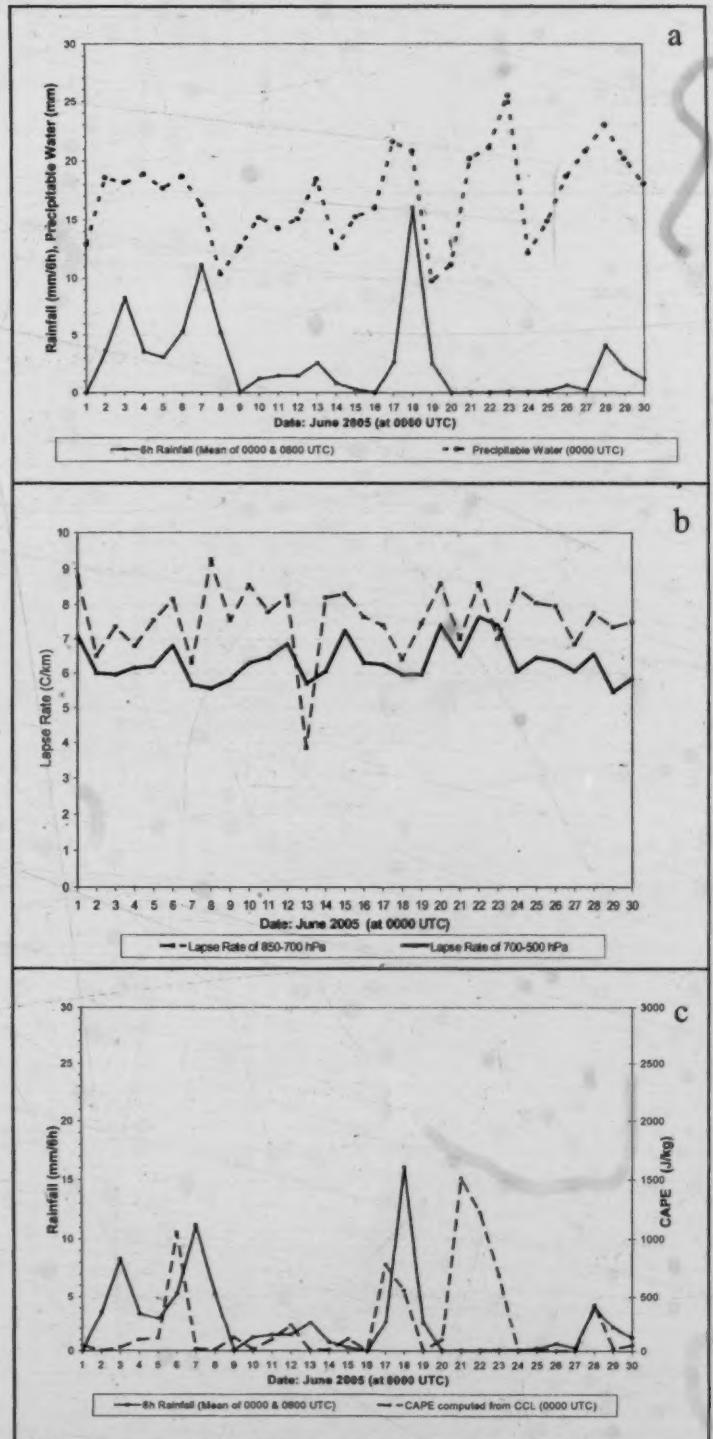
a
Rainfall (mm/6h), Precipitable Water (mm)
Date: June 2005 (at 0000 UTC)
6h Rainfall (Mean of 0000 & 0600 UTC)
Precipitable Water (0000 UTC)
b
Lapse Rate (C/km)
Date: June 2005 (at 0000 UTC)
Lapse Rate of 850-700 hPa
Lapse Rate of 700-500 hPa
c
Rainfall (mm/6h)
CAPE (J/kg)
Date: June 2005 (at 0000 UTC)
6h Rainfall (Mean of 0000 & 0600 UTC)
CAPE computed from CCL (0000 UTC)

Figure 5-4. Time series of sounding parameters and precipitation of June 2005. (a) Precipitable water and space-averaged 6h rainfall; (b) Ambient lapse rate; (c) CAPE and space-averaged 6h rainfall.

References:

Alberta Environmental Protection, Water Resources Operations Division, 1995: Oldman river dam June 1995 flood summary report. Alberta Environment Technical Note, Revision No.2, 35 pp.

Beckman, S. K., 1987: Use of Enhanced IR/Visible Satellite Imagery to Determine Heavy Snow Areas. *Mon. Wea. Rev.*, **115**, 2060-2087.

Bjerknes, J., 1951: Extratropical cyclones. Compendium of Meteorology, T. F. Malone, Ed., Amer. Meteor. Soc., 577-598.

——, 1954: The diffluent upper trough. *Arch. Meteor. Geophys. Bioklim.*, **A7**, 41-46.

Bleckman, J. B., 1981: Vortex generation in a numerical thunderstorm mode. *Mon. Wea. Rev.*, **109**, 1061-1071.

Bluestein, H. B., 1986: Fronts and jet streaks - A theoretical perspective. Mesoscale Meteorology and Forecasting. Amer. Meteor. Soc., 793 pp.

Brimelow, J. C. and G. W. Reuter, 2005: Transport of atmospheric moisture during three extreme rainfall events over the Mackenzie River Basin. *J. Hydrometeo.* **Vol. 6**, 423-440.

Browne, G., 1996: Southern Alberta heavy rain event, June 6-7, 1995. Environment Canada, Environmental Service Branch, Technical Note, Report 96-xx, 31 pp.

Browning, K. A., 1990: Organization of clouds and precipitation in extratropical cyclones. Extratropical Cyclones - The Erik Palmén Memorial Volume, Amer. Meteor. Soc., 129-153

Burrows, W. R. 1966: Heavy rainfalls in Edmonton. Meteorological Branch CIR 4477, TEC-626. 33 pp.

Carlson T. N., 1980: Airflow through midlatitude cyclones and the comma cloud pattern. *Mon. Wea. Rev*, **108**, 1498-1509.

Carr, F. H., and J. P. Millard, 1985: A composite study of comma clouds and their association with severe weather over the Great Plains. *Mon. Wea. Rev*, **113**, 370-387.

Chung, Y. S., and E. R. Reinelt, 1973: On cyclogenesis in the lee of the Canadian Rocky Mountains. *Arch. Meteor. Geophys. Bioklim., Ser. A*, **22**, 205-226

——, K. D. Hage, and ——, 1976: On lee cyclogenesis and airflow in the Canadian Rocky Mountains and the East Asian Mountains. *Mon. Wea. Rev.*, **104**, 879-891.

Cotton, W. R., and R. A. Anthes, 1989: Storm and cloud dynamics. Academic Press, San Diego, 883 pp.

Djurić, D., 1994: Weather analysis. Prentice Hall, New Jersey, 304 pp.

Doswell, C. A., H.E. Brooks, and R.A. Maddox, 1996: Flash flood forecasting: An ingredients-based methodology. *Wea. Forecasting*, **11**, 560-581.

Dupilka, M. L., G.W. Reuter, T. K. Flesch and R. D. D'Armours, 2007: On calculating source regions using a non-diffusive Lagrangian trajectory model. National Weather Association Electronic Journal of Operational Meteorology.

Hage, K. D., 1957: On the summer cyclogenesis in Western Canada associated with upper cold lows. Sci. Report No. 1, Contract No. AF 19 (604)-2179, Univ. of Chicago, 87 pp.

Holton, J. R., 2004: An introduction to dynamic meteorology. 4th edition, Academic Press, New York, 391 pp.

Hoskins, B. J., M. E. McIntyre and A. W. Robertson, 1985: On the use and significance of isentropic potential vorticity maps. *Quart. J. Roy. Meteor. Soc.*, **111**, 877-946.

——, 1990: Theory of extratropical cyclones. Extratropical Cyclones - The Erik Palmén Memorial Volume, Amer. Meteor. Soc., 63-80.

Kocin, P. J. and L. W. Uccellini, 1990: Snowstorms along the northeast coast of the United States, 1955 to 1985. Amer. Meteor. Soc., 280 pp.

Lin, Y., S. Chiao, T. Wang, M. Kaplan, L. Michael, and R.P. Weglarz, 2001: Some common ingredients for heavy orographic rainfall. *Wea. Forecasting*, **16,** 633-660.

Liu, J., and R. E. Stewart, 2003: Water vapor fluxes over the Saskatchewan River basin. *J. Hydrometeor.*, **4,** 944-959.

McKay, G. A., 1965: Statistical estimates of precipitation extremes for the prairie provinces. Hydrology Division, PFRA Regina, 29 pp.

Moran, J. M. 2002: Online weather studies, Amer. Meteor. Soc., 2nd Edition, 416 pp.

Nguyen, C. D., 1987: Synoptic study of two intense cold core cyclonic storms. M.Sc. Thesis, Univ. of Alberta, Edmonton, Canada, 176 pp. [Available from Univ. of Alberta, 114 St.–89 Ave., Edmonton, AB, T6G 2E2, Canada.]

Palmén, E., and C. W. Newton, 1969: Atmospheric circulation systems. Academic Press, New York, 603 pp.

Pan, Z., M. Segal, and R. W. Arritt, 2004: Role of topography in forcing low-level jets in the central United States during the 1993 flood-altered terrain simulations. *Mon. Wea. Rev.*, **132,** 396-403.

Petterssen, S., 1956: Weather analysis and forecasting. Vol. I, Motion and Motion Systems, 2nd Edition. Mc-Graw-Hill, New York, 428 pp.

Pierrehumbert, R. T., 1986: Lee cyclogenesis. Mesoscale Meteorology and Forecasting, Amer. Meteor. Soc., 793 pp.

Phillips, D., 1990: The climates of Canada. Minister of Supply and Service Canada, Environment Canada, 176 pp.

Phinney, R. B., 1982: Flood of June 1975 in the Oldman River Basin, Alberta. Environment Canada, Water Resource Branch (Inland Water Directorate), Technical Note, 48 pp.

RAOB, The Complete RAwinsonde OBservation Analysis Program, User's Guide, Version 4.0, 1997, 52 pp.

Reinelt, E. R., 1970: On the role of orography in the precipitation regime of Alberta. The Albertan Geographer, No. **6**. 45-58.

Reuter, G.W., 1990: Radar observations of precipitation production in thunderstorms. *Atmosphere-Ocean*, **28**, 216-229.

—— and C. D. Nguyen, 1993: Organization of the cloud and precipitation in an Alberta storm. *Atmospheric Research*, **30**, 127-141.

—— and L. Xin, 1998: Stratiform rainfall rates from water flux balance equation and cloud model. *Atmosfera*, **11**, 223-237.

——, 2000: Effects of available moisture content on the minimum recurrence interval between two major rainstorms. Alberta Environment Protection, Technical Report, 40 pp.

Rogers, R. R. and M. K. Yau, 1989: A short course in cloud physics. Butterworth-Heinemann, 3rd Edition, 290 pp.

Smith, S. B., and M. K. Yau, 1987: The mesoscale effect of topography on the genesis of Alberta hailstorms. *Beitr. Phys. Atmosph.*, **60**, 371-392.

Szeto, K. K., 2002: Moisture recycling over the Mackenzie Basin. *Atmos.–Ocean,* **40,** 181-197.

Taylor, G. H. and Hogg, W. D., 2005: An analysis of probable maximum precipitation for the province of Alberta. Alberta Infrastructure and Transportation, Edmonton, Alberta. 43 pp.

Taylor, N. M., 1999: Climatology of sounding parameters identifying the potential for convective storm development over central Alberta. M.Sc. Thesis, Dept. of Earth and Atmospheric Sciences, Univ. of Alberta, Canada, 121 pp. [Available from Univ. of Alberta, 114 St.–89 Ave., Edmonton, AB, T6G 2E2, Canada.]

Thompson, W. C., 1976: Three early severe flood producing storms in Alberta. Meteorological Branch TEC-827. 19 pp.

Tibaldi, S., A. Buzzi and A. Speranza, 1990: Orographic cyclogenesis. Extratropical Cyclones - The Erik Palmén Memorial Volume, Amer. Meteor. Soc., 107-127.

Uccellini, L. W., 1990: Processes of contributing to the rapid development of extratropical cyclones. Extratropical Cyclones - The Erik Palmén Memorial Volume, Amer. Meteor. Soc., 81-105.

Verschuren, J. P., and L. Wojtiw, 1980: Estimate of the maximum probable precipitation for Alberta river basins. Alberta Environment, Hydrology Branch, RMD-80/1, Edmonton, Alberta, 307 pp.

Warner, L. A., 1973: Flood of June 1964 in the Oldman and Milk River basins, Alberta. Environment Canada, Water Resource Branch (Inland Water Directorate), Technical Bulletin No. **73,** 89 pp.

Weldon, R. B., 1979: Satellite training course notes Part IV, Cloud patterns and upper air wind field. United States Air Force, AWS/TR-79/003.

Young, M.V., G. A. Monk and K. A. Browning, 1987: Interpretation of satellite imagery of a rapidly deepening cyclone. *Quart. J. Roy. Meteor. Soc.*, **113,** 1089-1115.